MASTER IN BIOMEDECINE

Role of TRAPP complexes in the glioblastoma sensitivity to treatment

Fillol Bruguera, Laura

Award date:
2022

Awarding institution:
University of Namur

Faculté de Médecine

ROLE OF TRAPP COMPLEXES IN THE GLIOBLASTOMA SENSITIVITY TO TREATMENT

Mémoire présenté pour l'obtention

du grade académique de master en sciences biomédicales

Laura FILLOL BRUGUERA

Août 2022

Université de Namur ©

FACULTE DE MEDECINE

Département des sciences biomédicales

Rue de Bruxelles 61 - 5000 NAMUR

Téléphone: + 32(0)81.72.43.22

E-mail: manon.chatillon@unamur.be - http://www.unamur.be/

Role of TRAPP complexes in the glioblastoma sensitivity to treatment

FILLOL BRUGUERA Laura

Abstract

Background − Glioblastoma (GBM) is a highly aggressive glioma with an average survival of 15 months. The current standard of care is a multimodal approach based on surgery, concomitant chemotherapy and radiotherapy as well as adjuvant chemotherapy. The intratumour heterogeneity poses as the greatest challenge in developing a better treatment as it makes this cancer highly resistant to treatment. Next-generation sequencing (NGS) technologies have improved the understanding of complex diseases such as cancer. Furthermore, the discovery of genome-editing techniques such as CRISPR-Cas endonucleases have provided scientists with the right tools to target specific genes within a given cell genome and manipulate their expression. Previously to the start of this project, a genome-wide CRISPR-Cas9 knockout (GeCKO) screening was performed on a GBM cell line upon a combined exposure to X-ray irradiation and temozolomide (TMZ) to determine which genes are implicated in the resistance to GBM treatment. The results suggested that TRAPPC genes, which participate in intracellular trafficking, may have a role in the sensitivity to GBM treatment.

Aim – In this study, the aim was to validate whether some of the TRAPPC genes play a role in the GBM sensitivity to treatment.

Methodology –The project was divided into two strategies: the knockout and the knockdown of TRAPPC1 gene. For the knockout of TRAPPC1 gene, three TRAPPC1-targeting-single-guide RNAs (sgRNA) were designed and cloned into a plasmid containing the CRISPR-cas9 endonuclease. For the knockdown of TRAPPC1 gene, three targeting TRAPPC1-shRNAs plasmids were designed. Using lentivirus as the gene-therapy vector system, the plasmids were delivered into the U87 cells. The validation of the knockout/knockdown was done at mRNA and protein levels. Additionally, a proliferation assay was performed. Then, TRAPPC1-knockdown GBM cells were treated with a combination of radiotherapy and TMZ and a clonogenic assay was performed to study the role of TRAPPC1 gene in the sensitivity to treatment.

Results – The knockout of TRAPPC1 was validated at mRNA and protein levels for one of the TRAPPC1-targeting sgRNA. The knockdown of TRAPPC1 was validated for one of the TRAPPC1-targeting shRNA at mRNA level. The validation at protein level was not successful. A decrease in cell proliferation was observed with the knockout and knockdown of TRAPPC1. After TMZ and X-ray treatment, TRAPPC1-knockdown cells seem to have a slight higher clonogenicity than controls.

Conclusions – TRAPPC1 appears to be involved in cell proliferation and thus, behaves like an essential gene. The implication of TRAPP genes in the sensitivity of GBM to treatment was not demonstrated and thus, further research needs to be done.

Keywords: Glioblastoma, Genome-wide-knockout screening, CRISPR-Cas9, TRAPP complexes, Intracellular trafficking

Mémoire de master en sciences biomédicales
August 2022
Thesis Supervisor: Prof. Dr Carine Michiels

Acknowledgements

I want to express my sincerest gratitude to my tutor, Jia-Wei Chen, who gave me the opportunity to work on this project and thus, be a minor participant in her doctoral research. Jia-Wei has taught me by example what it means to be a great scientist. I want to thank her for her excellence, perfectionism and strength, as I believe it has helped me become a better professional. I also want to extend my most special thanks to my principal investigator, Prof. Dr Carine Michiels, for her guidance, patience and support throughout this project.

I also wish to thank the TumHyp team for prepping me and challenging me throughout this project. I am grateful to Christoph Schifflers for his constructive feedback. I want to thank him for always speaking his mind and sharing his perspective on things, as it was inspiring.

Furthermore, I wish to acknowledge the important role played by Patrick Pabst and Tobias Kipfelsberger, my two managers at Merck KGaA. I want to thank them for their trust, understanding and respect. Additionally, I wish to extend a special thanks to the rest of the Procurement Healthcare Marketing and Sales team for facilitating the working relationship when I couldn't. A special mention goes to Monica Abril, my friend and colleague, for her unconditional support.

I thank the Unit of Research of animal Cell biology (URBC) for briefly welcoming me to their team. Thank you for allowing me to work and learn from you.
I also want to show my sincerest appreciation to all URBC students for always being willing to help and creating a warm work environment. Coline, Thomas, Louise, and Inès, thank you for your friendship.
Additionally, I want to express my sincerest gratitude to Dr Damien Detraux for not only assisting me in the lab but also for showing me kindness and encouraging me in moments of need.

Finally, I also wish to thank my boyfriend for his unlimited support throughout this challenging experience. Julian, thank you for your encouragement and understanding and for putting up with me in my not-so-great days. Also, I am grateful for my family, who, despite the distance, are my biggest supporters. Gràcies per ajudar-me a creuar la meta.

Being part of this project has been a beautiful, hardening experience, so thank you to all who had a role in it.

Table of contents

List of abbreviations

Abbreviation	Meaning
2-HG	2-hydroxyglutaric acid
Ago	Endonuclease Argonaut
AKT/PKB	Protein kinase B
ANOVA	Analysis of Variance
APS	Ammonium persulfate
ATG	Autophagy-related genes
BAK	Bcl2-antagonist/killer 1
BAX	Bcl-2-associated X protein
BBB	Blood brain barrier
Bcl-2	B-cell lymphoma 2
BH	Bcl-2 homology domain
BLAST	Basic Local Alignment Search Tool
BNIP3	Bcl2 Interacting Protein 3
CDK	Cyclin-dependent protein kinase
CDKN	CDK inhibitor
cDNA	Complementary DNA
C-Met	Tyrosine-protein kinase Met
CRISPR	Clustered Regularly Interspaced Short Palindromic Repeats
CRISPR-Cas9	CRISPR-associated protein Cas9
Ct	Cycle threshold
CTL	Control
CXR	Carboxy-X-Rhodamine
DMEM	Dulbecco's Modified Eagle Medium
DMSO	Dimethyl sulfoxide
DNA	Deoxyribonucleic acid
DSB	Double-strand break
dT	Deoxy-Thymidine
E2F	E2 Transcription Factor
EDTA	Ethylenediaminetetraacetic acid
EGFR	Epidermal Growth Factor Receptor
ER	Endoplasmatic reticulum
ERK	Extracellular-signal regulated kinases
FBS	Foetal bovine serum
GA	Golgi Apparatus
GAP	GTPase-activating proteins
GAPDH	Glyceraldehyde-3-Phosphate Dehydrogenase
GBM	Glioblastoma (multiforme)
GDP	Guanosine diphosphate
GeCKO	Genome-wide CRISPR-Cas9 knockout
GEF	Guanine nucleotide exchange factors
GFP	Green Fluorescent Protein
GSC	Glioma stem cell
GTP	Guanosine triphosphate
Gy	Gray
HDR	Homology directed repair
HeBS	HEPES-buffered saline

HIF1-α	Hypoxia-inducible factor 1-alpha
HPS	Hematoxylin phloxine saffron
IDH	Isocitrate dehydrogenase
IDT	Integrated DNA Technologies
Ig	Immunoglobulin
indels	Insertion–deletion mutations
IR	Ionizing radiation
ITH	Intra-tumoral heterogeneity
Kb	Kilobase
KO	Knockout
LB	Luria-Bertani
LTR	Long-Terminal Repeat
MAGeCK	Model-based Analysis of Genome-wide CRISPR/Cas9 Knockout
MAP	Mitogen-activated protein kinase
MDM2	Mouse double minute 2 homolog
MEK	MAPK/ERK kinase
MEM	Minimum Essential Medium
MGMT	O6-methylguanine-DNA methyltransferase
MOI	Multiplicity of infection
MOMP	Mitochondrial outer membrane permeabilization
MRI	Magnetic Resonance Imaging
mRNA	Messenger RNA
MTIC	Monomethyl triazeno imidazole carboxamide
mTORC	Mechanistic target of rapamycin complex
Neaa	Non-essential aminoacids
NFkB	Nuclear factor 'kappa-light-chain-enhancer' of activated B-cells
NGS	Next generation sequencing
NHEJ	Non-homologous end joining
NIBP	NIK-and-IKK2-binding protein
NSC	Neural stem cells
NT	Non-targeting
PBS	Phosphate-buffered saline
PCR	Polymerase chain reaction
PDGFR	Platelet-derived growth factor receptor
PE	Plating efficiency
PFA	Paraformaldehyde
pH	Potential of hydrogen
PI3K	Phosphatidylinositol 3 kinase
PIB	Phosphatase inhibitor
PNK	Polynuclease kinase
PTEN	Phosphatase and tensin homolog
PTGs	Post-transcriptional gene silencing
PVDF	Polyvinylidene fluoride microporous membrane
qPCR	Quantitative polymerase chain reaction
Rab	Ras-associated binding (Rab) proteins
Raf	Rapidly accelerated fibrosarcoma
Ras	Rat sarcoma
RB	Retinoblastoma

Rheb	Ras homolog enriched in brain
RISC	RNA-induced silencing complex
RNA	Ribonucleic acid
RNAi	RNA interference
ROS	Reactive Oxygen Species
RQ	Relative quantification
RTK	Receptor tyrosine kinase
RT-qPCR	Reverse transcription- quantitative PCR
S.O.C.	Super Optimal Broth
SA-βgal	Senescence-associated beta-galactosidase
SD	Standard deviation
SDS-page	Sodium dodecyl sulfate-polyacrylamide gel electrophoresis
SF	Surviving Fraction
sgRNA	Single-guide RNA
Shh	Sonic hedgehog
shRNA	Short-hairpin RNA
siRNA	Small interference RNA
STAT3	Signal transducer and activator of transcription 3
STRING	Search Tool for the Retrieval of Interacting Genes/Proteins
SVZ	Subventricular zone
TALEN	Transcription activator-like effector nuclease
TCGA	The Cancer Genome Atlas
TEMED	Tetramethylethylenediamine
TERT	Telomerase Encoding Reverse Transcriptase
TME	Tumor microenvironment
TMZ	Temozolomide
TP53	Tumor protein 53
TRAPP	Transport Protein Particle
URBC	Unit of Research of Cell Biology
UT	Untransduced
VSV-G	Vesicular stomatitis virus glycoprotein
WHO	World Health Organization
X-gal	5-Bromo-4-chloro-3-indolyl β-D-galactopyranoside
Ypt	Yeast protein transport
ZFNs	Zinc-finger nucleases

1. Introduction

1.1. Foreword

The etymology of the word cancer is Greek, originally called καρκίνος, which reads as karkinos; its literal meaning is crab. In 400 bC, Hippocrates named cancer "crab" after the resembling of the cancer cells progressing and expanding to the crab legs.
Today, we know cancer to be a disease caused by alterations to the genome.

According to the World Health Organization (WHO), cancer is a leading cause of death worldwide. In 2020, approximately 19 M new cancer cases were detected while 10 M people died of cancer[1]. Despite the development of better diagnostic devices, preventive techniques and new treatments, it is predicted that the burden of cancer incidence and mortality will continue to grow over the next years.

The reason why cancer is still a major cause of death among humans is explained by Hanahan and Weinberg, who have investigated the similarities of all cancer types and have defined what we know now as the hallmarks of cancer. The hallmarks of cancer are aberrations shared with most, if not all, cancer cell types, which provide an advantageous survival upon the healthy cells. These hallmarks are summarized in the figure 1[2].

The definition of the hallmarks of cancer, together with the recent biotechnological advancements, have allowed to shift cancer therapies towards a more personalized approach, aiming to target one specific gene/protein, which is specifically dysfunctional in cancer cells.

All in all, it is imperative that we expand our knowledge on how the molecular processes regulate aberrant gene expression to develop more successful anticancer therapies.

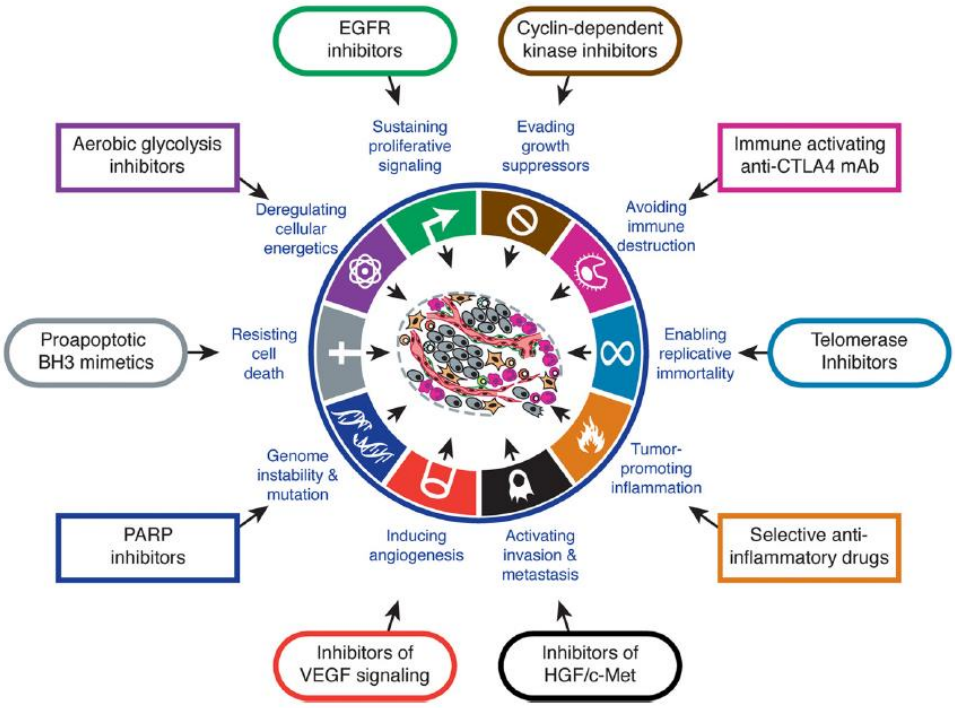

Figure 1. The hallmarks of cancer. The six acquired capabilities (framed in a circle) together with emerging hallmarks (framed in a square). In the future, these hallmarks may be useful to develop therapeutic targets that can be relevant for the treatment of different cancer types[2].

1.2. Glioblastoma Multiforme

Brain malignancies are relatively rare in comparison to other types of cancers. However, when they occur, they raise special challenges when it comes to their treatment, mainly due to their protected location due to the Blood Brain Barrier (BBB).

Glioblastoma multiforme (GBM) is the most common and most malignant brain cancer in humans. After its diagnosis, the patient normally has an average survival of 14 to 16 months. The current standard of care consists of a multimodal approach, combining surgery resection of the tumour, radiotherapy and concomitant chemotherapy followed by adjuvant chemotherapy[3].

Despite the aggressive treatment, all the years invested in understanding the molecular tumorigenesis of this cancer and the development of novel precision therapies, GBM remains an incurable cancer.

1.2.1. Epidemiology and aetiology of glioblastoma

The incidence of GBM is low, reporting an annual age-adjusted incidence rate of 5-8/100.000 people in Europe[4]. However, compared to other brain malignancies, it is the most common, accounting for more than 70% of all brain cancers in adults[5]. Due to its poor prognosis, GBM is also among the most studied types of cancer.

This cancer incidence increases with age, the peak being at 55-65 years old. It is more typically found in men than in women. However, until now, no risk factors accounting for GBM have been found, indicating that the appearance of this cancer is mainly sporadic.
Several studies have concluded that there is no substantial evidence of GBM association with lifestyle factors like smoking, alcohol consumption, drug use or even mobile phone use[6]. However, there is evidence indicating that previous irradiation exposure is a potential risk factor for GBM occurrence[7].

This cancer lethality and the lack of prevention methods make this disease a public health issue that needs substantial research and investigation.

1.2.2. Classification and pathology hallmarks of glioblastoma

Glioblastoma is a diffuse glioma, which means that the cancer cells can infiltrate into the surrounding normal brain parenchyma and even recur after total gross resection[8].

In 2016, the WHO published the current international standard for the nomenclature and diagnosis of gliomas[5,9] based on their malignancy level, determined from tumour morphology and molecular alterations. This classification stratifies gliomas into four grades, with I being the lowest and IV being the highest and consequently, the most malignant tumour. GBM is currently classified as IV grade glioma.

Traditionally, GBM has been identified as a primary brain tumour, when the cancer arises with no precedent, or as a secondary brain tumour, when the glioma evolves from a low grade into a more malignant neoplasm[8]. These two subtypes closely correlate with the isocitrate dehydrogenase (IDH) gene mutation status and show similar histological characteristics, but they differ at a molecular level and are also thought to develop from different cells of origin[10]. Currently, the WHO classifies GBM based on the mutational status of isocitrate dehydrogenase (IDH) genes, as it is an indicator of the cancer malignancy and

consequently, serves as prognostic for the outcome of GBM treatment (Supplementary data, Figure 1).

IDH is an enzyme that catalyses the oxidative decarboxylation of isocitrate into alpha-ketoglutarate and carbon dioxide (Figure 2). IDH has two different isoforms: NADP-dependent (IDH1 and IDH2) and NAD-dependent (IDH3). IDH1 is found in cytoplasm and peroxisomes and has mainly an antioxidant function. IDH2 and IDH3 are found in mitochondria, where they are involved in the TCA cycle, and thus, play a key role in the cell metabolism.

Mutated IDH1/2 show association with several human diseases, such as brain cancers. Mutations in the IDH3 isoform are not frequent.
Generally, when IDH1/2 is mutated, the product of the decarboxylation of isocitrate is converted into 2-hydroxyglutaric acid (2-HG), which acts as an oncometabolite by promoting the formation of tumor microenvironment, glioma cells invasion and blocking stem cells differentiation. The accumulation of 2-HG can inhibit αKG-dependent dioxygenases, which are enzymes involved in many critical biological processes, such as post-translational modifications, epigenetic regulations; and thus, contribute to alterations in cell metabolism and cancer cell differentiation[11]. Furthermore, 2-HG can also inhibit chromatin-modifying enzymes, namely 2-oxoglutarate-dependent dioxygenases, which in turn can cause DNA and histone methylation which can promote tumourigenesis.

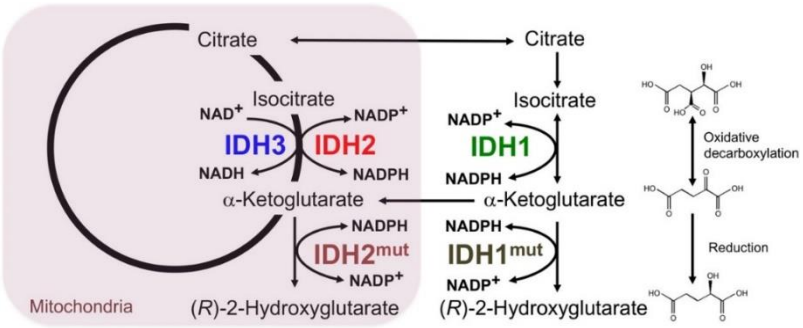

Figure 2. Schematic representation of the role of IDH1/2 and IDH3 in the Krebs cycle based on their subcellular localisation and their mutagenic status[12]. IDH2 and IDH3 are located in the mitochondria while IDH1 is found in the cytosol. Mutated IDH1/2 convert α-KG into 2-HG regardless of their location.

In the context of GBM, 2-HG can sensitise glioma stem cells to alkylating agents by inhibiting the ALKBH repair enzyme. However, it can also favour tumour microenvironment (TME) formation and induce high levels of hypoxia-inducible factor-1α (HIF1-α), promoting glioma invasion[13].

The patients with primary GBM usually have the IDH-wildtype status, which has been correlated to a poorer prognosis than those with the IDH-mutant status. On the other hand, patients having a secondary GBM commonly have the IDH-mutant status, either with a mutation in IDH1 or IDH2. This latter group of patients has been associated with a longer survival[14].

Other common genetic aberrations that are present in GBM are the methylation of O^6-methylguanine-DNA methyltransferase (MGMT) promoter, epidermal growth factor receptor (EGFR) gene amplification, phosphatase and tensin homolog (PTEN) mutation, TP53 mutation and telomerase encoding reverse transcriptase (TERT) promoter mutation, among others[5].

The forementioned genetic aberrations can be clustered based on their effect on the processes that are contributing to gliomagenesis. These are mainly three: initiating tumour growth, evading senescence and enabling immortal growth.

In 2017, Noroxe et al.[15] published a review highlighting the hallmarks of cancer in the context of GBM based upon the previous extensive work done by Hanahan and Weinberg[2]. In Figure 3, the three processes that are based on the molecular signature of GBM cells are summarised by colours in relationship to three core common disrupted pathways: receptor tyrosine kinase (RTK)/rat sarcoma (RAS)/PI3K, p53 and RB pathways. They will be described in more detail hereunder.

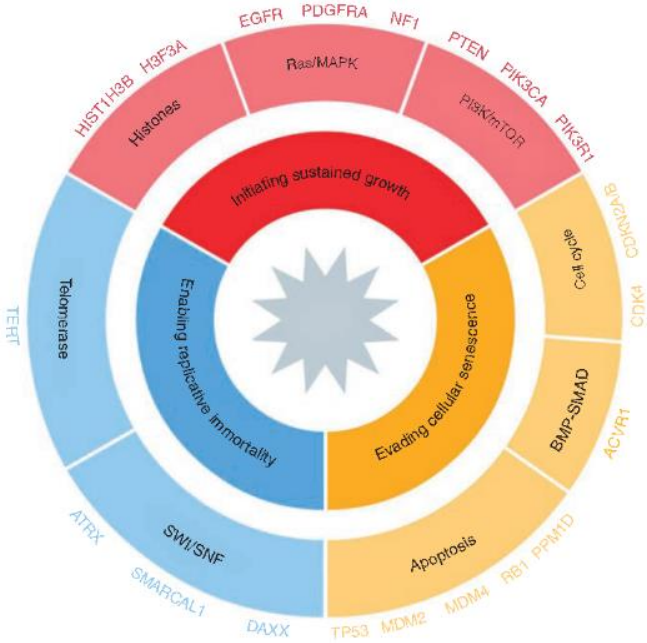

Figure 3. Molecular aberrations of GBM highlighting the 3 pathways (shown in blue, orange and red) as pathological hallmarks of this cancer[3].

RTK/RAS/PI3K signalling pathway

The RTK/RAS/PI3K pathway regulates the proliferation, differentiation and survival of normal cells upon the activation of RTK (Supplementary data, Figure 2). In any cancer, genetic aberrations in genes involved in this pathway result in increased proliferation, survival and metastasis. RTK act as receptors for growth factors, hormones, etc., and comprise several subfamilies, including EGFRs, platelet-derived growth factor receptors (PDGFRs) among others[16].

In GBM, several genes that encode proteins involved in the RTK/RAS/PI3K signalling pathway are considerably altered. For example, as we have previously mentioned, the EGFR gene is overexpressed in GBM and thus, has a role in sustaining the high proliferative rate of cancer cells.
In 2018, he Cancer Genome Atlas (TCGA) published an investigation on molecular aberrations for GBM. In this investigation, they found that EGFR activation mutation is the most common alteration in the RTK/RAS/PI3K pathway with a 45% incidence[17], as presented in Figure 4. On the other hand, other relevant mutations participating in this pathway can be found, like the inactivation of PTEN, causing increased proliferation and decreased apoptosis[15].

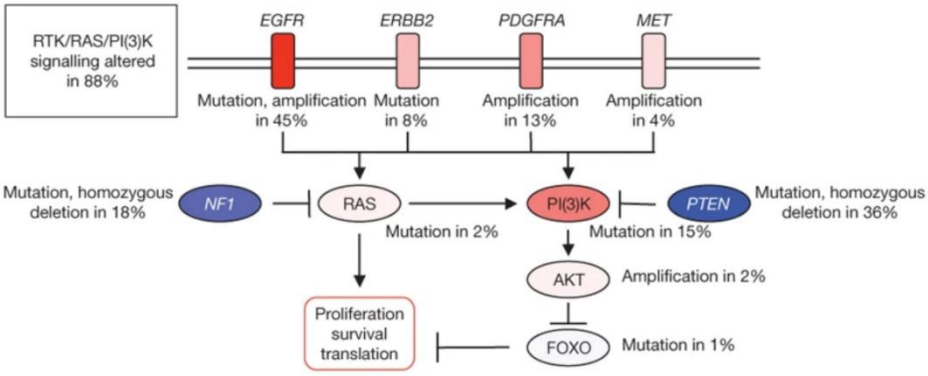

Figure 4. Schematic view of the altered RTK/RAS/PI3K pathway in GBM and the presence of mutations in human samples evaluated in 2008. Extracted from TCGA research network[17]

p53 pathway

p53, also known as the guardian of the genome, is a 53-kDa protein that regulates the cell cycle and has a direct implication on growth arrest and apoptosis, meaning that it has the capability to induce cell death in response to DNA damage[18].

In a normal healthy cell, the protein level of p53 is low thanks to E3 Ubiquitin ligase Mouse double minute 2 homolog (MDM2). p53 and MDM2 work in a negative feedback loop where p53 activates MDM2, which in turn promotes p53 degradation[19]. In the "supplementary data" section, figure 3 shows how p53 is activated upon diverse stress stimuli, including oncogene expression and DNA damage. Other factors like hypoxia, metabolic dysfunction and replicative stress also activate p53, which results in a variety of responses aiming to stop cancer initiation[20].

The loss of function in p53 is common in many cancer types, allowing cancer cells to sustain proliferation, avoid cell death and evade growth suppressors. In other words, p53 is a tumour suppressor protein playing a fundamental role in preventing cancer development and thus, is a very well-studied biomarker for cancer therapy research as it is mutated in ~50% of all cancers[19].

The TCGA GBM molecular investigation[17] shows that the alteration of the p53 pathway was present in 87% of the cases, from which 35% display the loss of p53 (Figure 5).

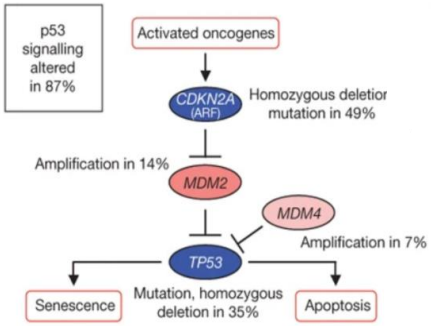

Figure 5. Schematic view of the p53 altered pathway in GBM and the incidence of common mutations in human GBM samples evaluated in 2008. Extracted from TCGA research network[17]

RB pathway

The RB pathway counts with the well-coordinated interaction of 5 protein families that work together to ensure the proliferation of the cell (Supplementary data, Figure 4). These protein families are the Rb-pocket protein family, E2F transcription factors, D-type cyclins, cyclin-dependent protein kinases (CDK) and CDK inhibitors (CDKN). Since genetic and epigenetic changes in this pathway are consistently found in most human cancers, it is essential to better understand how this pathway participates in cancer initiation and tumour growth[21].

Retinoblastoma (Rb) is a tumour-suppressor gene and key participator in regulating cell cycle, differentiation and apoptosis[22]. The main activity of Rb is to inhibit the G1 phase of the cell cycle to repair detected damage or cause apoptosis to the cell[15,23]. The activity of Rb can be E2F dependent or independent. E2F are transcription factors that act as activators or repressors of genes required for DNA synthesis. They participate in the Rb-pathway by forming a complex with Rb-pocket proteins, thus inhibiting the cell division.

Other proteins may interact with Rb-pocket proteins. For example, CDK4 and CDK6 can disrupt the interaction between Rb-E2F by phosphorylating Rb, which leads to the activation of the E2F regulated gene expression, promoting cell cycle progression[21]. These two kinases are negatively regulated by CDKN2A/B, which means CDKN usually inhibits them. When the cell suffers a genetic loss of CDKN2A or of Rb, the cell indirectly displays a functional Rb inhibition[15] and thus, a sustained proliferation but also evades growth suppressors and resists cell death.

In the TCGA molecular investigation of GBM[17] (Figure 6), researchers observed that Rb-pathway was altered in 78% of the human samples. From this 78%, CDKN2A/B was mutated in approximately 50% of the cases, and Rb gene deletion happened only in 11%.

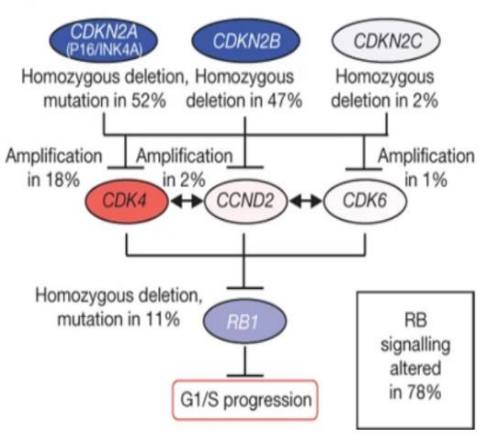

Figure 6. Schematic view of the alteration of Rb-pathway in GBM and the presence of mutations on the human GBM samples evaluated in 2008. Extracted from TCGA research network[17]

Altogether, RTK/RAS/PI3K signalling, p53 and Rb pathways remain a focus for further biomarker investigation and targeted molecular therapy development for GBM.

1.2.3. Histopathology, symptomatology and clinical signs of glioblastoma

The typical histological features for GBM include hypercellularity, nuclear atypia, microvascular proliferation and necrosis[3,10] (Figure 7).

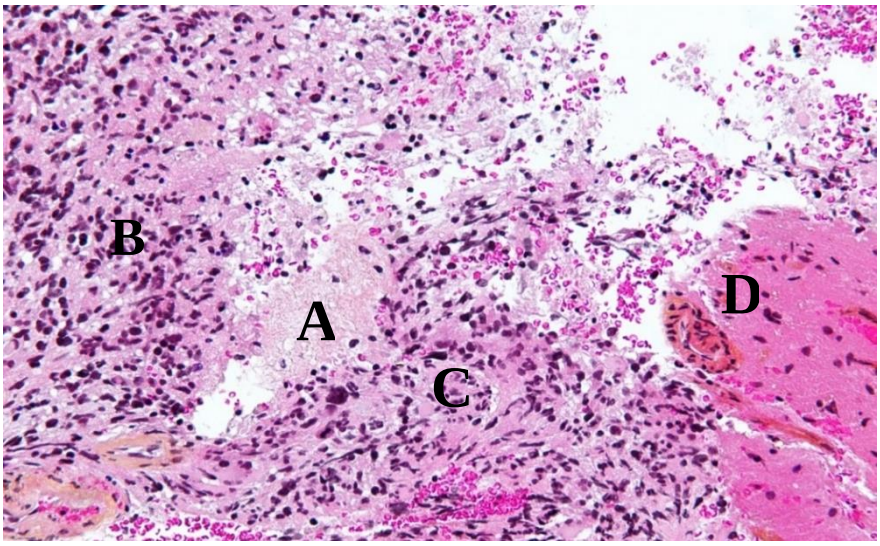

Figure 7. Histological sample of GBM in HPS staining with high magnification. We can observe necrotic areas (A), nuclear pleomorphism (B), microvascular proliferation (C) and a piece of near-normal white matter (D) for comparative reasons[24].

The most frequent location for GBM is in the cerebral hemispheres, where 95% of these tumours arise in the supratentorial region[5]. Contrast-enhanced MRI is the diagnostic tool for GBM[3]. Figure 8 presents an MRI from a patient suffering from GMB[25]. This tumour typically manifests as large, has thick margins and a central necrotic mass surrounded by oedema and infiltrative tumour[26].

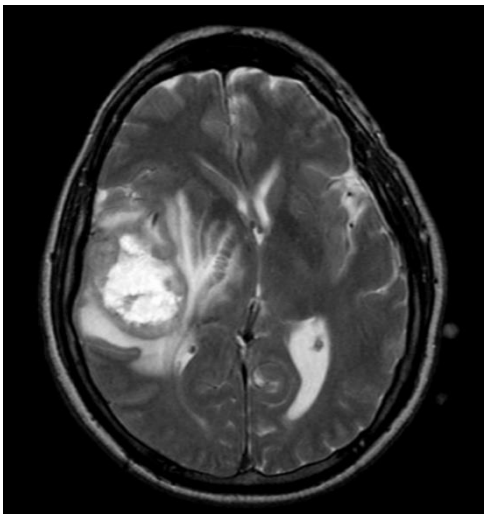

Figure 8. Axial T2 MRI of a patient suffering from GBM. In this case, there is a large mass in the superior part of the right temporal lobe surrounded by edema. The high T2 signal in the central region suggests a necrotic area. The GBM was confirmed by biopsy[25].

1.2.4. Biology and origin of glioblastoma

A tumour is developed after a first healthy cell acquires a cancer-promoting mutation. This cell is called the cell of origin, and it differs from the cancer stem cells, which are a subset of cells that sustain malignant growth[27]. The nature of the cell of origin for GBM has always been controversial. Initially, GBM was classified as astrocytoma, arguing that this cancer arises from differentiated glial cells such as astrocytes, based upon histological samples from patients suffering from GBM[28].

Recent evidence supports the theory that GBM arises from a subpopulation of neural stem cells (NSC) located in the brain's subventricular zone (SVZ).

Lee et al.[29] performed deep genome sequencing of triple-matched tissues from patients with isocitrate dehydrogenase (IDH) wildtype GBM to compare somatic mutations. The tissues compared were 1) normal SVZ tissue (away from tumour mass), 2) tumour tissue, and 3) normal cortical tissue (or blood). They found that 56.3% of patients had low-level GBM driver mutations in the normal SVZ tissue that were observed similarly at higher levels in the associated tumour tissue. These results indicated that either the cells harbouring the driver mutations from GBM migrated to SVZ or those from the SVZ harbouring driver mutations underwent clonal evolution. They performed single cell cloning in the cancer cells carrying the driver mutations shared with SVZ tissue. Then, they examined the aetiology of somatic mutations in the SVZ-tumour free tissue by single-cell sorting and sequencing. A few clones harbouring the shared mutations lacked tumour-private mutations; the others had normal alleles. This observation, together with the experimental results they obtained after analysing the glioma progression in genome-edited mice (carrying low-level driver mutations in NSCs from SVZ tissue), led to the deduction that the cells of origin are NSCs from SVZ tissue, and after that, these cells clonally evolve to GBM.

Despite these results, astrocytes are still considered as potential cells of origin for glioblastoma. It has been observed that after traumatic brain injury some astrocytes re-enter the cell cycle, meaning that some proliferating astrocytes may still be present in the postnatal brain[30].

Therefore, the characterization of this cancer's cell of origin needs to be further investigated as it can provide fundamental value in the development of better treatments for patients.

1.2.5. Standard care of treatment and treatment resistance

The high cellular heterogeneity of GBM poses a significant challenge when treating this cancer. As already mentioned, cancer cells harbour mutations that provide them with selective growth advantages and promote proliferation, survival and resistance to treatment. These mutations differ from cell to cell, which means that GBM has a high intra-tumoral heterogeneity (ITH). This ITH contributes to the high percentage of patients suffering from cancer recurrence, which represents 90% of the cases[31].

Sottoriva et al. [31] presented an integrated analysis of ITH at different levels (e.g., genetic, phenotypic) within one patient displaying different subtypes of GBM to describe the clonal evolution of GBM cells after treatment. They concluded that it is possible to characterise the different cellular subtypes of a tumour within one patient based on gene expression levels. This is interesting for designing a better treatment as the cell population presents genetic aberrations that make them more sensitive to treatment[32,33].

The current standard of care of GBM comprises surgery, radiotherapy (RT) and chemotherapy. The most successful chemotherapeutical agent is temozolomide (TMZ), and therefore it is the most used. However, due to the intra-tumoral heterogeneity and inter-tumoral heterogeneity (patient-to-patient), treatment must be tailored to each patient based on sex, age, weight and GBM molecular signature.

Generally, the treatment for GBM after surgery consists of RT (30 X-ray fraction x 2 Gy, so a total dose of 60 Gy) with concurrent TMZ (75 mg/m^2/day x 6 wk.) and maintenance of TMZ (150-200 mg/m^2/day x 5 days for six 28-day cycles)[3] (Supplementary data, Figure 5).

1.2.5.1. Temozolomide-based chemotherapy

Temozolomide (TMZ) (Figure 9A) is an alkylating agent able to cross the BBB and thus, it is widely used in the therapy against malignant brain tumours. This drug is orally administered and has an excellent uptake and distribution behaviour[31].

TMZ is a prodrug converted at a physiological pH to a short-live active compound named monomethyl triazeno imidazole carboxamide (MTIC). This compound is cytotoxic because it is responsible for methylating DNA at the O6 and N7 positions of guanine[34] and the N3 position of adenine. This methylation results in the inaccurate pairing of the methylated guanine (with incorporated thymine) during DNA replication, resulting in DNA double-strand breaks, irreparable DNA damage and cell death[35].

Even though TMZ is shown to be the most efficient drug when combined with RT in the GBM treatment, there are known resistance mechanisms to TMZ in GBM (e.g. MGMT methylation, DNA mismatch repair pathway, glioblastoma stem cells and autophagy) [36]

We have mentioned that GBM cells can harbour MGMT promoter methylation. MGMT is an enzyme that participates in the DNA-repairing mechanism by removing methyl groups from O6-MeG lesions. The expression of MGMT inversely correlates to the sensitivity of cancer cells to alkylating agents, meaning that elevated levels of MGMT show increased TMZ-chemoresistance. Patients with low methylated MGMT promoter have a higher survival when treated with RT and TMZ-based chemotherapy, while patients with methylated MGMT do not benefit from this treatment[31].

Besides, as mentioned previously, GBM patients with IDH1/2 mutations have better survival prognostic (Figure 9B), which can also be explained by the fact that they have better treatment response as IDH1/2 mutations may be involved in MGMT methylation, which eventually leads to DNA strand breaks, apoptosis, autophagy and cell death.

The methylation of MGMT promoter happens in 45% of newly diagnosed GBM patients, and thus, it is an acceptable prognostic for the response to TMZ treatment. While 45% is a good ratio, it means there is a significant number of patients with TMZ resistance[31].

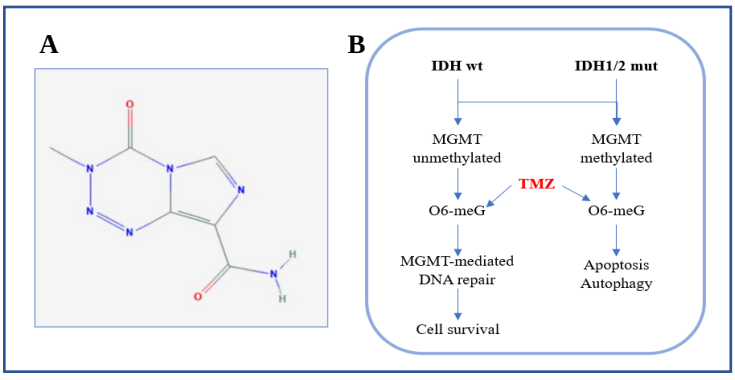

Figure 9. A: 2D chemical structure of TMZ[34]; B: Response to TMZ treatment upon IDH genetic status and MGMT methylation status in GBM cells.

1.2.5.2. Radiotherapy

Irradiation of the remaining tumour cells after surgery aims to prevent disease relapse. Together with temozolomide, it has been demonstrated to increase survival in patients suffering from GBM[5,37]. However, it has a countereffect; there is evidence that the damage caused by X-ray irradiation might create tumour-susceptible niches facilitating proliferation and invasion of residual cancer cells and, thus, cancer recurrence.

The main consequence of ionizing radiation (IR) is the over-production of ROS, which affects the cells' proper function at different levels, especially their ability to grow and proliferate. IR can be divided into two types of treatment: photon and particle radiation therapies[38]. Photon radiation is the most common, in which the patient receives high-energy X-rays from a photon beam; whilst particle radiation, and more specifically proton radiation, is a more innovative approach in which the patient receives charged particles that release their energy at a precise location, without damaging the cells nearby. Both strategies cause oxidative stress, leading to cell damage.

One of the mechanisms of radiotherapy resistance in GBM (Supplementary data, Figure 6) lies on the hypoxic niches that limit the formation of ROS necessary for cell killing, on hyperactivated DNA damage response machinery and on active environmental crosstalk across multiple signalling pathways (e.g. Wnt, Notch, Shh and NFkB)[13] that collectively induce radiotherapy resistance in glioma stem cell populations (GSCs). Besides, a long radiation exposure may promote epigenetic changes that can add to the cancer radio-resistance[39].

Altogether, both chemotherapy and radiotherapy treatments are known to enrich the tumour mass heterogeneity and thus, contribute to the resistance treatment by activating DNA damage response pathways and inducing autophagy, among others[31].

1.3. Intracellular trafficking, autophagy and cancer

Intracellular communication and trafficking of proteins and lipids within cells are vital processes for cell viability as they help maintain cellular homeostasis, morphology, cell polarity, motility, secretion and synaptic function in the case of neuronal cells[40,41]. Because cell membranes are semi-permeable, many molecules need to cross the cell through carrier proteins. Moreover, the cell needs bulk transport mechanisms when the molecules are larger. These mechanisms are the endocytic and exocytic pathways, and they both imply the critical participation of many molecules, particularly small GTPases, primarily Rab GTPases.

1.3.1. Endocytosis

Endocytosis is the active transport of large molecules, bacteria, apoptotic bodies and other components into a cell. Generally, the cell plasma membrane invaginates to engulf the target particle. When it is entirely closed, it pinches off from the membrane, resulting in an intracellular vesicle. The purposes of endocytosis are various, from nutrient intake for cellular growth and repair to pathogen capture and elimination of senescent/damaged cells. Two main types of endocytosis are described: pinocytosis (cell drinking) and phagocytosis (cell eating).

1.3.2. Exocytosis

Exocytosis, also an active transport, is the reverse process of endocytosis. The content of an intracellular vesicle, such as waste products, is expulsed from the cell. This pathway lies in the fusion between the membrane of the intracellular vesicle with the plasma membrane so its content can exit the cell. The purposes that serve exocytosis are toxin/waste removal, protein secretion, cell to cell communication and cellular membrane growth[42].

1.3.3. Autophagy, apoptosis and senescence crosstalk in cancer

Autophagy, apoptosis and senescence are crucial cellular processes that respond to stress, and thus, it makes sense that these processes are interconnected in cancer cells and participate in the cancer treatment resistance. When focusing on GBM's molecular pathogenesis and the high intra-and inter-tumoral heterogeneity, understanding how these relationships work is vital in developing a successful anti-cancer therapy against GBM.

Autophagy is a cell-survival pathway by which the cells degrade and recycle cellular content to use it as source of energy, in response to stress or starvation. It is a highly regulated and very well-conserved pathway (Supplementary data, Figure 7). Autophagy has been identified as a mechanism related to several diseases, among them, cancer.

In cancer, autophagy is like a double-edge sword. It can have a tumour-suppressor role or tumour-protective[43] depending on the stimuli that activate this pathway and on the genetic status of the cells.
Autophagy, also called macroautophagy, is mainly regulated by autophagy-related-gene (ATG) proteins whose mechanism of action has been studied thanks to gene-editing techniques and thus, some ATGs have been identified as key molecules for the autophagosome biogenesis[44]. Up to date, we know about 20 core ATG proteins implicated in autophagosome biogenesis. Those can be divided into six functional groups: 1) ULK protein kinase complex, 2) ATG9-containing vesicles, 3) autophagy-specific PI3K, 4) ATG2-WD-repeat protein, 5)ATG12-ATG5-ATG16L1 complex, and 6) ATG8-family protein lipidation system[45]. Each of these groups of ATG proteins takes responsibility for a function in the autophagosome biogenesis.
In the context of GBM, autophagy seems to contribute to tumour cell survival and progression in a hostile environment as it can be triggered by intrinsic and or extrinsic GBM cell signals, contributing to cell proliferation, cell invasion and cell resistance to therapy[46].

Autophagy is activated upon chemotherapy and radiotherapy. TMZ-induced autophagy displays a cytoprotective role, leading to TMZ resistance through mTORC signalling and by inhibiting apoptosis. On the other hand, the cytotoxicity caused by TMZ can be enhanced with the combination of other drugs and therefore in this case, autophagy would be increased and implicated in type II cell death [47].

Of note, radiation induces cell death by apoptosis in GBM cells. However, some cells activate autophagy and escape apoptosis. This can be explained by the existing crosstalk between autophagy and apoptosis that enables the coregulation of these pathways[43].

Apoptosis is a genetically programmed cell death that helps to maintain cell homeostasis and to remove unwanted cells. As we have seen, cancer cells have inherent mutations that help them to avoid or escape apoptosis (e.g., p53 mutation). Anti-cancer therapies aim to induce apoptosis in cancer cells.

Intrinsic or extrinsic death pathways can induce apoptosis. The intrinsic pathway is triggered by an intracellular injury provoked by cellular stress such as nutrient detriment, hypoxia, or chemotherapy/radiotherapy. The extrinsic pathway is triggered by death ligands produced by other cells in the microenvironment.
Both pathways lead to the activation of caspases that act as common death effector molecules in various forms of cell death[48]. The intrinsic pathway is regulated by pro-/anti-apoptotic proteins belonging to the family of Bcl-2 proteins. These proteins are characterised by the presence of homologous regions named Bcl-2 homology domains (BH)[49].

The BH3 domain is essential for the pro-apoptotic function of the Bcl-2 family proteins. Generally, in response to apoptotic stimuli, the BH3 pro-apoptotic proteins are activated and inhibit anti-apoptotic proteins, releasing the pro-apoptotic factors (Bax, Bak) and allowing them to oligomerise and cause mitochondrial outer membrane permeabilisation (MOMP)[49]. MOMP, in turn, will support the release of the cytochrome C, which will activate the caspases and bring the cell to death (Supplementary data, Figure 8).

B-cell lymphoma 2 (Bcl-2) anti-apoptotic protein is a crucial regulator of apoptosis. The gene Bcl-2 is overexpressed in many cancers, e.g. B cell lymphoma and lung cancer[50], which means that upregulation of this gene is associated with cancer. Furthermore, Wang et al.[49] observed that, in starvation conditions, senescent human fibroblasts showed increased Bcl-2 gene expression compared to non-aged fibroblasts. This study was the first to identify the direct link between the increase in Bcl-2 level and senescence.

Cellular senescence is a cellular state in which the cell cannot divide due to the loss of mitotic activity, but it is still metabolically active. There exist replicative and premature forms of senescence. Replicative senescence is associated with an end replication problem, which means that DNA polymerase cannot initiate replication of the very ends of linear chromosomes, which leads to shortening of chromosomal ends and consequently, the cells stop dividing[51]. The premature senescence is not associated with telomere erosion but with oxidative, genotoxic or replicative stress. Senescence is irreversible, and therefore, it has been a focus when developing anti-cancer therapies.

1.3.4. Rab GTPases and their emerging role as oncogenes

Rab GTPases belong to the Ras superfamily. They are well-conserved proteins responsible for regulating all membrane-bound intracellular trafficking pathways in eukaryotic cells. Consequently, they are known to be key for the cell wellbeing and for human health[52].

In humans, there are more than 60 Rab GTPases. Alterations in Rab GTPases (and their effectors) are associated with multiple human diseases, including neurodegenerative diseases and cancer. Recently, in addition to their key role in intracellular trafficking processes, Rab GTPases have emerged as oncogenes due to their implication in regulating cell growth, survival and programmed cell death or apoptosis[40,53].

Rab GTPases cycle between a GTP-bound active form and a GDP-bound inactive form (Figure 10). The GTP-bound form interacts with different effectors that trigger membrane trafficking events.

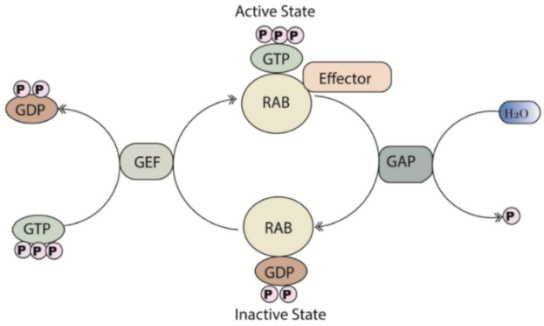

Figure 10. GTP-bound state of Rab GTPases. Guanine nucleotide exchange factors (GEF) are responsible for the activation of Rab GTPase by catalysing the exchange of GDP for GTP, while GTPase-activating proteins (GAP) are responsible for the inactivation of Rab proteins[40].

Literature review identifies Rab GTPases as compartment-specific rather than function-specific. It also seems that GEFs are crucial for their function whereas GTPase-activating proteins (GAPs) play a role in their cycling across membranes and vesicles[53].

1.3.5. TRAPP complexes

Transport Protein Particles or TRAPP are a highly conserved multi-subunit protein complexes[54,55] that act as Rab GTPase guanine nucleotide exchange factors (GEFs) and are therefore responsible for the GDP/GTP exchange.

In mammals, like in yeast, there are 3 TRAPP complexes: TRAPP I, TRAPP II and TRAPP III. The main difference between these complexes lies on their function and even though TRAPP I acts as a core subunit for all forms, they have also different structures[56].

TRAPP complexes have been very well characterised in yeast. However, in mammals, TRAPP structure and function remain to be further studied. Yet what we know is that most mammal TRAPP complexes are homologous to yeast ones and thus, have similar functions (Figure 11).

TRAPP complexes are key regulators of the vesicle trafficking between ER and the GA[57]. In the context of cancer, it is worth to mention that some recent studies in yeast and mammals have linked some subunits from TRAPP II and III complexes to autophagy regulation[54]. Knowing how autophagy plays an important role in cancer cell survival and further understanding of the implication of TRAPP II and III in autophagy, is needed.

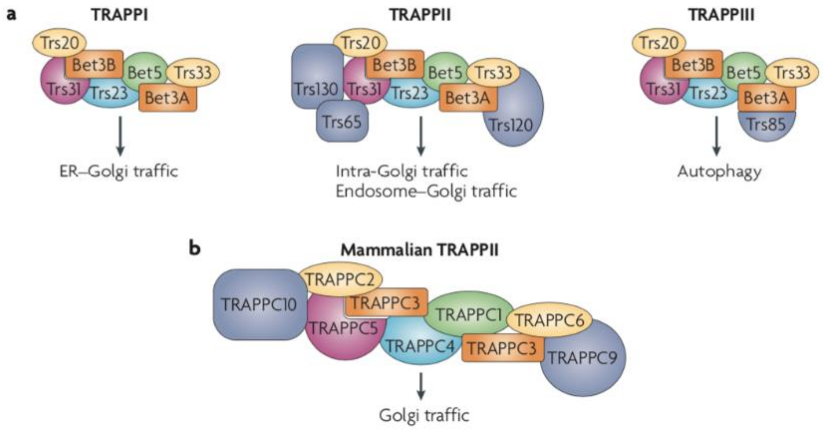

Figure 11. TRAPP complexes and their constituent subunits. A: TRAPP complexes present in yeast: TRAPP I, TRAPP II and TRAPP III. B: homologous TRAPP II complex from yeast in mammals[57].

Zhang et al.[58] studied the TRAPP II complex in mammals. More specifically, they discovered that the subunit TRAPPC9/NIBP acts as a key mediator of tumourigenesis of cancer cells through NFkB signalling. Nuclear Factor kappa B (NFkB) is a transcriptional factor that participates in important biological processes such as inflammation, immunity and anti-apoptotic activities. The activation of this transcription factor is found elevated in many types of human cancer (e.g., breast cancer). In this study, they induced the knockdown of TRAPPC9/NIBP in breast and colon cancer cells. Results indicated that TRAPPC9/NIBP-knockdown cancer cells significantly lost their proliferation, migration and colony formation capabilities. These capabilities are directly or indirectly dependent on intracellular trafficking processes. So, this is an example of how TRAPP complexes may be regulators of tumour growth[58].

Even though TRAPP I, II and III are functional as complexes, there is also evidence that each subunit has an individual role, as several pathologies (also referred to as TRAPPopathies[59]) have been linked to the mutation of one of the different TRAPP subunits or TRAPP-associated proteins. For example, Brunet et al.[60] found that TRAPPC4 is overexpressed in colorectal cancer lines, increasing cell proliferation and invasiveness of these cancer cells, which led to the assumption that TRAPPC4 contributes to tumour growth through the Ras-Raf-MEK-ERK signalling pathway[60].

The Ras-Raf-MEK-ERK pathway couples extracellular signals from the cell surface receptors to transcription factors, which regulate the expression of genes that induce cell cycle progression or prevent apoptosis[61]. Many members of this pathway have been defined as oncogenes, and aberrant activation of this pathway is commonly found in cancer cells. TRAPPC4 is involved in this pathway by interacting with the MAP kinase ERK2, which is part of the complex ERK1/2 that participates in the ERK-MAPK pathway[62(p4)]. In this study, they induced the downregulation or the overexpression of TRAPPC4 to examine its contribution to the ERK1/2 phosphorylation. The results showed a relationship between TRAPPC4 depletion and the decrease in ERK1/2 phosphorylation and vice versa when TRAPPC4 was overexpressed.

These examples highlight the importance of further studying TRAPP complexes and their role in intracellular secretory and excretory trafficking pathways in the context of cancer research[63].

1.4. Next-generation sequencing and genome-editing technologies

Over the past decade, the application of next-generation sequencing (NGS) technologies or also known as high-throughput sequencing, have contributed to the profiling of several cancer types by revealing their underlying genomic drivers[64].
NGS technologies serve as a tool to massively sequence numerous DNA/RNA strands at the same time. This has revolutionised the genomic research by allowing to decipher the complete genome sequence of any living being in a short period of time, e.g., the human genome. In the context of cancer, obtaining the genomic sequence of one tumour or even of one cancer cell has revealed the complexity of the intratumour heterogeneity. Furthermore, it can bring us closer to personalised cancer therapies.

In parallel, genome editing helps understanding the contribution of a single gene to a specific disease. The development of genome-editing techniques has promoted the creation of more accurate in vitro and in vivo models by directly targeting and modifying genomic sequences in almost all types of eukaryotic cells[65]
The editing of the genome editing had its origin with the discovery of restriction enzymes in the late 1960s by Stuart Linn. However, the most advanced genome editing technologies are based on engineered or bacterial nucleases. Recently, the discovery of the prokaryote-derived CRISPR-Cas technology has revolutionised genome engineering in translational research due to its ease of use and robustness[66,67] and it has opened the door to a lot of different applications including the genome-wide CRISPR screening.

1.4.1. Clustered regularly interspaced short palindromic repeats (CRISPR)

CRISPR is a natural available system in prokaryotes serving as an immune-like defence against foreign DNA.

The principle behind the CRISPR technology consists in the design of a short single-stranded endogenous RNA component that guides the nuclease to a specific site complementary to that sequence and induces a double-strand break (DSB)[68], which will in turn promote the activation of DNA damage repair mechanisms existing in all mammalian cells.

Generally, when a DNA damage occurs in a mammalian cell, it induces an endogenous response mechanism to repair it. There are several responses that allow the cell to cope with the DNA damage, however in the framework of genome-editing we benefit from two major repair mechanisms to resolve the DSB: nonhomologous end joining (NHEJ)-mediated repair and the homology-directed repair (HDR)[69] (Figure 12).

NHEJ is an error-prone repair mechanism that normally leads to a small insertion or deletion (indels) mutation. It is frequently used to produce gene knockouts (KO) whereas HDR integrates an homologous donor DNA template in the targeted genomic site, such as point mutation or long DNA insertion[66].

These two natural DNA damage responses can be useful in the context of genome-editing by artificially inducing a targeted-DSB to either delete, insert or alter genetic information within the genome. CRISPR-Cas9 technology and others such as transcription activator-like effector nucleases (TALENs), and zinc-finger nucleases (ZFNs) are the most successful technologies in editing the genome.

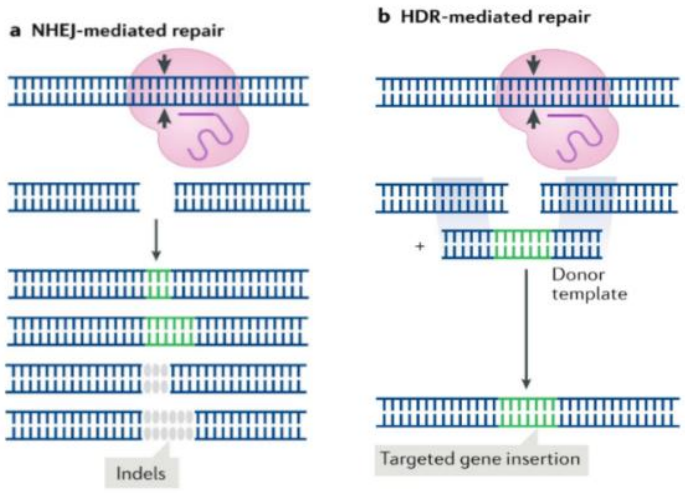

Figure 12. Mammalian reparation mechanisms after DNA DSB. A: NHEJ-mediated repair induces small indels which may lead to mRNA degradation or truncated protein. B: HDR resulting in a targeted integration using a DNA template. Adapted image from Pickar-O. A. *et al*.[66]

1.4.2. RNA interference (RNAi) and short hairpin RNA (shRNA)

RNAi, also known as post-transcriptional gene silencing (PTGS), is a biological process by which RNA molecules can silence the expression of a targeted gene with high selectivity and specificity[70]. RNAi presents as a valuable genome-editing tool for personalised cancer therapy as the RNAi gene silencing machinery can be hijacked to regulate the expression of genes of interest.

This gene-silencing process is controlled by the RNA-induced silencing complex (RISC). RISC can be triggered with the introduction of a small double-stranded fragment of RNA is loaded into the RISC. This complex separates the two strands of the siRNA, one of the strands will serve as a guide for cleavage in a targeted mRNA sequence homologous to the strand. The endonuclease Argonaut (Ago) is responsible for slicing of the targeted mRNA sequence, and thus, the targeted gene silencing[71](Figure 13).
Endogenously, the ribonuclease Dicer produces the siRNA by cutting a long double-stranded RNA into a precise 22-25 nucleotide sequence with a dinucleotide overhang in the 3´end and a monophosphate group in the 5´end to allow the recognition by RISC.

To apply this natural process in in vitro targeted cancer research, we can use two different types of molecules: the chemically synthesised siRNA or the vector-based short hairpin RNA (shRNA). The shRNA, unlike siRNA, are synthetized in the nucleus of the cell and then transported into the cytoplasm. SiRNAs and shRNAs need to be delivered into the cell. To do so, virus-based delivery systems (e.g., lentiviral transduction) and non-viral delivery systems (e.g., chemical modification of siRNA, liposome formulation) are used[71]. For shRNA, it is common to use viral-delivery systems, as they offer a stable and effective integration of exogenous DNA and a high transfection affinity.

The lentivirus is a type of retrovirus that is widely used in as gene-delivery system in the research field. Lentiviruses use the host cellular machinery to amplify and package their genetic material[72]. The lentivirus shRNA knockdown vector system is a high-efficient method for permanently knocking down the expression of a target gene in a wide variety of

mammalian cells. However, it has some safety concerns as lentivirus have the capability of infecting primary cells and their manipulation demands a complex technical procedure.

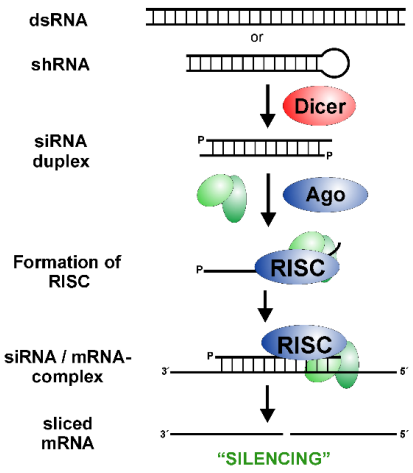

Figure 13. Graphic representation of the gene-silencing process controlled by RISC[73].

1.5. Objectives and strategy of this project

1.5.1. Previous results

In the Unit of research of animal cell biology (URBC), previously to the start of this project, a genome-wide CRISPR-Cas9 knockout (GeCKO) screening was performed. This screening was done on a GBM cell line upon a combined exposure to X-ray irradiation and TMZ in vitro to determine which genes are implicated in the resistance to GBM treatment.

The GeCKO screening was performed under the guidance of the protocol published in Nature (2017) from Joung et al.[74]. In the figure 14 is presented a diagram of the protocol used in this screen.

To perform the knockout screening, they used the GeCKO v2 Human CRISPR knockout pooled library from Addgene, which is a pooled library of sgRNAs targeting 19050 human genes. To ensure the specificity and efficiency of the screen, each gene is targeted by 6 different sgRNAs. As controls, 1000 non-targeting sgRNA are included.

After amplification of the GeCKO v2 libraries, the lentiviral pooled sgRNA plasmid library was transfected into HEK293T cells to obtain the lentiviral particles. Thereafter, U87 cells, which is a human GBM cell line, were transduced with the lentiviral library at a multiplicity of infection (MOI) of 0.3 to ensure that most cells received only one stably integrated sgRNA.

After one week of selection with puromycin (2 µg/ml), the U87 cells were treated with TMZ at a final concentration of 200 µM together with an X-ray exposure of 7 Gy every two days for 2 weeks.
Subsequently, the genomic DNA was harvested and the sgRNA region was amplified in a 2-step PCR and deep-sequenced. The results were analysed with the MAGeCK computational tool to identify positively or negatively selected sgRNA/genes. Therefore, the results from the genome-wide CRIPSR-cas9 KO screening were subdivided into two categories: the genes/sgRNA that are positively enriched, which means that they may contribute to cell

treatment-resistance pathways and genes that are negatively enriched, which may contribute to the cell sensitivity to a treatment or are considered as essential genes.

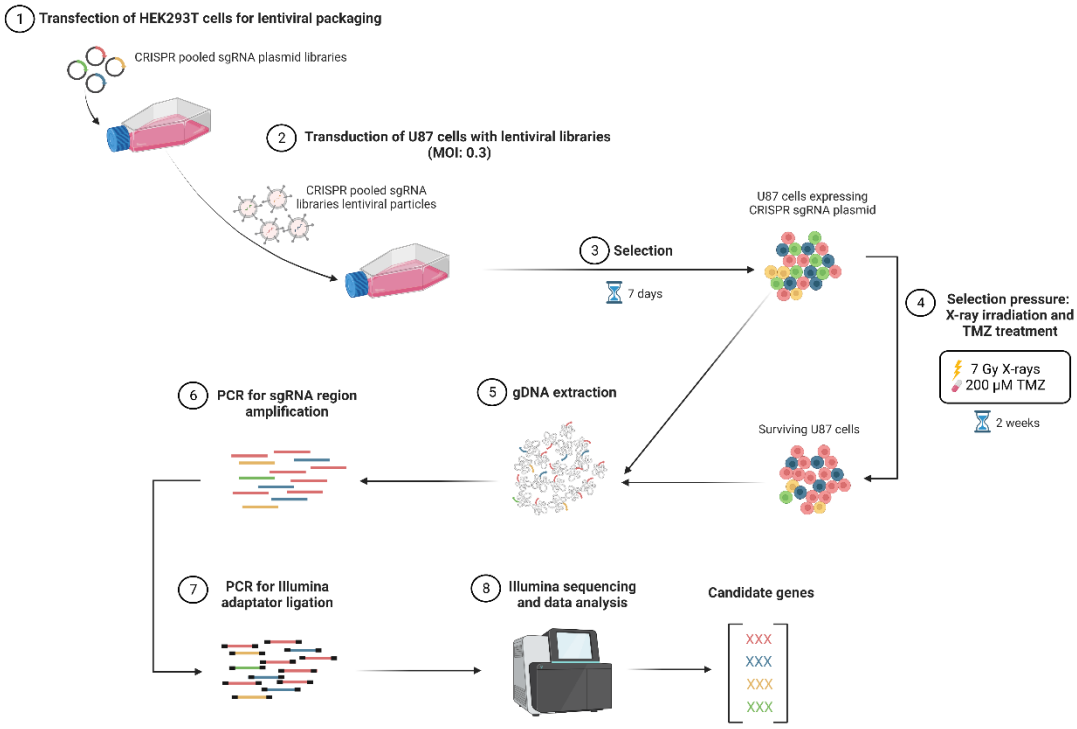

Figure 14. Explanatory diagram of the GeCKO screening performed in U87 cells. This figure was made with Biorender.

Since the results showed no significant positive-enriched genes upon GBM treatment, it was decided to shift the approach of this project to study the sensitivity to GBM treatment. Among the negatively enriched genes, there were multiple genes coding for TRAPP complex subunits (e.g., TRAPPC1, TRAPPC4, TRAPPC8, TRAPPC2L). This, together with the fact that the intracellular trafficking pathways were also significantly negatively enriched, led us to study the role of TRAPP complexes in the sensitivity to GBM cell treatment.

1.5.2. Objective and experimental strategy

In this project, the main goal is to study the potential implication of TRAPP complexes in the sensitivity to treatment of U87 cells, a GBM cell line.

Initially, the strategy was based on performing the knockout of 3 TRAPPC genes (TRAPPC1, TRAPPC4, TRAPPC8) in a U87 cell line using the lentiCRISPRv2 plasmid. During the development of this project, we also developed another approach by performing the knockdown of the same TRAPPC genes, together with TRAPPC2L in a U87 cell line using shRNA. Both experimental strategies are described in figure 15.

The two strategies can be divided in three phases. The first phase happens differently in each strategy but the second and the third phases follow the same protocols.
The knockout strategy (Figure 15A, upper panel) started with the digestion of a small sequence of the Cas9-containing plasmid vector, LentiCRISPRv2 puro, to which we subsequently cloned the sgRNA of interest into it. After the recombination of the plasmid, it was

transformed into Stbl3 bacteria for amplification purposes, followed by purification and Sanger sequencing to confirm the success of the cloning steps.

The knockdown strategy (Figure 15B, upper panel) started with the transformation of the shRNA lentiviral vector into Stbl3 bacteria for amplification purposes, followed by purification and Sanger sequencing to confirm the success of the cloning steps.
The second phase, common for both strategies (Figure 15A, 15B, lower panel), consisted in inducing the gene knockout/knockdown in U87 cells. To do so, we used lentivirus as delivery system, for which we had to perform two necessary steps, the lentiviral transfection and posterior transduction. Lentiviral transfection was performed in HEK293T cells, in which step three different plasmids were given to HEK293T: lentiviral packaging vector, lentiviral envelope vector and the Cas9-lentiviral transfer plasmid, encoding the sgRNA of interest. The lentivirus was assembled by HEK293T cells and then collected from the supernatant. They were then transduced into U87 cells at a low MOI (MOI<0.5). Posterior to transduction, there was a selection period of 7 days with puromycin to select the knockout clones.

The third phase is the validation of the knockout/knockdown, which have been done at mRNA and protein levels with a RT-qPCR and Western Blot, respectively. Additionally, we evaluated the cell viability after knockout/knockdown with a proliferation assay.

After validating the targeted gene knockout/knockdown, we assessed the sensitivity to treatment with a clonogenic assay after exposing the lentiviral transduced cells to concomitant TMZ-based chemotherapy and radiotherapy.

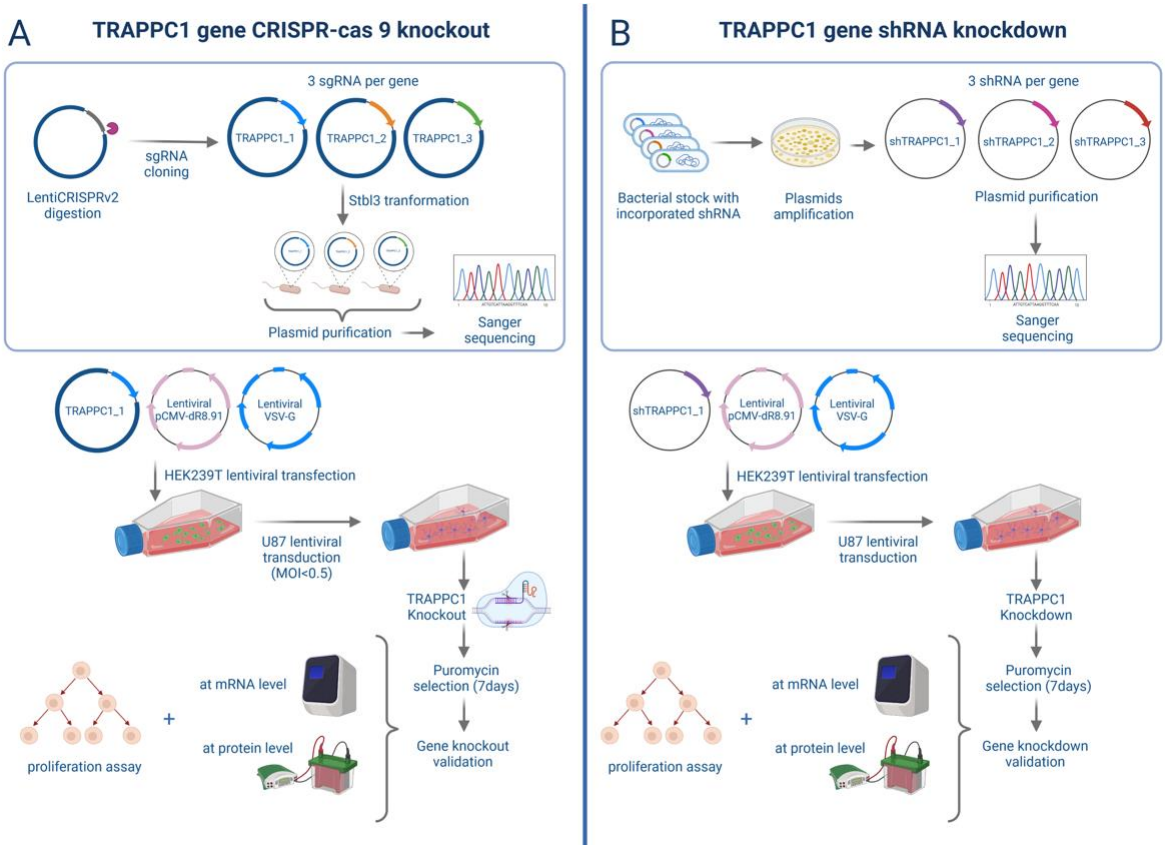

Figure 15. Explanatory diagram of the strategies followed in this project. A: Diagram illustrating the gene knockout process. (A, upper quadrant): Cloning of sgRNA into the lentiviral plasmid, Stbl3 bacteria transformation and plasmid purification followed by sanger sequencing as cloning validation. B: Diagram illustrating the gene knockdown process. (B, upper quadrant): amplification of the bacterial plasmids containing the shRNA of interest and sanger sequencing to ensure that we work with the right sequence. The validation of the gene knockout coincides with the validation for the gene knockdown. This image was made with Biorender.

2. Material and Methods

Cell culture

HEK293T cells

HEK293T cells were cultured into 75 cm^2 cell culture flasks with 15 mL of Dulbecco's Modified Eagle Medium (DMEM) (Thermo Fisher, 31885023) supplemented with 10 % of Fetal Bovine Serum (FBS) and incubated at 37ºC with 5 % of CO_2. Cells were sub-cultured every 3-4 days.

U87 cells

U87 glioblastoma cells were cultured into 75 cm^2 cell culture flasks with 15 mL of Minimum Essential Medium (MEM) (Thermo Fisher, 42360024) supplemented with 10 % of FBS, 1 % of pyruvate (Thermo Fisher, 11360039), 1 % of antibiotic mix of Penicillin-Streptomycin (Thermo Fisher, 15140122) and 1 % of non-essential amino acids (Neaa) (Thermo Fisher, 11140035) and incubated at 37ºC with 5 % of CO_2. Cells were sub-cultured every 3-4 days.

Cloning of sgRNA

The cloning of all TRAPPC-sgRNAs and NT-sgRNAs (table 1) into the lentiCRISPRv2 plasmid was made following the Zhang Lab instructions[75].

Lentiviral plasmid digestion

The lentiCRISPRv2 plasmid (Addgene, 52961) was digested and dephosphorylated using the BsmBI restriction enzyme site and the thermosensitive alkaline phosphatase, respectively. To do so, a sample mix was prepared with a final volume of 60 µL, containing 5 µg of the lentiCRISPRv2 plasmid, 3 µL of the FastDigest BsmBI (Thermo Fisher, FD0454), 3 µL of the FastAP (Thermo Fisher, EF0651), 6 µL of the 10X FastDigest buffer (Thermo Fisher, B64), 0.6 µL of 100 mM DTT (freshly prepared) and ddH_2O. Digestion mix was incubated at 37°C for 30 minutes.

Subsequently, digestion mix was run into a 0.6% agarose gel with 20 µL of ethidium bromide (Sigma Aldrich, 15585011). After migration, digested lentiCRISPRv2 plasmid was extracted by cutting the gel and purified with the Macherey-Nagel DNA purification kit following the manufacturer instructions.

Oligo annealing

Before the ligation step, phosphorylation and annealing of 2 complementary oligos forming the sgRNA was performed with T4 polynucleotide kinase via thermocycler using the following parameters: 30 min at 27ºC, 5 min at 95ºC and ramp down to 25ºC at 5ºC/min.

Annealing mix was prepared in a final volume of 10 µL per oligo pairs, containing each oligo at 100 µM, 10X T4 ligation buffer (NEB), ddH_2O and T4 PNK (NEB, M0201S)
Once the annealing was finished, the annealed oligos were diluted at 1:100 into sterile water for the ligation step.

Ligation of sgRNAs

The set-up of ligation reaction was done by adding 1 µL of the diluted oligo pairs to the BsmBI digested mix (50 ng) together with 5 µL of 2x Quick ligase buffer (NEB) and ddH_2O.

Subsequently, 1 µL of Quick Ligase (NEB, M2200S) enzyme was added to the mix and then incubated at room temperature for 1h.

Gene-sgRNA	Forward (5'→3')	Reverse (5'→3')
TRAPPC1-1	CACCGCAGGAGTATAAGCTGATGTA	AAACTACATCAGCTTATACTCCTGC
TRAPPC1-2	CACCGTGTGTCTGCACTACAGCGAA	AAACTTCGCTGTAGTGCAGACACAC
TRAPPC1-3	CACCGCACTGACCGCACTGTAGATG	AAACCATCTACAGTGCGGTCAGTGC
TRAPPC4-1	CACCGGTACACGGCCGACGGGAAAG	AAACCTTTCCCGTCGGCCGTGTACC
TRAPPC4-2	CACCGGGGGACTTACGAGTGGAACA	AAACTGTTCCACTCGTAAGTCCCCC
TRAPPC4-3	CACCGGATGCATACCTGTCAGTGTC	AAACGACACTGACAGGTATGCATCC
TRAPPC8-1	CACCGAAAGGATACATGCTAAATAG	AAACCTATTTAGCATGTATCCTTTC
TRAPPC8-2	CACCGGTGATTATTCCTACCCCAAG	AAACCTTGGGGTAGGAATAATCACC
TRAPPC8-3	CACCGTCTTCAGTCGATGCCAGCAT	AAACATGCTGGCATCGACTGAAGAC
NT-1	CACCGGCGTGCGTCCCGGGTTACCC	AAACGGGTAACCCGGGACGCACGCC
NT-2	CACCGTGAGGATCATGTCGAGCGCC	AAACGGCGCTCGACATGATCCTCAC

Table 1. Designed oligo pairs for each sgRNA by adding overhangs matching the restriction sites (highlighted in red)

Bacterial transformation

DNA ligated vectors were transformed into One Shot Stbl3 Chemically Competent bacteria (InvitroGen, C737303) at a ratio of 1:10. The process involved the incubation of the bacteria with 50 ng of the ligated vector on ice for 30 minutes, a subsequent heat shock at 42 ºC for 45 seconds and finally 2 min on ice. Subsequently, samples were supplemented with 250 µL of *E. coli* S.O.C. medium (Invitrogen, 15544034) and incubated during 1h at 37 ºC in a shaking incubator. Finally, bacteria were plated on Petri dishes containing Luria-Bertani (LB) agar (Roth GmbH, X965.1) and 1:1000 ratio of ampicillin (Sigma Aldrich, A9393) as a selection pressure. Petri dishes were incubated upside down overnight at 37ºC.

PCR in colony

Following the bacterial transformation, each bacterial clone was transferred into a new Petri dish and incubated at 37ºC during 6h for stock reasons. In parallel, for each bacterial clone, we performed a PCR using the Gotaq2 DNA polymerase (Promega, M7841) aiming to amplify the sequence containing the sgRNA and thus, validating the ligation steps. The PCR mix contained two verification primers.

PCR settings: 1x 94ºC (2 min) cycle x 30, 94ºC for 30 seconds, 55ºC for 30 seconds, 72ºC 1:30 min, 1x 72ºC (5 min), and end temperature of 4ºC.

Purification and sequencing of DNA

The product of the PCR in colony was purified with the Macherey-Nagel DNA purification kit and prepared for Sanger Sequencing following Eurofins kit instructions. We used the forward primer as the sequencing starting point and a final plasmid concentration of 15 µg based on the size of the plasmids of interest and the manufacturer´s instructions.

Mini prep and maxi prep

Mini prep and maxi prep were performed on bacterial clones with successful lentiCRISPRv2 plasmid cloning and on bacterial clones carrying pLKO.1-puro TRC shRNA lentiviral vectors (Sigma Aldrich). This step aimed to amplify the plasmids of interest for posterior use.

The mini prep was performed by incubating one bacterial clone supplemented with 2 mL of LB media (Roth GmbH, X964.2) and ampicillin (Sigma Aldrich, A9393) at a ratio of 1:1000 during 5-6 hours at 37ºC in a shaking incubator. After approximately 5 hours, maxi prep was launched. To do so, we added 1 mL of the bacterial mini prep sample into a 500 mL-sterilized Erlenmeyer, which was supplemented with 250 mL of LB media (Roth GmbH, X964.2) and ampicillin (Sigma Aldrich, A9393) at a ratio of 1:1000. Maxi-prep samples were then incubated overnight at 37°C in the shaking incubator.
Subsequently to the maxi prep, the samples were purified using the InvitroGen PureLink kit to obtain the amplified plasmids of interest. The end product was diluted with nuclease free water and stored at -20ºC.

Transfection of HEK293T cells

HEK293T cells were transfected at a 70 % confluence in T75 flasks. Transfection with the plasmid of interest was performed at a ratio of 1.5:2:1 by adding pCMV-dR8.91 (Addgene, 8455) as packaging lentiviral plasmid and VSV-G (Addgene, 8454) as enveloping lentiviral plasmid together with the plasmid of interest. The reagent mix was prepared based on plasmid concentrations (Table 2).
All three plasmids were mixed in an Eppendorf containing sterile water according to Table 2. Subsequently, 2.5 M of $CaCl_2$ (sigma-Aldrich; C7902) was added and the mix was vortexed.

Previously to the experiment, 250 mL of 2x phosphate-containing 4-(2-hydroxyethyl)-1-piperazineethanesulfonic acid-buffered saline (HeBS) solution was prepared. HeBS was added dropwise to the lentiviral plasmid mix and samples were vortexed immediately for 5 seconds.
After an incubation time of 30 minutes at room temperature, the mix was added dropwise to HEK293T cells flask. The control for transfection was a plasmid encoding Green Fluorescent protein (GFP) (Addgene, 19070).

Cells were incubated at 37ºC with 5 % of CO_2. 24h after transfection, HEK293T cell medium was replaced by fresh medium.

Flask	Surface (cm^3)	ADNc (µg)	VSVG (µg)	Delta 8.9 (µg)	$CaCl_2$ (µL)	Water (µL)	HeBS (µL)
T25	25	1.35	0.7	1	28.5	180	200
T75	75	4	2	3	85	540	600

Table 2. Quantities of reagents used in the lentiviral transfection according to the type of flask.

Lentiviral particle titer by qPCR

Lentiviral vector RNA was titered by qPCR using a qPCR Lentivector Titration Kit (Applied Biological Materials) according to the manufacturers' protocol[76]. Briefly, samples were diluted 1:100, 1:1000, 1:10000 and 1:100000 in phosphate-buffered saline prior to lysis to calculate the dilution factor. Viral lysis was performed using 2 µl of diluted supernatant added to 18 µl Virus Lysis Buffer provided. The mixture was incubated for 3 minutes at room temperature to obtain the viral lysate.

The RT-qPCR program was performed following RT-qPCR parameters: 1 cycle of reverse transcription was performed at 42°C for 20 minutes, 1 cycle of enzymatic activation was performed at 95°C for 10 minutes, 35 cycles (denaturation was performed at 95°C for 15 seconds, followed by cycles of annealing/extension at 60 °C for 1 minute). Sample titers were calculated from C_t (cycle threshold) values using the following equation:

Titer of viral lysate = $5 \times 10^7/2^{3(Ctx-Ct1)/(Ct2-Ct1)}$ * (dilution factor) where C_{tx} equals the average of three C_t sample values, C_{t1} equals the average of three C_t values from Standard 1 values and C_{t2} equals the average of three C_t values from Standard 2.

Transduction of U87 cells

U87 cells were transduced at 70 % confluency per T25 flask. First, the lentiviral supernatant of the transfected HEK293T cells was collected 48h post-transfection and filtered using a 0.2 µm filter (Sarstedt AG &Co, 83.1826.001) and a 5 mL syringe. Secondly, the medium of the U87 cells was replaced by the filtered lentiviral supernatant.

For the knockout cells, transduction was performed at a multiplicity of infection (MOI) < 0.5 with polybrene (5 µg/mL; Sigma Aldrich, TR-1003) whereas for the knockdown cells, the total supernatant collected was used for U87 cell transduction.

Cells were transduced in triplicates and then were incubated at 37ºC with 5 % of CO_2. After 24h, the medium containing the lentivirus was removed and replaced by fresh U87 cell medium.

Transduction selection was performed during a 7-day period with puromycin (2 µg/ml; Invivogen, QLL-41-02) where puromycin was added every 2 days. Untransduced (UT) U87 cells were used as killing control of puromycin.

Cell proliferation assay

For the knockout samples and their respective control sample, $3x10^5$ U87 cells were seeded into 25 cm^2 flasks. For the knockdown samples and their respective control sample, the equivalent number of 1.15 $x10^5$ U87 cells were seeded into 6-well plates. After 24h, cell numbers were assessed manually using a Neubauer's chamber and are presented in the results as Time 0 (t0), Time 24 (t24), Time 48 (t48) and Time 72 (t72) hours. First, we removed the supernatant and rinsed the U87 cells with pre-heated PBS at 37°C. Secondly, we performed the trypsinization of the U87 cells with Trypsin-EDTA and incubated them for 2 minutes at 37°C. Subsequently, cells were collected with medium into a falcon tube and centrifuged for 5 min at 1 rpm. Following this step, supernatant was removed and cells were resuspended with the same small volume of pre-heated medium. The number of cells in each cell suspension was counted 8 times and the average of the counts was calculated. In the end, we calculated the growth percentage of each condition at each time (assuming t0 as 100%) and normalised the proliferation of each condition based on t0.

RNA cell extraction

$8x10^5$ cells were seeded into 25 cm^2 flasks. After 24h, total cell RNA extraction was performed at room temperature using the kit Promega ReliaPrep in a free RNAse environment. Briefly, the supernatant of the T75 flasks was removed and then the cells were rinsed with PBS. After removing the PBS, freshly prepared lysis buffer with thioglycerol (1:5) was added. Note that for $5x10^6$-$2x10^6$ cells, 250 µL of lysis mix is added. Then, the surface of the flask was scratched, and lysed cells were collected in an Eppendorf microtube. At this step, usually

samples were frozen at -80°C and 1-2 days after, RNA content from the cells was purified using the ReliaPrep RNA Miniprep system kit´s minicolumns and following manufacturer´s instructions. The concentration of the RNA samples was assessed with the Implen NanoPhotometer™ N60 c spectrophotometer.

Precedent to the reverse transcription, RNA samples were diluted with free RNAse H_2O considering that the desired final cDNA quantity for the qPCR was 1 µg and the final volume was 12 µL. Then, to denaturalise the RNA chains, diluted RNA samples were incubated 5 min at 70 °C in a thermocycler.

For each sample, reverse transcription was carried out using the complete reverse transcription kit from Promega, containing 2 µL of the reverse transcriptase enzyme mix, 2 µL of the master mix with Oligo-dT and 2 µL of Random Primers. Described reagents were added together with 2 µL of free RNAse H_2O to the denatured RNA product considering a final volume of 20 µL. Then, reverse transcription was run in the thermocycler with the following parameters: 5 min at 25°C, 60 min at 42 °C, 15min at 70 °C and the end temperature of 4 °C. Obtained cDNA samples were stored at -20 °C.

Primer design and RT-qPCR

All primers used for qPCR were designed via BLAST software and or GETPRIME software. To ensure the correct annealing of the primers to the sequence of interest, we ordered different primers (Table 3) and tested their efficiencies. Briefly, we diluted the cDNA 1:10, 1:100, 1:1000, 1:10000 and 1:100000 and we used each primer pair at two different concentrations, 3 µM and 6 µM. Quantitative real-time PCR was performed with the Applied Biosystems StepOne Real-Time PCR system. Results were analysed and compared based on their melting curve and efficiency percentage.

Gene	Forward (5'→3')	Reverse (5'→3')	Source
TRAPPC1	GTAACTCTTGACGGGCACT	TACTCCTCCTCCTTGGGAATC	BLAST
TRAPPC4	TGGAATAGATTCTCTTCTCCG	AGAGCTCACACCTGATAG	GETPRIME
TRAPPC8	ACATCAGTCCCACTACTC	GAAATTCATGATCCAATGCTGG	BLAST
TRAPPC2L	TTGCCAAGGAGAATTACCC	GATCTTCTCATCCACCACG	GETPRIME

Table 3. Primer pairs designed with BLAST and GETPRIME software for targeting TRAPPC mRNA

Quantitative real-time PCR was conducted with Applied Biosystems StepOne Real-Time PCR system. Samples of cDNA were diluted (1:100) and 4 µL of each sample were mixed with 10 µL Taq® qPCR Master mix reagent (Promega, A600A), 2 µL of each primer (3 µM; IDT) and 1.8 µL of nuclease free water with 0.2 µL of CXR (Carboxy-X-Rhodamine; Promega, C541A). Relative glyceraldehyde-3-phosphate dehydrogenase (GAPDH) expression was used for gene expression normalisation. Relative mRNA expression levels were quantified based on the obtained Ct with the following formulas:

ΔCt = Ct gene of interest- Ct GAPDH; $\Delta\Delta Ct = \Delta Ct$ sample 1 - ΔCt GAPDH; ΔCt GAPDH is set to the value of 1. Relative quantification (RQ) = $2^{-\Delta\Delta Ct}$; RQ is the fold change compared to GAPDH.

Protein cell extraction and Western Blot

$8x10^5$ U87 knockout cells were seeded into 25 cm^2 flasks. 24h later, protein extraction was performed on ice using lysis buffer [50 mM of tris-HCl (pH 7.4), 150 mM NaCl, 1 mM Ethylenediaminetetraacetic acid (EDTA), 1% NP40 mixed with phosphatase inhibitor (PIB) (1:25)]. Protein concentration was determined with a Pierce 660 nm Protein assay. Quantified protein extracts were separated by SDS-page with a 15% or 8% acrylamide separator gels to identify the protein abundance of TRAPPC1 and Cas9, respectively. To prepare the different gels we used water, separation buffer or stacking buffer, acrylamide 30%, ammonium persulfate (APS) 10% and TEMED (Table 4).

	3,75%		15%	8%
Stacking buffer	1.25 mL	Separation buffer	1.2 mL	1.2mL
Acrylamide	0.5 mL	Acrylamide	2.5 mL	1.3 mL
Water	2.25 mL	Water	1.3 mL	2.5 mL
APS 10%	50 µL	APS 10%	25 µL	25 µL
TEMED	5 µL	TEMED	5 µL	5 µL

Table 4. Quantities and materials used for the acrylamide gel preparation for western blotting

After gel preparation, sample proteins were prepared based on the concentration results of the Pierce 660nm protein assay and the final volume per well of 30 µL. Bromophenol blue was diluted 5x in the total amount (30:5 = 6µL) per sample. Proteins were loaded together with 1 µL of protein ladder (Bio-Rad, 1610373) and electrophoresis was performed with the following parameters: 200 V, 400 mA for 45 minutes. Once proteins finished migration, they were transferred onto a polyvinylidene fluoride microporous membrane (PVDF) in a semi-liquid transfer. After transfer, membrane was blocked for one hour with protein-free blocking buffer (PBS) (LI-COR, 927-90001). Subsequently, membrane was probed with the appropriate primary antibodies. To identify TRAPPC1 relative protein abundance, we used a mouse monoclonal anti-TRAPPC1 IgG antibody (1:1000; Santa Cruz Biotechnologies, 377024). To identify Cas9 relative protein abundance, a mouse monoclonal anti-CRISPRCas9 IgG antibody (1:1000; BioLegend, 844302) weas used. After incubating the membrane on the agitator at 4°C overnight, the membranes were probed with the secondary antibody, a goat anti-mouse IgG antibody (1:10000) for 1h. In both membranes, GAPDH was used as loading control to normalise the relative abundance of both proteins. To do that, both membranes were probed with mouse monoclonal anti-GAPDH IgM antibody (1:20000; Sigma Aldrich, G8795). Membrane scanning and fluorescence quantification were performed with Amersham Typhoon Biomolecular Imager at 700 nm.

U87 cell treatment

$8x10^5$ U87 (untransduced) cells were seeded in four 25 cm^2 flasks. Treatment was divided in 4 conditions: 1) untreated, 2) treated with TMZ and X-rays, 3) treated with TMZ and 4) treated with X-rays. Temozolomide (TMZ) (Sigma Aldrich, T2577) was added at a final concentration of 200 µM half an hour before X-rays exposure. Cells were treated three times a week, every 2 days at approximately the same time of the day. Medium was removed and replaced each time.

For the untreated cells, dimethyl sulphoxide (DMSO) (Carl Roth, A994.2) was added equally to the volume added for TMZ. Cells were exposed to a total dose of 7 Gy using a X-RAD 225 XL cabinet irradiator.

Clonogenic assay

2000 U87 (untransduced) cells were seeded in in triplicates in 15 cm^3 petri dishes after treatment.
Knockdown U87 cells were seeded in triplicates in 15 cm^3 petri dishes with different densities for each independent cell population: 1) 500 cells, 2) 1000 cells, 3) 2000 cells. Treatment was divided in 3 conditions: 1) untreated, 2) treated with 25µM TMZ and 2 Gy and 3) treated with 25 µM TMZ and 4 Gy. Treatment was applied 24 h after cell seeding and left until clonogenic assay was stopped. Cells were exposed to TMZ half an hour before X-rays irradiation.
Cells were incubated for 10-15 days at 37 ºC with 5 % of CO_2.

Clonogenic assay was stopped 10-14 days after cell treatment by fixating the cells with paraformaldehyde (PFA) for 5 min and after rinsing the colonies were stained with crystal violet.

Crystal violet was prepared with 1g crystal violet, 10 mL of ethanol and 2490 mL of ddH_2O. Colonies were counted and based on the calculated plating efficiency (PE), surviving fraction (SF) was calculated as followed:

For the untreated cells:
PE= (number of counted colonies/number of cells seeded)
SF= PE/PE = 1

For the treated cells:
PE= (number of counted colonies/number of cells seeded)
SF= PE/PE of untreated cells

Beta-galactosidase assay

U87 cells were seeded at a low density (10,000 cells/well) in a 6 well-plate (Corning, 3516), with 3 replicates for each condition.

After 24h hours, cells were rinsed twice with PBS before fixating them. The fixation solution contained formaldehyde 2% (Merck, 4005) and glutaraldehyde 0.2% (Fluka, G6257), and was left in contact with the cells for 5 minutes at room temperature. Then, cells were rinsed twice with PBS and each well was incubated with 2 mL of the staining solution for 16 hours at 37°C without CO_2.

Staining solution was made of 5-bromo-4-chloro-3-indolyl-β-D-galactoside (X-gal; Thermo Scientific, R0404), N,N dimethylformamide (Janssen Chimica, C_3H_7NO), pH 5.8 phosphate buffer containing NaH_2PO_4 (Merck, 6346) and Na_2HPO_4 0.1 M (Merck 6580), potassium ferrocyanide 100 mM ($K_4Fe(CN)_6.3H_2O$, 1.04934.0100, Merck), potassium ferricyanide 100 mM ($K_3Fe(CN)_6$, 1.04973.0100, Merck), sodium chloride 2.5 M (NaCl, 6404, Merck), magnesium chloride 1 M ($MgCl_2$, 1.05833.0250, Merck) and distilled water.

After 16 hours, staining solution was removed, and each well was rinsed twice with 2 mL of non-sterile PBS and then once with 2 mL of methanol (CH_4O, 8388.5, Carl Roth).

The proportion of SA-βgal-positive cells was determined by counting at least 200 cells per well.

Hypoxia

$8x10^5$ U87 cells were seeded in 25 cm^2 flasks. After 24h, U87 cells medium was replaced by 4 mL of CO_2 independent medium (Thermo Fischer Scientific, 18045-054), both for hypoxic and normoxic conditions. Hypoxic environment was created with an environment of 99% of N_2 and less than 1% of O_2. Cells were incubated at 37°C for 24, 48 and 72 hours.

Statistical analysis

All statistical analyses in this study have been performed with GraphPad prism.

3. Results

3.1. CRISPR-Cas9 induced knockout

As explained in the "Objectives" section, two approaches were used to invalidate the expression of the genes of interest: CRIPSR/cas9 and shRNA technologies. These approaches were performed in U87 cells. U87 is a human glioblastoma astrocytoma cell line, which is commonly used in cancer research. It derives from a malignant glioma from a female patient. This cell line has a mutation in the hTERT promoter and is IDH1 wildtype, among others.

The knockout of the subunits of TRAPP complexes identified in the previous GeCKO screening was performed using the CRISPR-Cas9 technology. These genes were TRAPPC1, TRAPPC4 and TRAPPC8.

Target guide sequence cloning

The nuclease Cas9 together with a target-specific sgRNA must be delivered in the U87 cells to knock out the TRAPP gene of interest. Therefore, the first step was to clone each of the three gene-targeting sgRNAs into the lentiCRISPRv2 plasmid, which encoded the sequence of the nuclease Cas9. As experimental negative control we used a non-targeting sgRNA (NT-1), which was also cloned into a separate lentiCRISPRv2 plasmid.

To clone the sgRNAs, the lentiCRISPRv2 plasmid was first digested with the BsmBI restriction enzyme. The digestion resulted in a linearised plasmid and a ~2 kb band corresponding to the product digestion located within the enzyme restriction sites (Figure 16).

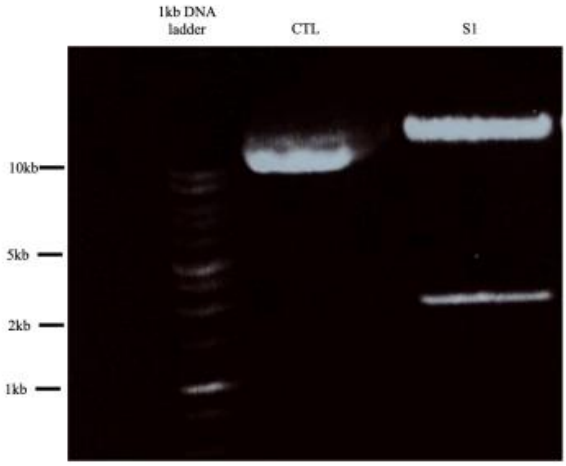

Figure 16. Digested LentiCRISPRv2 plasmid ran into an agarose gel 0.6%. Image taken after sample migration. From left to right; DNA ladder 1kb, control sample (CTL) without adding the restriction enzyme and the digested lentiCRISPRv2 plasmid (S1) with the ~ 2kb digested product band below.

After gel extraction, purification and subsequent elution, each sgRNA was ligated into the linearised plasmid. The sgRNAs were constructed by the annealing of one forward and one reverse oligonucleotide sequence designed with overhangs matching the restriction sites (Table 1).

In the next step, the ligated products were transformed into Stbl3 bacteria, which are recombination-deficient and adapted for lentiviral plasmids containing Long-Terminal Repeats (LTRs). After transformation, each bacterial colony had its sequence amplified by PCR and was subsequently sequenced by the Sanger method to verify successful cloning. The

results indicated that each target guide sequence was correctly cloned into a bacterial clone (Figure 17). The ten cloned sequences were named as TRAPPC1-1, TRAPPC1-2, TRAPPC1-3, TRAPPC4-1, TRAPPC4-2, TRAPPC4-3, TRAPPC8-1, TRAPPC8-2, TRAPPC8-3 and NT-1 as mentioned in the "Materials and Methods" section of this manuscript (Table 1).

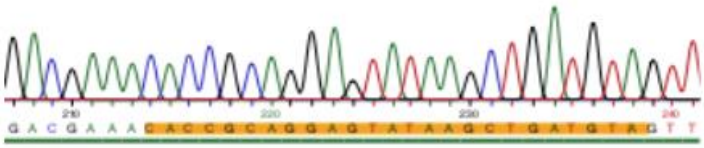

Figure 17. Sequencing results show inserted sgRNA in lentiCRISPRv2 plasmid sequence. Highlighted in yellow is the designed forward TRAPPC1-1 sgRNA sequence with the overhang CACCG at the 5' end.

Since the Sanger sequencing results indicated that all the sgRNAs of interest were correctly cloned and ligated to the vectors, amplification by miniprep and maxiprep and then DNA purification were performed to isolate the ligated vectors for U87 cell transduction.

Lentiviral transfection and U87 cell transduction

Lentiviral transfection and U87 transduction was only performed for the TRAPPC1 sgRNAs because, due to the lack of time, we did not proceed further with the knockout of TRAPPC4 and TRAPPC8 as initially planned.

Lentiviral particles were produced by the transfection of HEK293T cells with each lentiCRISPRv2 plasmid encoding one of the TRAPPC1 sgRNA of interest together with the addition of the lentiviral packaging and envelope plasmid. A plasmid encoding the GFP was used as a transfection control (Figure 18).

Subsequently to transfection, lentiviral particles were collected and transduced to the U87 cells. The aim was to perform the lentiviral transduction at a low MOI to prevent from multiple DNA cleavage within a single cell and thus avoid off-target mutagenesis. With this intention, lentiviral titers were quantified by performing a qPCR. Finally, U87 cells were transduced with the lentiviral particles enclosing the clone plasmid at a MOI of <0.5 with biological triplicates.

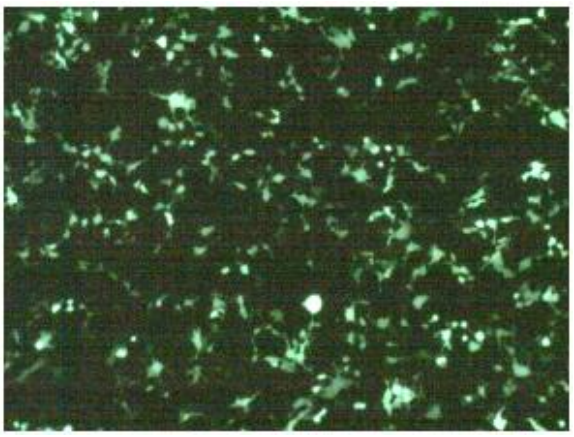

Figure 18. GFP transfected HEK293T under the epifluorescent microscope at a magnification of 10x. Green fluorescence confirms that the transfection procedure was successful.

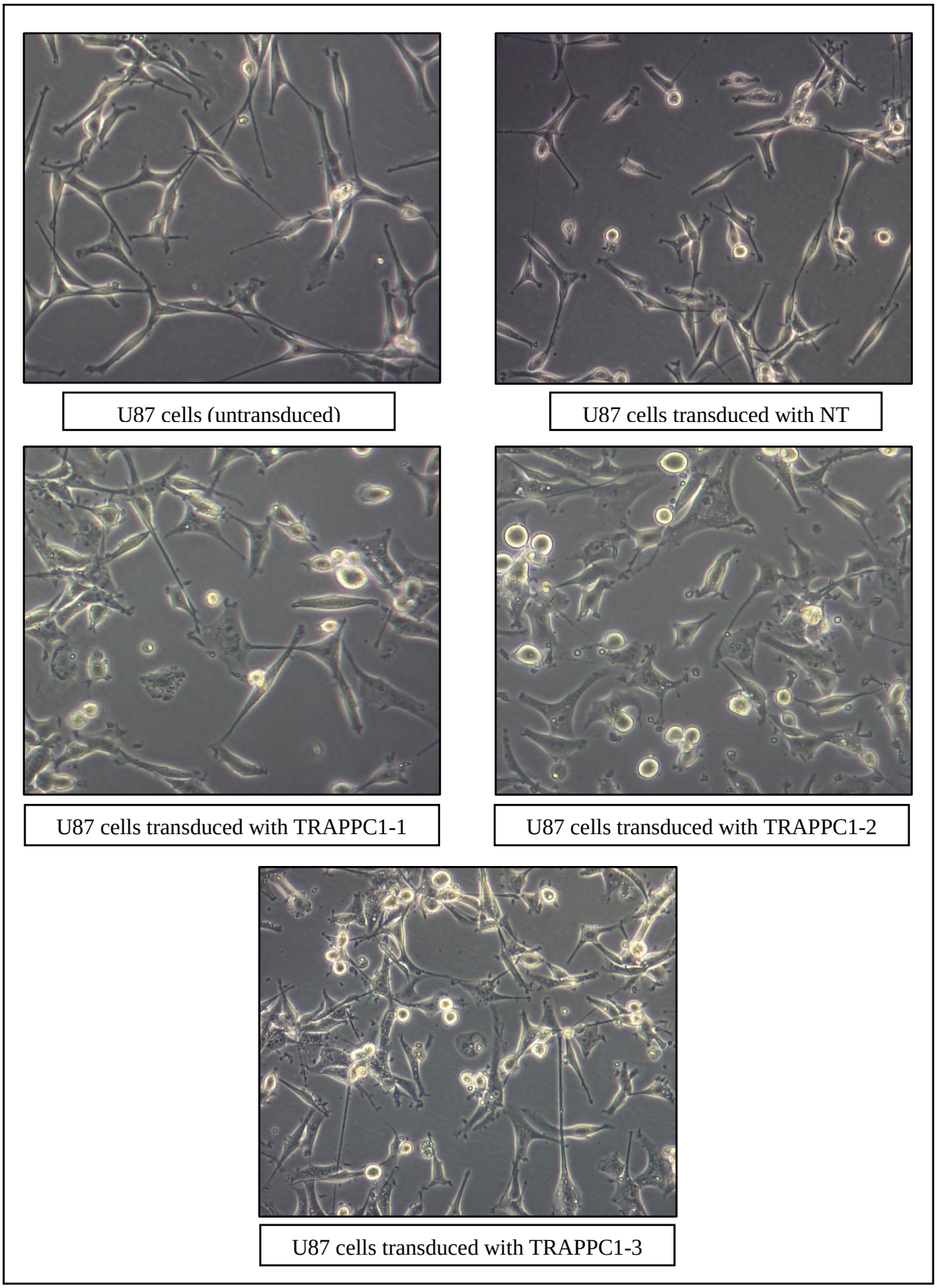

Figure 19. U87 cell morphology after transduction with TRAPPC1 sgRNAs and NT sgRNA compared to untransduced U87 cell phenotype under phase-contrast microscopy at a magnification of 10x. These images were taken two weeks after the selection period with puromycin.

Cell morphology from TRAPPC1 transduced U87 cells were compared to untransduced U87 cells to identify whether the transduction and/or the knockout affected U87 cell phenotype.

As mentioned, U87 cells are astrocytes, and therefore, their phenotype is determined by a bipolar appearance, together with the presence of multiple nuclei and giant nuclei and many intracellular vesicles/lipid droplets. The images in Figure 19 were taken two weeks after the puromycin selection since once the selection period was stopped, death of cells transduced with TRAPPC1 sgRNAs was observed. Altogether, the surviving U87 cells maintained their morphology: no differences were visible between transduced and untransduced cells.

3.2. Validation of knockout in U87 cells

3.2.1. For TRAPPC1-1, TRAPPC1-2 and TRAPPC1-3 sgRNAs

To validate the knockout for TRAPPC1, mRNA relative expression and protein abundance of TRAPPC1 were quantified by RT-qPCR and Western Blot, respectively. Results shown in this section belong to the first biological replicate for TRAPPC1 knockout with each sgRNA, so no statistical significance could be assessed. All results presented were normalised to the untransduced U87 cells condition to study the transduction effect in U87 cells.

At the mRNA level (Figure 20), the three cell populations transduced with lentiviral particles harbouring sgRNA-targeting TRAPPC1 displayed a lower relative TRAPPC1 mRNA expression than cells transduced with the negative control sgRNA NT and the wild-type U87. Additionally, in the case of the TRAPPC1- 1, and compared to TRAPPC1-2 and TRAPPC1-3, the fold change is lower, suggesting a higher decrease in the relative TRAPCC1 mRNA expression.

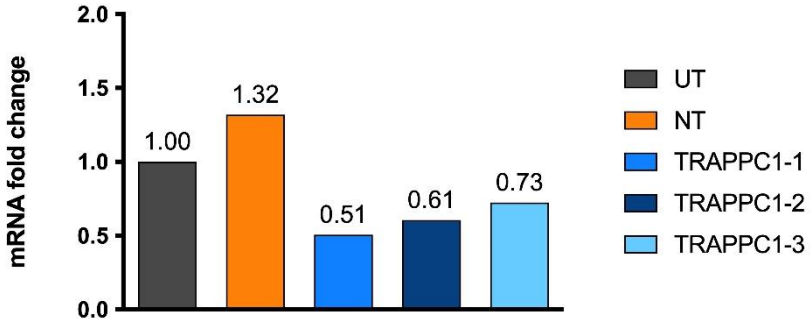

Figure 20. Relative TRAPPC1 mRNA expression in U87 cells. TRAPPC1 mRNA level of U87 cells transduced with the three TRAPPC1 sgRNA or with the NT sgRNA compared to untransduced cells (UT) assessed by RT-qPCR. GAPDH was used for gene expression normalisation.

At the protein level, protein extracts from untransduced U87 cells showed no relative abundance for protein Cas9, as we would have expected (Figure 21A, B). On the other hand, transduced cells displayed a high relative expression of the protein Cas9 (Figure 21A, B). These results indicate that U87 cells were correctly transduced with the cloned plasmids. Along with these results, we could also identify a band corresponding to TRAPPC1 protein in untransduced U87 cells and NT transduced cells (Figure 21C). However, the band is also present in the cells that were transduced with TRAPPC1-2 and TRAPPC1-3 sgRNAs. Only the cells transduced with TRAPPC1-1 sgRNA displayed a lower protein abundance of TRAPPC1, suggesting a possible partial knockout for the TRAPPC1 gene in this condition (Figure 21C, D).

Altogether, considering the mRNA and protein level results for the first biological replicate of the CRISPR-cas9 TRAPPC1 induced KO in U87 cells, we can suggest that there appears to be a partial KO for the first sgRNA, TRAPPC1-1, and that no knockout for TRAPPC1-2 and TRAPPC1-3 sgRNAs was evidenced.

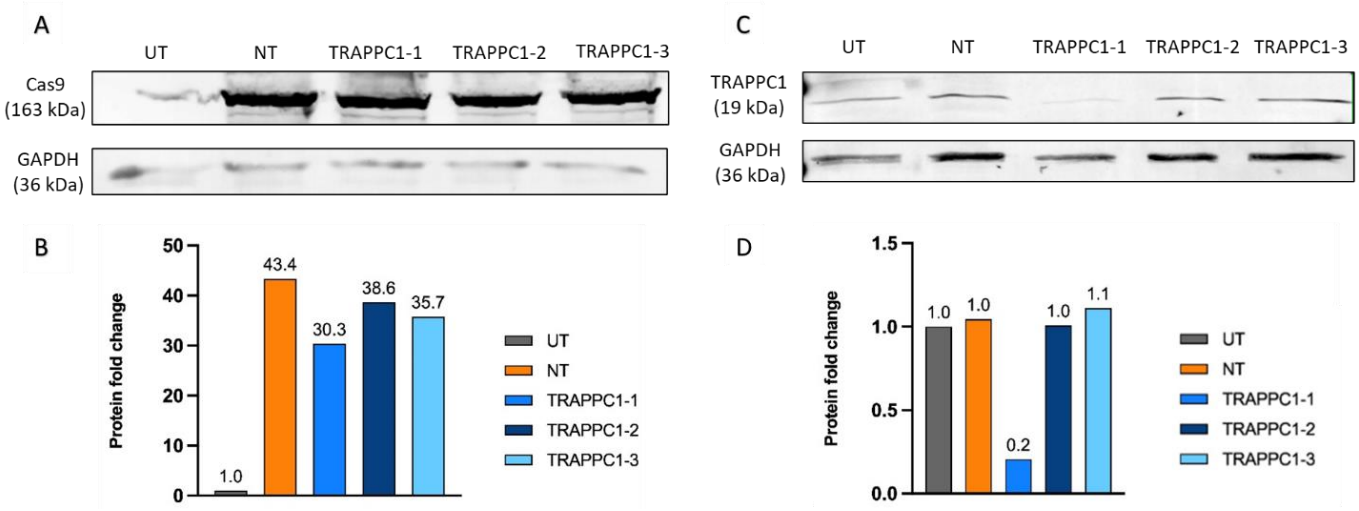

Figure 21. Left panel (A, B): Cas9 protein abundance in U87 cells transduced with TRAPPC1 sgRNA or with the NT sgRNA in comparison to untransduced cells (UT). A: Separation of protein extracts with 8% polyacrylamide gel and subsequent identification of Cas9 by western blot analysis. (Above) Band around 160 kDa, corresponds to Cas9 (163 kDa). (Below) GAPDH (36 kDa) as loading control. B: Quantification of protein fold change compared to control-untransduced sample; Right panel (C, D): TRAPPC1 protein abundance in U87 cells transduced with TRAPPC1 sgRNA or with the NT sgRNA in comparison to untransduced cells (UT). C: Separation of protein extracts with 15% polyacrylamide gel and subsequent identification with mouse monoclonal anti-TRAPPC1 IgG antibody. (Above) Band around 19kDa, corresponds to TRAPPC1. (Below) GAPDH (36 kDa) as loading control. D: Quantification of protein fold change compared to control-untransduced cells.

Besides validating the knockout, the cell proliferation rate of U87 cells after TRAPPC1 gene KO was also assessed (Figure 22). We performed a cell proliferation assay for TRAPPC1 KO U87 cells, NT transduced cells and untransduced cells. Cell counting was performed manually after cell resuspension at time 0, time 24h, time 48h and time 72h after seeding.

TRAPPC1 KO cells appeared to have a lower proliferation rate over the 72 hours of the experiment compared to NT transduced cells and untransduced cells. Among the three cloned sgRNAs, the TRAPPC1-1 cell population had the lowest cell proliferation rate. Interestingly, as we had previously observed, TRAPPC1-1 was the sgRNA giving the most efficient knockout at mRNA and protein levels.

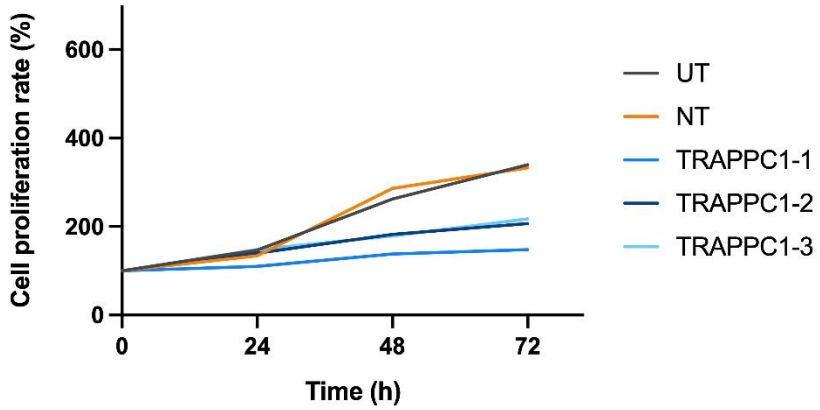

Figure 22. Effect of TRAPPC1 knockout on U87 cell proliferation. The proliferation rate of U87 cells transduced with TRAPPC1 sgRNAs or with the NT sgRNA and of untransduced cells (UT) was calculated for the first biological replicate. Actual cell numbers were counted eight times for each cell suspension of each sample at time 0, time 24h, time 48h and time 72h after seeding. Average cell counts and respective cell rate proliferation were calculated.

3.2.2. For TRAPPC1-1 sgRNA with biological replicates

Since TRAPPC1-1 sgRNA seemed to be the most efficient in inducing the TRAPPC1 gene knockout, the significance of the previous results was studied by validating the knockout induced by TRAPPC1-1 sgRNA with biological replicates. TRAPPC1 relative expression at mRNA level and relative protein abundance, with RT-qPCR and Western blot, respectively, was analysed in three different cell cultures that had been transduced independently with TRAPPC1-1 sgRNA. Results shown in this section are normalised to the untransduced U87 cells to evaluate the transduction effect in U87 cells. However, statistical analysis was performed using the actual control, NT, to study the knockout significance of TRAPPC1 in the transduced U87 cells.

At the mRNA level (Figure 23), the U87 cell population transduced with lentiviral particles harbouring sgRNA-targeting TRAPPC1-1 displayed a significant lower relative TRAPPC1 mRNA expression when compared to the U87 cell population transduced with lentiviral particles harbouring non-targeting sgRNAs (p-value of 0.0021).

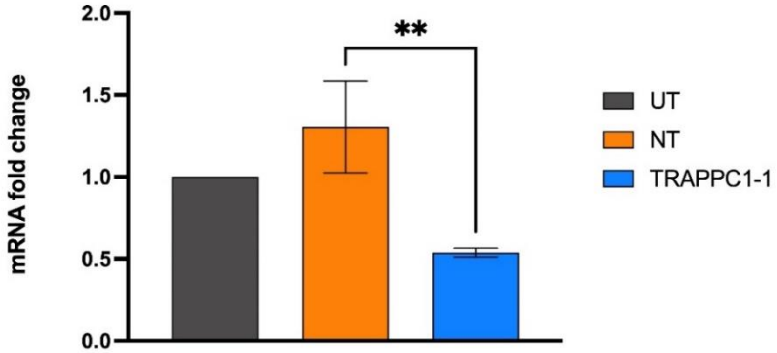

Figure 23. Relative TRAPPC1 mRNA expression in TRAPPC1-1 knockout cells. The TRAPPC1 mRNA level of U87 cells transduced with TRAPPC1-1 sgRNA or with the non-targeting (NT) sgRNA was assessed by RT-qPCR. GAPDH was used for gene expression normalization. Results are presented as means ±1SD for three independent cell populations. Significance of results was analysed with a one-way ANOVA with multiple comparisons ** p-value < 0.001).

Results at a protein level regarding the Cas9 protein abundance indicate that the U87 transduced cells was successful in all biological triplicates (Figure 24). However, GAPDH protein abundance detection was unsuccessful for the second and third replicates and thus, relative quantification for Cas9 protein was not possible. This is because an error in the secondary antibody preparation.

Regarding the detection of TRAPPC1 protein abundance, the western blot performed with the second and third biological replicates was unsuccessful. Expression of TRAPPC1 protein could not be assessed nor quantified in any of the two replicates left for the TRAPPC1-knockout cells.

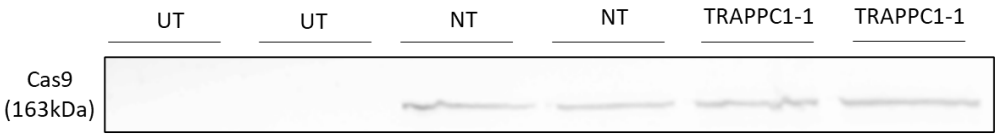

Figure 24. Cas9 protein abundance in U87 cells transduced with TRAPPC1-1 sgRNA or with the NT sgRNA compared to untransduced cells (UT). A: Separation of protein extracts with 15% polyacrylamide gel and subsequent identification of Cas9 by western blot analysis. Band around in between 180 kDa and 130kDa, corresponds to Cas9 (163 kDa). Results are presented for two independent cell populations.

Additionally, besides validating the TRAPPC1-1 knockout, we also performed the proliferation assay for the other biological replicates of TRAPPC1-1-transduced U87 cells (Figure 25). To do so, cell counting was performed at time 0, time 24h, time 48h and time 72h after seeding.
Results confirmed what we had previously observed, i.e. that there was a lower proliferation rate for TRAPPC1-1 transduced U87 cells than for NT and UT cells. The simple linear regression analysis showed a significant difference in slope between the three curves (p-value of 0.0284). However, the two-way ANOVA analysis indicated that the differences observed in the cell proliferation rate between NT-transduced U87 cells and TRAPPC1-1-transduced cells (at each point in time) were not significant (p-value of 0.1853).

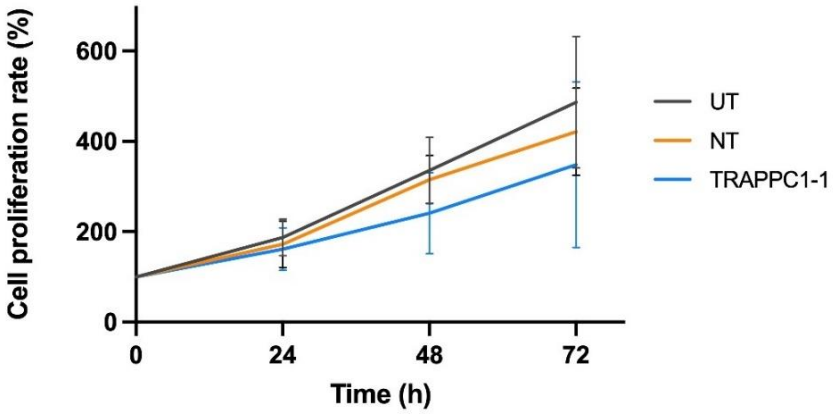

Figure 25. Proliferation rate of TRAPPC1-1 knockout U87 cells. Actual cell numbers were counted eight times in each cell suspension at time 0, time 24h, time 48h and time 72h after seeding. Average cell counts and respective cell rate proliferation were calculated. Results are presented as means ±1SD for three independent cell populations. Significance of the slope cell proliferation curve differences was analysed with a simple linear regression test whilst significance of each of the data points in the cell proliferation curves was studied with a two-way ANOVA with multiple comparisons.

Altogether, we can conclude that the decreased cell proliferation rate observed in TRAPPC1-1 knockout cells was not significant. However, because after lentiviral transduction we observed cell death in the TRAPPC1-knockout U87 cell population, we decided to shift the approach of this project towards the knockdown of TRAPPC1.

3.3. TRAPPC1 knockdown in U87 cells

The knockdown in U87 cells was performed for TRAPPC1 with two different shRNA, shTRAPPC1-1, and shTRAPPC1-2, keeping a non-targeting shRNA as negative control for the validation of the knockdown (shCTL) and untransduced U87 cells as negative control for studying the effects of the transduction.

Lentiviral transfection and U87 cell transduction

The first step to obtain TRAPPC1-shRNA-encoding lentiviral particles was to deliver the shRNA vector containing the TRAPPC1 mRNA-targeting sequence and the lentiviral packaging plasmids to the HEK293T cells.

Transfection of HEK293T cells was performed for the two shRNAs for TRAPPC1 knockdown, and for one non-targeting shRNA as the control for the following transduction. We used a plasmid encoding GFP as transfection control (Figure 26). After 24h, cells transduced with the GFP encoding plasmid displayed a green fluorescence, indicating that the transfection of plasmids in HEK293T was successful. However, roughly only 10-15% of the HEK293T cell population seemed to be successfully transfected and thus, expressed GFP.

Once the lentiviral particles were produced, we independently transduced the U87 cells in three different cell populations. In this case, the lentiviral titers were not assessed as we used all lentiviral supernatant for transduction to maximize the knockdown of TRAPPC1.

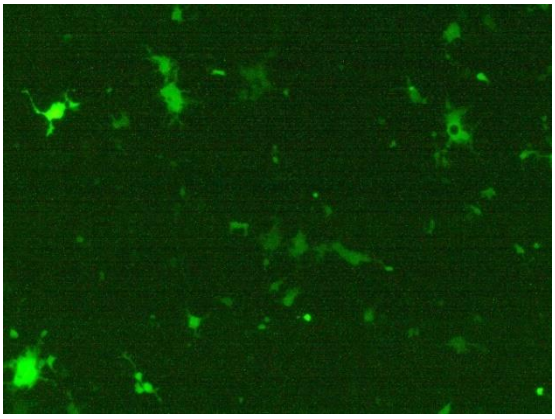

Figure 26. Transfection of HEK293T cells with GFP plasmid and observation by epifluorescence microscopy (10x). This image was taken 48 hours after transfection showing about 10-20% of cells expressing GFP.

U87 cell morphology was analysed after transduction (Figure 27). The lentiviral transduction did not appear to have any influence the U87 cell morphology.

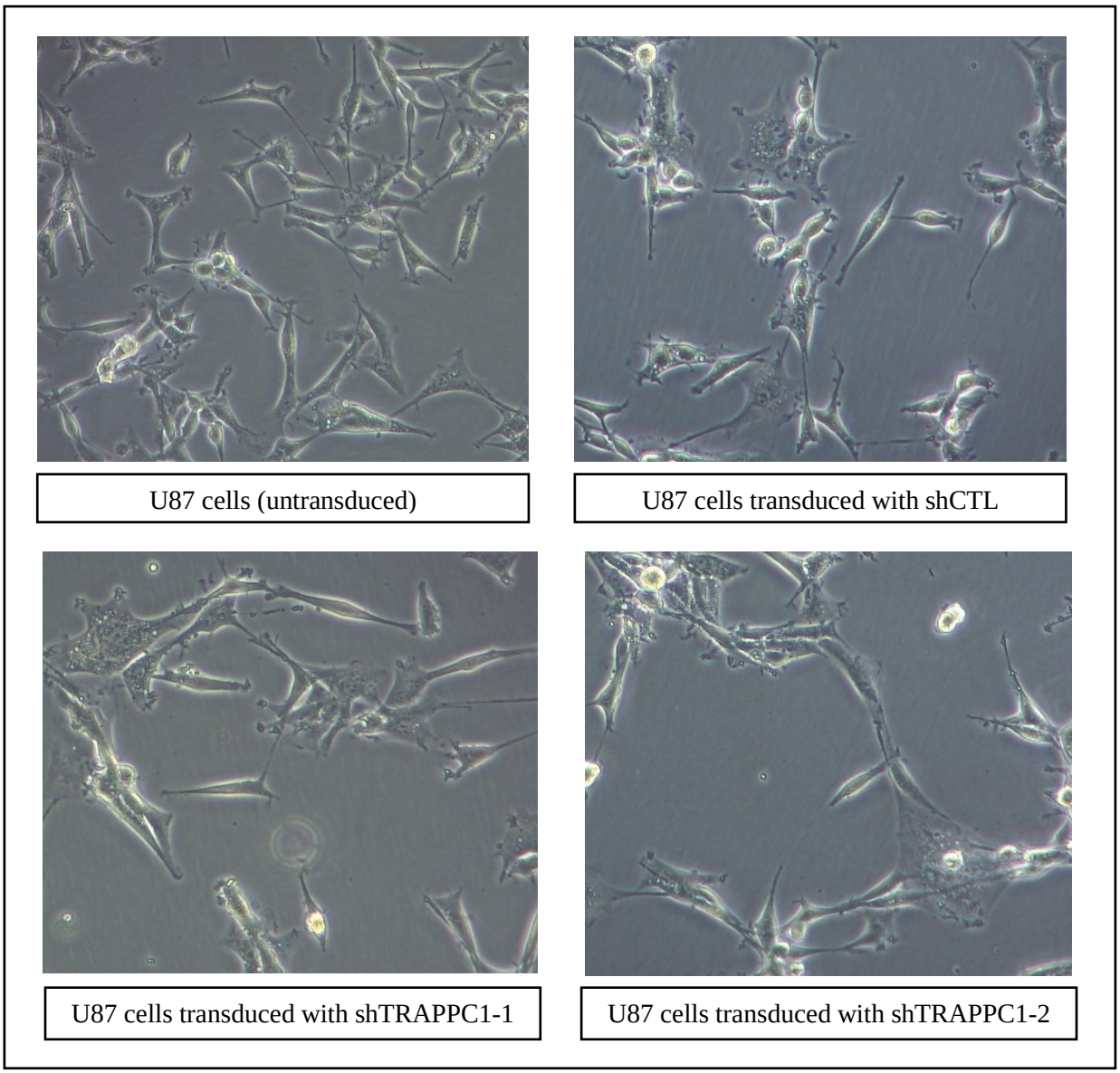

Figure 27. U87 cell morphology after transduction with TRAPPC1 shRNAs or CTL shRNA compared to untransduced U87 cell phenotype under phase contrast microscopy at a magnification of 10x.

3.4. Validation of TRAPPC1 knockdown

We assessed the TRAPPC1 knockdown at the mRNA level using RT-qPCR and at the protein level by performing a Western blot. Results in this section are presented for the three biological replicates and are normalised to the untransduced U87 cell condition to study the effect of transduction. Furthermore, statistical analysis was applied to study the significance of TRAPPC1 difference of expression (both at mRNA and protein levels) in the TRAPPC1-knockdown cells compared to NT-transduced control.

At the mRNA level, cells transduced with both TRAPPC1-targeting-shRNAs presented a significantly lower expression of TRAPPC1 than the NT-transduced cells (Figure 28). The second TRAPPC1-targeting-shRNA, shTRAPPC1-2, presented a lower fold change compared to shTRAPPC1-1 and thus gave the most efficient TRAPPC1 knockdown (p-value of 0.005).

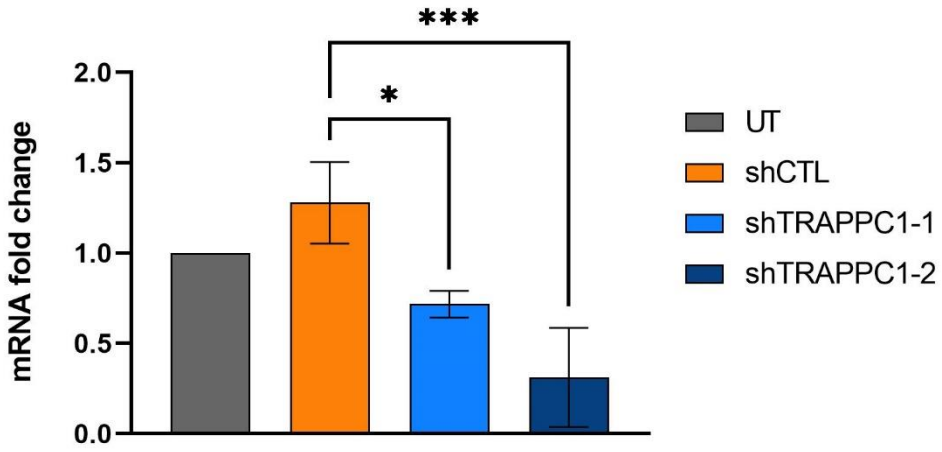

Figure 28. Relative TRAPPC1 mRNA expression in TRAPPC1 knockdown cells. TRAPPC1 mRNA level of U87 cells transduced with two different TRAPPC1 shRNA or with the non-targeting (CTL) shRNA compared to untransduced U87 cells (UT) assessed by RT-qPCR. GAPDH was used for gene expression normalisation. Results are presented as means ±1SD for four independent cell populations. Significance of results was analysed with a one-way ANOVA with multiple comparisons (* p-value < 0.05, *** p-value < 0.0005).

To validate the knockdown effect at the protein level, we performed a western blotting to assess the relative protein expression for TRAPPC1. However, at the protein level (Figure 29 A), we could not observe a clear band around 19 kDa, which coincides with the molecular weight of TRAPPC1. Furthermore, we could identify a band around the molecular weight of 35 kDa, which matches to the GAPDH molecular weight (Figure 29 B). Given that GAPDH protein expression was previously chosen as the endogenous control for U87 cells, we proceeded to reactivate the membrane by rehydrating it for 1 min with Methanol, and incubate it with GAPDH antibody (primary and secondary). After GAPDH antibodies incubation for GAPDH protein detection, a band was detected at a molecular weight of 35 kDa (Figure 29 C).

Because the secondary antibody solution used for TRAPPC1 antibody detection was reutilized from the previous KO TRAPPC1-detection experiment, these results suggest that the secondary antibody solution was contaminated. Altogether, neither TRAPPC1 nor GAPDH protein could be detected. Hence their abundance could not be quantified for any of the biological triplicates of U87 knockdown cells.

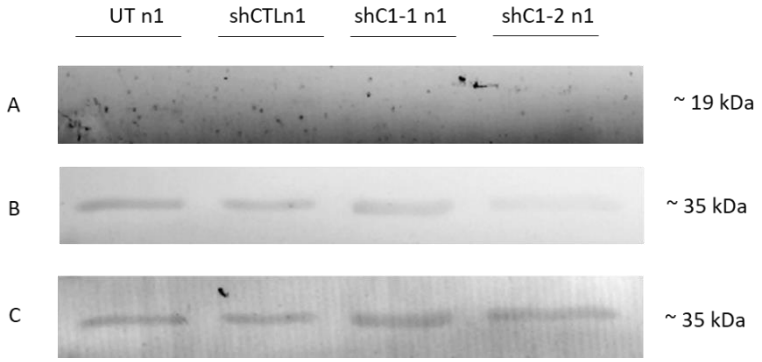

Figure 29. TRAPPC1 protein relative abundance in TRAPPC1 knockdown U87 cells. The sequence shows three images belonging to the same membrane. Upper and middle panels (A, B): images taken after TRAPPC1 antibody membrane incubation for TRAPPC1 protein detection. Below panel I: image taken after the GAPDH antibody membrane incubation for GAPDH protein detection as endogenous control. A; Band at a MW of 19 kDa, where TRAPPC1 protein should be detected is not visible for any of the samples. B; Band at a MW of 35 kDa, is visible, which coincides with the MW of GAPDH. C; Band at 35 kDa.

Besides validating the knockdown of TRAPPC1, we also assessed cell proliferation by cell counting at time 0, time 24h, time 48h and time 72h after cell seeding (Figure 30).

Results indicated that all transduced samples displayed a decreased proliferation rate at time 48h and time 72h when compared to untransduced cells. Assuming a simple linear regression of each slope, statistical analysis concludes that the differences observed between each line were very significant (p-value of 0.0019). In the Figure 30, we can observe that the cell proliferation rate for the U87 cells transduced with the second TRAPPC1 shRNA, shTRAPPC1-2, seemed to have a more decreased proliferation rate compared to the other transduced and also untransduced U87 cells. However, when a two-way ANOVA was applied in order to compare each time point to the transduced control, shCTL, none of the transduced and untransduced U87 cells showed significant differences in cell proliferation rate.

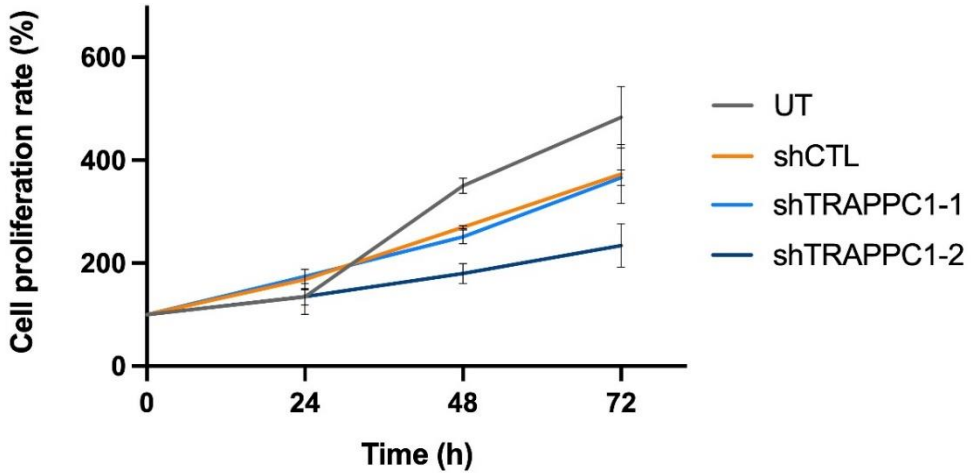

Figure 30. TRAPPC1 knockdown effect on proliferation was assessed with a proliferation assay by manually counting the cells eight times after resuspension at time 0, time 24h, time 48h and time 72h. Note that time 0 is assessed 24 hours after cell seeding. Average cell counts and respective cell rate proliferation were calculated. Results are presented as means ±1SD for four independent cell populations. Significance of the slope cell proliferation curves differences was analysed with a simple linear regression test whilst significance of each of the data points in the cell proliferation curves was studied with a two-way ANOVA with multiple comparisons.

Considering the results obtained from the proliferation assay for the knockout and knockdown of TRAPPC1 in U87 cells and the results obtained at the mRNA level, we can say that cell proliferation seems to inversely correlate with TRAPPC1 abundance. Altogether, we can conclude that TRAPPC1 seems to influence cell proliferation.

3.5. Effect of treatment on U87 cell morphology, senescence, proliferation and gene expression

Before studying the effect of TRAPPC1 on the sensitivity of U87 cells to treatment, we treated U87 untransduced cells to better characterize their response to TMZ-chemotherapy and x-ray irradiation as it is well known that they take part in some cell responses to damage and stress, i.e., apoptosis, senescence, autophagy.

The two treatments where used alone or in combination.

Previously, in the genome-wide CRISPR-Cas9 screening experiment, U87 cells were treated with TMZ at a final concentration of 200 µM and an exposure of 7 Gy X-rays at a 2 Gy/min dose rate. That is why we chose the same parameters for these experiments. Four different conditions were used: untreated U87 cells (CTL), U87 cells treated with 200 µM TMZ (TMZ), U87 cells exposed to 7 Gy X-rays (X-rays) and finally U87 cells treated with both 200 µM of TMZ and 7 Gy X-ray (TMZ + X-rays). TMZ was added to the cells half an hour before cells were exposed to x-ray radiation.

After treatment, cells were seeded for RNA extraction, beta-galactosidase assay and clonogenic assay.

3.5.1. Study of U87 cell morphology

U87 cell morphology was analysed after treatment (Figure 31).

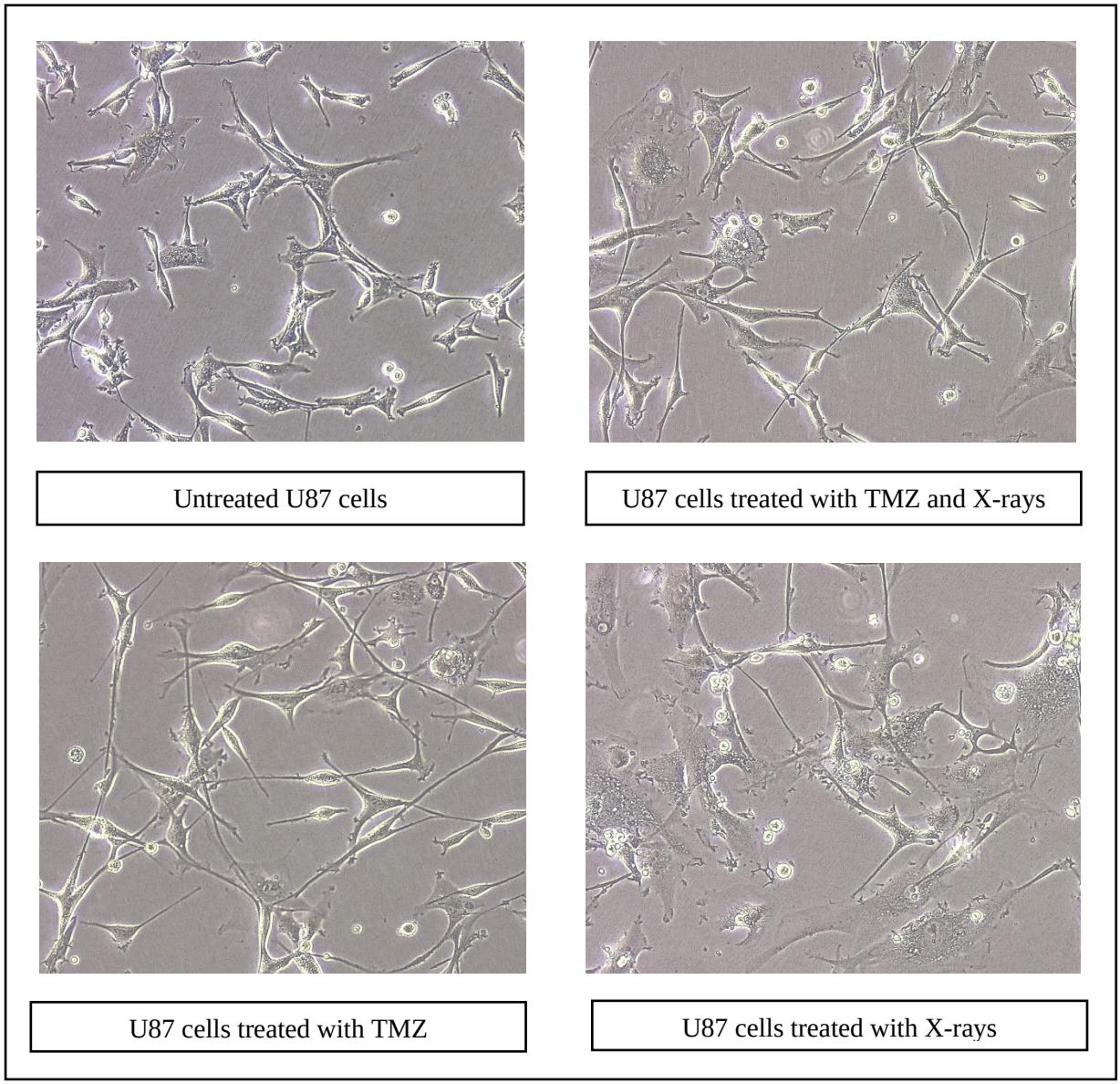

Figure 31. U87 cell morphology after treatment with 200 µM of TMZ, 7 Gy X-rays and with 200 µM TMZ half an hour before exposing cells to 7 Gy X-rays compared to untreated U87 cells under phase contrast microscopy at a magnification of 10x.These images were taken 24h after chemotherapy and radiotherapy exposure.

U87 cells treated with TMZ seemed to have a more accentuated, elongated bipolar appearance, whilst the U87 cells exposed to X-rays lose structure and seemed to have a higher intracellular vesicle content than TMZ treated cells and control cells. We observed the same features in U87 cells that were treated with both chemotherapy and radiotherapy.

3.5.2. Cell proliferation

A clonogenic assay was performed in order to study the effect of the TMZ-treatment and X-rays irradiation to the cell proliferation in U87 cells. This in vitro method is used to study the cell reproductive death after ionizing radiation and thus, it helps measuring the cells that survive treatment and that are capable to grow into colonies.

For the clonogenic assay, the results are presented for four independent cell populations ten days after cell seeding (Figure 32). After 10 days in culture, the assay was stopped by fixating and staining the cells on the petri dish in order to calculate the surviving fraction.

Initially, the number of cells seeded was the same for all four cell populations, which was 2000. Because the cell seeding density influences the cell proliferation and colony growth, it is important to determine the plating efficiency of each independent cell population prior to calculating the surviving fraction. The PE is a percentage of the proportion of single cells growing in a colony based on the number of cells seeded. The PE of the control group, which in this case were the untreated U87 cells, is used as surviving fraction normalisation for the other conditions.

In Figure 32, we can observe that after 10 days in culture, it was impossible to assess the number of colonies for the control group, and thus, their PE could not be calculated. This is because the seeded number of cells should have been lower for this cell population, such as 500 instead of 2000. Altogether, SF could not be calculated for any of the conditions. Based on the counted colonies, the cells exposed to X-rays irradiation seem to have a slight higher capacity to grow into colonies compared to the other two treatment conditions. However, nothing can be concluded from this experiment.

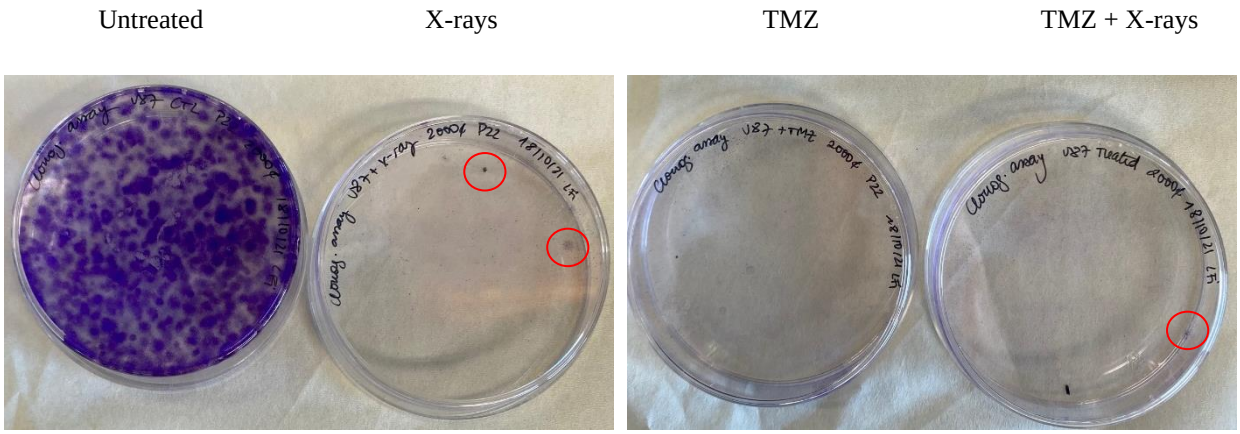

Figure 32. Clonogenic assay on U87 treated cells stopped ten days after cell seeding. From left to right: (1) U87 untreated, (2) U87 cells treated with X-ray, (3) U87 cells treated with TMZ and (4) U87 cells treated with both chemotherapy and radiotherapy. Colonies are highlighted with a red circle.

3.5.3. Senescence

X-ray irradiation has been described to induce senescence in addition to apoptosis and cell cycle arrest[77]. In order to assess the induction of senescence, senescence-associated beta-galactosidase assay was performed.

The senescence-associated beta-galactosidase is an enzyme that catalyses the hydrolysis of beta-galactosidase into monosaccharides whose expression has been shown to be higher and whose activity can be measured at neutral pH in senescent cells. We compared the proportion of SAβ-gal positive cells after each of the treatments with four biological replicates.
After performing the beta-galactosidase assay, a senescence ratio was obtained for each condition (Figure 33).

The results indicated that TMZ alone and x-ray irradiation alone, both induced senescence in U87 cells. The combination of both treatments induced a similar percentage of senescent cells compared to TMZ treatment alone, which had the higher percentage of senescent cells. A statistically significant increase in senescence was observed in all treated groups when compared to the untreated control (One-way ANOVA analysis, p-value of 0.0003).

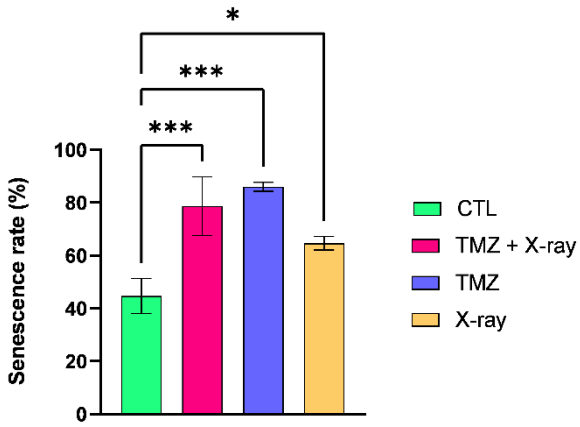

Figure 33. Senescence of U87 cells treated with TMZ and or X-rays. The proportion of senescent cells in 200 cells was counted manually under the phase contrast microscope. Results are presented as means ±1SD for four independent cell populations. One-way ANOVA with multiple comparisons was applied to study the statistical significance of the results (* p-value < 0.05, *** p-value < 0.0005).

3.5.4. Gene expression

RT-qPCR was performed in order to investigate whether both treatments may affect the expression of the genes of interest, which included some TRAPPC genes, as they function in a complex. Besides, based on the beta-galactosidase results, we also studied the relative mRNA expression level of p21, a gene marker for senescence. Furthermore, because we know that both chemotherapy and radiotherapy treatments induce autophagy and apoptosis responses, we found it valuable to study the levels of expression for Bcl-2, a gene marker for apoptosis. GAPDH gene was used for gene expression normalisation (Figure 34).

The RT-qPCR results indicate that even though we observed a slightly higher TRAPPC1 relative mRNA expression in treated cells compared to untreated cells, there was no significant difference in the relative expression for TRAPPC1.

The results obtained for the other TRAPPC genes expression are comparable. Although it may seem that the treatment with TMZ induces a slight increase in TRAPPC gene expression, results were non-significant. Altogether it can be concluded that TRAPPC gene expression was not influenced by the treatment with chemotherapy or radiotherapy both given individually or concomitantly.

p21 displayed a higher expression in the TMZ-treated cells, in X-ray irradiated cells and in cells treated with both TMZ and X-rays. However, this increase of p21 gene expression is not significant in any of the treated cell populations when compared to the untreated cells.

Conversely, for Bcl-2, the gene expression seemed to be decreased in all treated-cell groups. We can observe significant lower expression in the X-ray treated group when compared to the control group (p-value <0.0001).

All in all, although no significance was found, the results with regards to the relative p21 gene expression seem to be coherent with the results observed in the beta-galactosidase assay, which point to TMZ treatment and X-rays irradiation inducing senescence. On the other hand, the decrease in Bcl-2 expression in cells treated with radiotherapy and or chemotherapy may indicate that apoptosis was upregulated in these cells. Furthermore, the treatment of glioblastoma cells with both radiotherapy and TMZ-chemotherapy, did not seem to affect the gene expression of any of the studied TRAPPC genes.

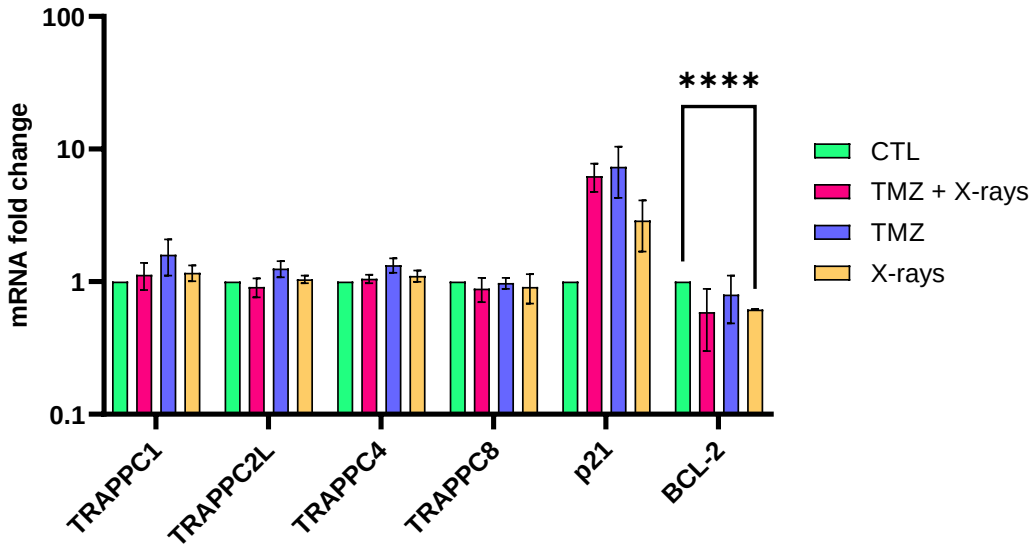

Figure 34. Relative mRNA expression level for TRAPPC1, TRAPPC2L, TRAPPC4, TRAPPC8, p21 and Bcl-2 genes in U87 treated cells compared to untreated U87 cells. Results presented are based on biological triplicates and gene expression was normalized with GAPDH. Results are presented as means ±1SD for four independent cell populations. Two-way ANOVA with multiple comparisons was applied to study the statistical significance of the results (**** p-value <0.0001).

3.5.5. U87 cells under hypoxic conditions

Given that hypoxia is frequent in solid tumours, we analysed the relative TRAPPC gene expression under hypoxia in comparison to normoxia to study a potential relationship between cancer survival in hostile conditions and TRAPPC genes.

The bipolar phenotype of U87 cells seems to be conserved over time both in hypoxic and normoxic conditions (Figure 35). However, what we can observe is that hypoxic cells tended to form a close network which goes in line with the expected cell behaviour in a hostile environment.

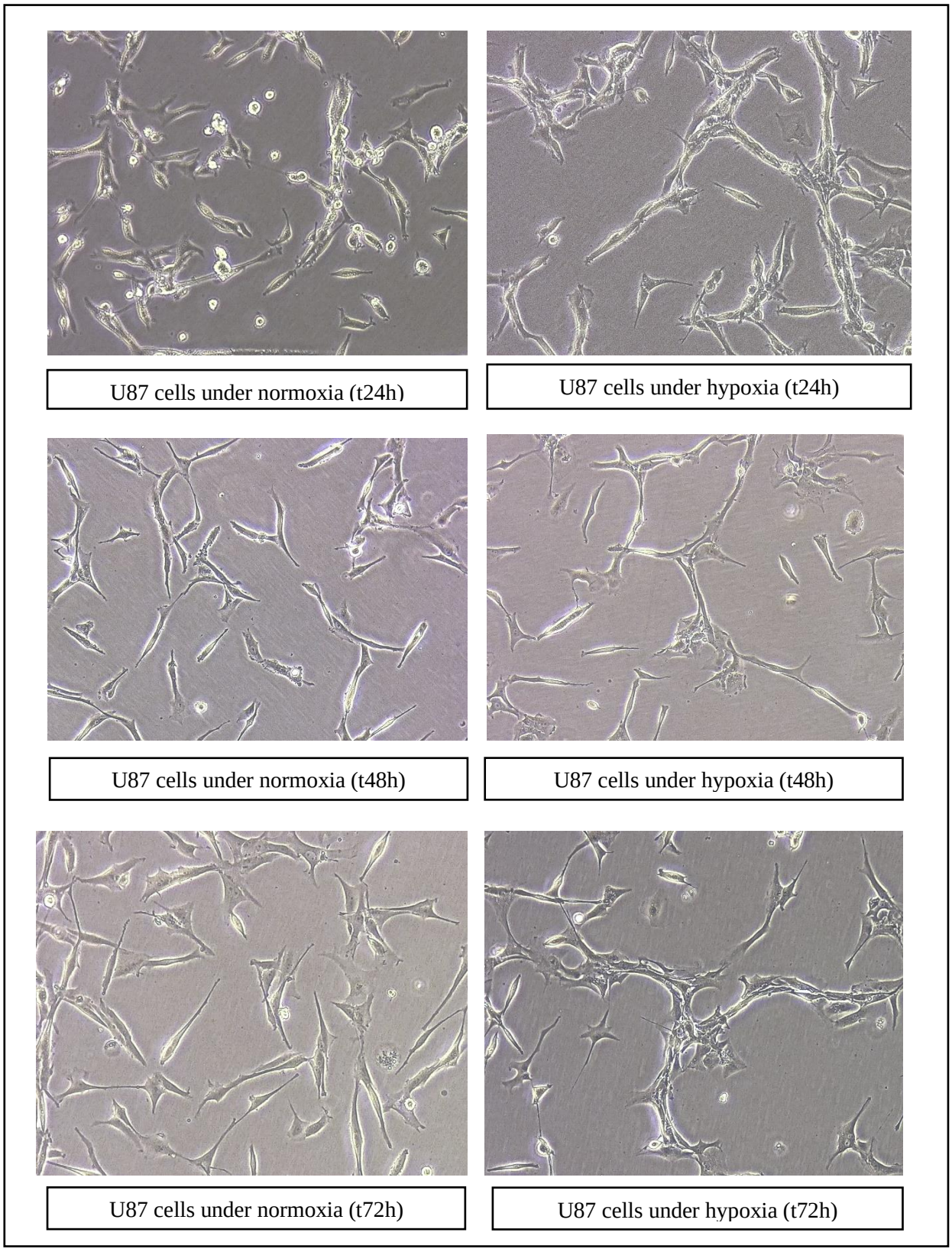

Figure 35. U87 cell morphology under hypoxic versus normoxic conditions. Images taken under the phase-contrast microscopy at 10x magnification.

TRAPPC1, TRAPPC2L, TRAPPC4, TRAPPC8 and BNIP3 relative gene expression was studied by RT-qPCR. Results are presented for two independent biological replicates (Figure 36).

BCL2 Interacting Protein 3 (BNIP3) is a pro-apoptotic protein localised in the mitochondria that has been implicated in hypoxia-induced tumour cell death. There is an association between the deregulation of BNIP3 expression in hypoxic regions of a tumour and hereafter, BNIP3 serves as a negative prognostic for cancer aggressivity. BNIP3 was used as a positive control of hypoxia. Figure 43 shows that BNIP3 mRNA level was indeed increased by hypoxia, already after 24h of exposure.

When looking at the relative levels of expression for all TRAPPC genes, it seems that there was a decrease over time under hypoxic conditions. This is especially true for TRAPPC8 and TRAPPC4.

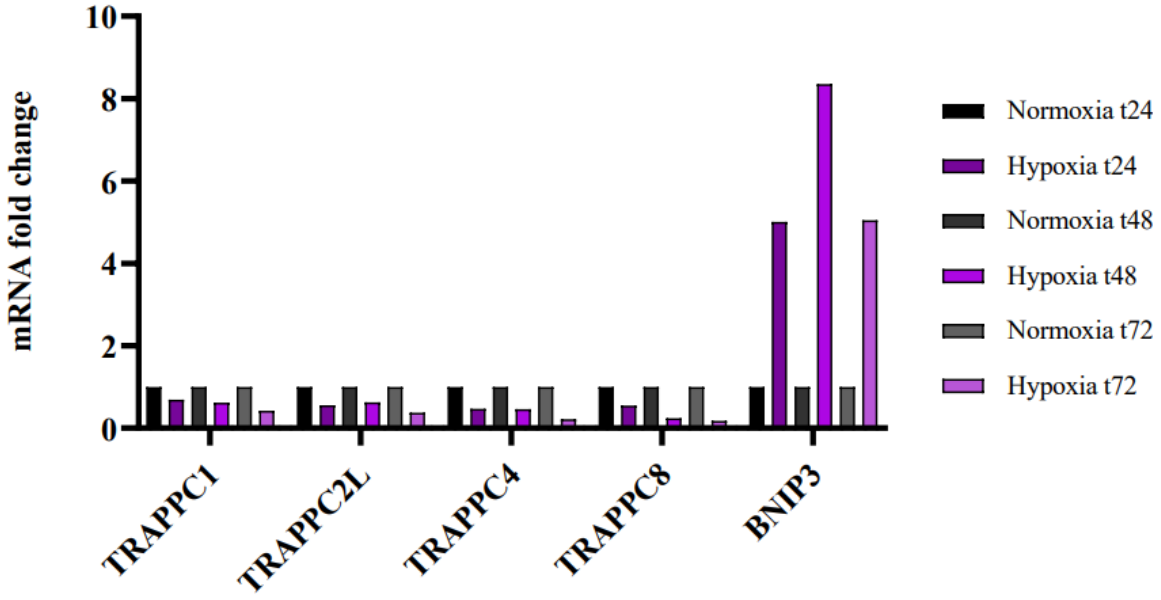

Figure 36. Effect of hypoxia on the mRNA levels of genes of interest. U87 cells were exposed to hypoxic and normoxic conditions for 42, 48 and 72 hours. RT-qPCR was performed for TRAPPC1, TRAPPC2L, TRAPPC4, TRAPPC8 and BNIP3 gene expression analysis. Gene expression normalisation was done with GAPDH in normoxic conditions for each time point. Results are presented for two independent biological replicates.

3.6. Effect of TRAPPC1 knockdown on U87 cell sensitivity to treatment

After validating TRAPPC1 knockdown in U87 cells, the sensitivity of these cells to GBM treatment was evaluated with a clonogenic assay. Given the previous results, the conditions chosen for this experiment were: shCTL as the negative control and the second TRAPPC1-targeting-shRNAas it seemed to give the most successful knockdown.

The treatment of transduced U87 cells was performed with chemotherapy and concomitant radiotherapy. U87-transduced cells were treated with TMZ at a final concentration of 25 µM and exposed to two different dosages of X-rays, 2 Gy or 4 Gy (Figure 37).

Transduced U87 cells were seeded 24h before treatment. Cells were exposed to treatment once. TMZ was added half an hour previously to X-ray irradiation.

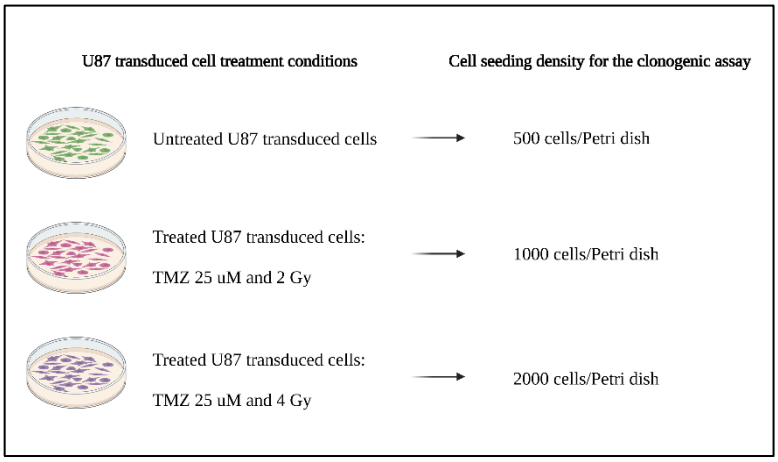

Figure 37. Diagram summarising the cell seeding densities for the clonogenic assay based on the different treatments of transduced U87 cells. The results obtained are presented for three independent cell populations with technical replicates. This image was made with Biorender.

When looking at the untreated conditions, we observed that most of the transduced cells have the capability to form colonies (Figure 38). However, the number of colonies that had grown in both transduced-typed U87 cells decreased significantly when treated with both treatments as compared to their untreated control. Furthermore, it seemed that with the increase of X-ray irradiation dose, the colonies lose structure and thus, surviving cells are more dispersed.

The Table 5 indicates the calculated averaged surviving fraction ratio for each sample within the two independent cell populations.

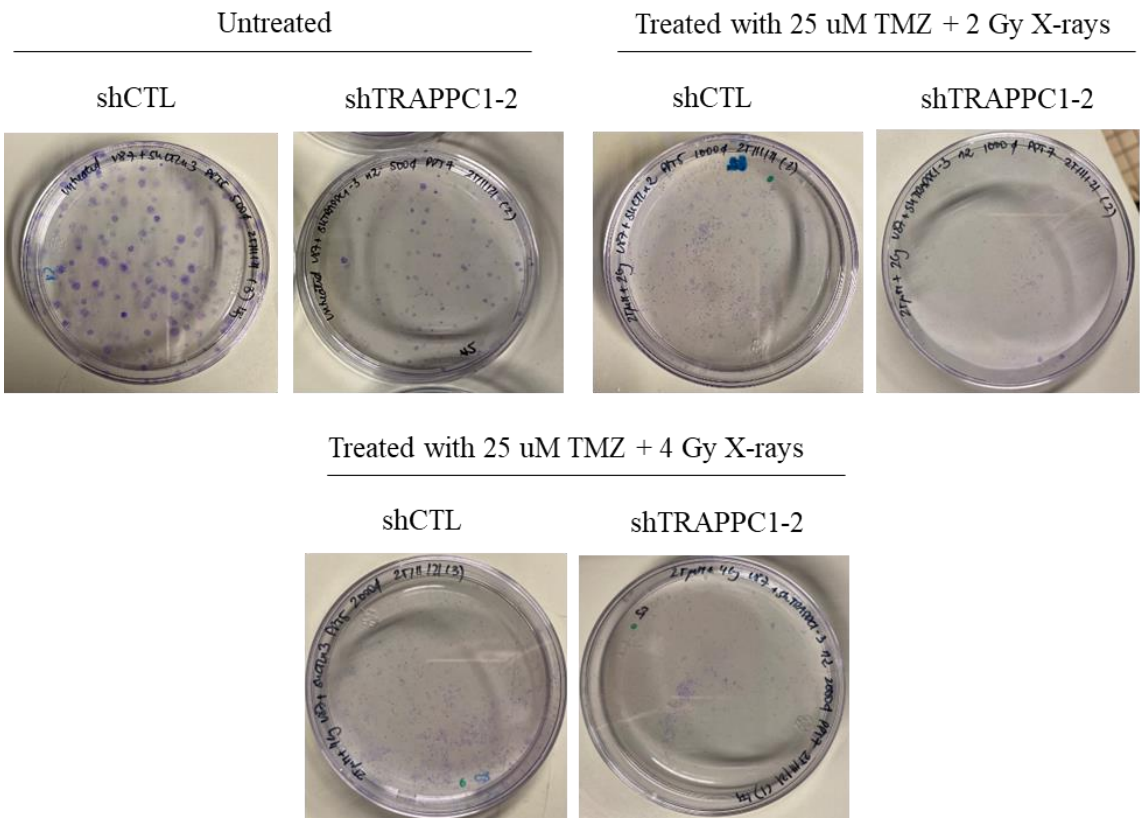

Figure 38. Clonogenic assay images comparing the untreated condition to the treated with 25 uM TMZ and 2 Gy X-rays and the treated with 25 uM TMZ and 4 Gy X-rays in both transduced cell populations.

	Averaged SF ratio for each transduced-U87 cell group					
Treatments	shCTL			Sh-TRAPPC1-2		
Untreated	1	1	1	1	1	1
TMZ + 2 Gy X-ray	0.040	0.032	0.034	0.043	0.050	0.080
TMZ + 4 Gy X-ray	0.008	0.016	0.006	0.013	0.010	0.015

Table 5. Surviving fraction ratio calculated after assessing the plate efficiency of each sample within the two individual cell populations exposed to three different treatments. For the treatment conditions, each SF ratio was obtained after normalisation to the corresponding untreated control.

Treatment of shCTL-transduced cells with TMZ and 4 Gy X-rays displayed a lower surviving fraction than the same cells exposed to TMZ and 2 Gy X-rays instead. The same happens for the shTRAPPC1-2-transduced cells, where their surviving fraction decreased with the increase in ionizing radiation dose (Figure 39).

Interestingly, when we individually compared each treatment effect on the surviving fraction within both of the cell populations, we observed that shTRAPPC1-2-transduced cells seemed to have a higher clonogenicity capacity when treated with concomitant chemotherapy and radiotherapy compared to the shCTL-transduced cells.

The statistical analysis indicated that there was a significantly higher surviving fraction ratio in shTRAPPC1-transduced cells that were treated with TMZ and 2 Gy X-rays compared to the shCTL-transduced cells (p-value of 0.0233).

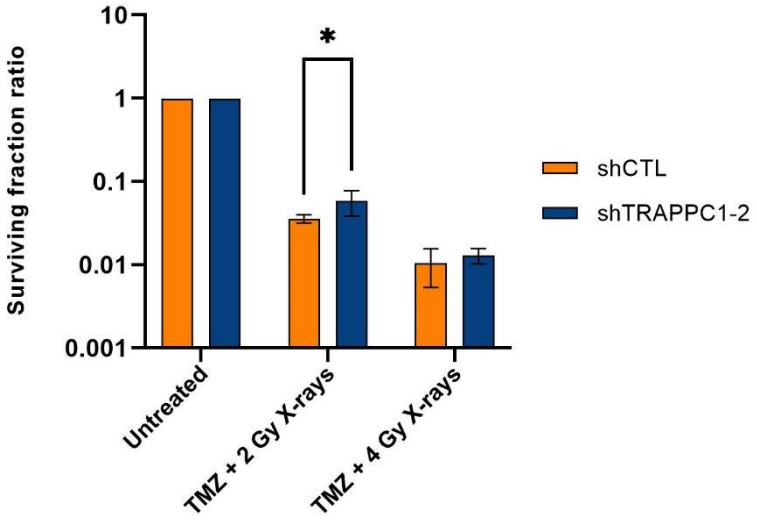

Figure 39. Surviving fraction ratio plotted in a log scale representing the clonogenicity differences between TRAPPC1-knockdown U87 cells and non-targeting transduced cells when exposed to different chemotherapy and radiotherapy treatments. Results are presented as means ±1SD for two independent cell populations. Surviving fraction was calculated in each cell population based on their plating efficiency and normalized to the untreated cell population. Significance of these results was studied with a two-way ANOVA with multiple comparisons (* p-value < 0.05)

4. Discussion

Intracellular communication and cellular trafficking of proteins and lipids are key processes for the cell viability as they help maintaining cellular homeostasis, cell morphology, polarity, synaptic function (in case of neuronal cells) and motility or secretion[40,78].

In the context of the hallmarks of cancer cells, the shared pathological behaviours, such as sustaining chronic proliferation, invasion and migration abilities or high metabolic adaptations, highlight the relevance of studying intracellular trafficking pathways in cancer research[79].

Rab GTPases are the largest subfamily of Ras superfamily of small GTPases and similar to TRAPP complexes, Rabs have been very well characterised in yeast. Additionally, human Rabs are also evolutionary conserved to yeast (Ypt)[53]. However, there are still many questions unresolved when it comes to mammals.

As we have mentioned before, Rab GTPases regulate all membrane-bound intracellular trafficking pathways in eukaryotic cells[52] and consequently, they are known to be key for the cell wellbeing and for human health.
In consequence, aberrant expression of Rab might be predictor for tumourigenesis and cancer progression[80].
For example, Rab25 has been found overexpressed in ovarian and breast cancer and associated with decreased survival[81]. The overexpression of Rab25 lead to apoptosis inhibition and increased cell proliferation associated to a decreased expression of BAK and BAX (BCL-2 family) and activation of phosphatidylinositol 3 kinase (PI3K) and AKT/PKB (protein kinase B) pathways, respectively.

In another study, Janice et al.,[82] identified Rab1A GTPase as a colorectal oncogene. Rab1A, homologue to Ypt1 in yeast, is located at the ER exit and pre-Golgi and it mediates ER-Golgi trafficking[80]. They demonstrated that Rab1A is responsible for activating the mechanistic target of rapamycin complex 1 (mTORC1) signalling by engaging the interaction of mTORC1 with Rheb in the Golgi[82]. mTOR is a serine/threonine kinase present in several subcellular compartments (e.g., mitochondria, lysosome, ER nucleus and plasma membrane). Upon activation, mTOR promotes cell growth and survival whilst limiting autophagy-mediated catabolism[83]. Altogether, we can assume that the overexpression of Rab1A positively impacts cell growth in this cancer type through mTORC1 signalling.

TRAPPC1 is part of the TRAPP I, also known as the TRAPP core complex, which plays a role in the vesicular transport from the ER to the GA. Additionally, the TRAPPC1 subunit has been located in the Golgi apparatus, cytosol and the ER.

When human Rab1A's protein interactions are analysed in the STRING software (Figure 40), the network of interactors shows TRAPPC1 to have a physical and functional interaction with Rab1A. We also can find other TRAPPC subunits interacting with Rab1A, like TRAPPC4 and TRAPPC5, amongst others.

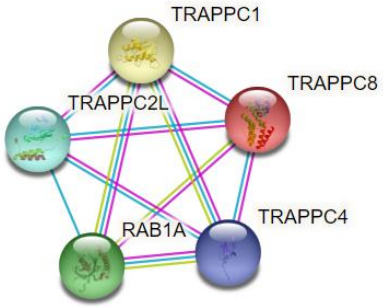

Figure 40. Network of physical interactions that have been experimentally demonstrated (pink edge) or obtained from databases (blue edge). Predicted interactions are also illustrated (green edge). Please note that this figure does not represent all interactors of Rab1A.

In our study, we observed that after the knockout of TRAPPC1, some cells were dying. From the surviving cells, we were able to validate a successful but partial knockout of TRAPPC1 at the mRNA level and only for the first TRAPPC1-targeting sgRNA. Moreover, although not statistically significant, a lower proliferation rate was observed for TRAPPC1-KO cells compared to NT-transduced and untransduced U87 cells. Altogether, it can be argued that after lentiviral transduction, TRAPPC1-KO cells survived because the KO of TRAPPC1 was only partial, and thus, TRAPPC1 KO could also not be fully validated.
Furthermore, taking in account that GBM is a highly mutagenic type of cell, and that we were working with a heterogeneous population of clones, we could also argue that some cells were able to repair the knockout after lentiviral transduction and thus, the cells either had a partial knockout or no knockout of TRAPPC1 at all.

Another explanation as why there was not a complete knockout in U87 cells is related to the off-target mutagenesis level of CRISPR-Cas9 method. CRISPR-cas9 technology enables the generation of in-/del mutations in targeted genes[84]. The ideal scenario lies on having a single cell mutation and thus, creating in our case, CRISPR-induced knockout clones. To avoid off-target mutagenesis, we performed the U87 transduction at a very low MOI (<0.5). Despite the low MOI, we must bear in mind that at the end of the selection period, our population was still a mix of cells KO for TRAPPC1, which explains the challenges of the validation of the KO, and perhaps the lack of significance on the proliferation results, as we may have incomplete target ablation, off-target mutations and/or a gene repair that have not led to the complete gene deletion[84].

Conversely, despite not studying the significance of our results, it seemed that the second and third sgRNA for TRAPPC1 were not successful in inducing the knockout of TRAPPC1.What´s more, cells transduced with these two sgRNAs displayed a slightly higher proliferation rate compared to the first TRAPPC1-sgRNA.

Altogether, this leads to the thought that TRAPPC1 may have a role in GBM cell survival given the observed decreased cell viability after TRAPPC1 knockout.

Since proliferation rate affects the response of cells to TMZ and to X-ray irradiation, it would have been difficult to interpretate the data regarding the effect of TRAPPC1 knockout on cell sensitivity to treatment. If an effect would have been observed, we could not have understood if whether the reason would have been due to TRAPPC1 knockout or due to the lower proliferation rate.

Furthermore, the review published in frontiers in Cell and Developmental Biology by Jane J. Kim et al.[54], brought us to the decision of shifting the project's approach towards the knockdown of the TRAPPC genes with shRNA instead. The mentioned review studied the essentiality of TRAPP subunits both in yeast and mammals and identified TRAPPC1, TRAPPC4 and TRAPPC8 as essential human genes (Figure 41).

Essential genes are genes crucial for an organism as they are required for cellular growth, proliferation, and survival[85]. The deletion of an essential gene leads to death or severe defect in proliferation, and thus, it is impossible to generate cells with an essential gene knockout.

Consequently, as our study could not validate the complete knockout of TRAPPC1 in U87 cells after lentiviral transduction, we decided to invalidate TRAPPC1 expression using shRNAs. shRNAs affect the gene expression without modifying the cell genome, because they act at mRNA and protein levels; adapting this as the new strategy would allow to study the TRAPPC1 gene function without severely influencing the survival of the cell.

Ideally, it would have been of great interest to invalidate the expression of a non-essential TRAPPC gene, such as TRAPPC2L, which was also identified as a potential gene with a role in the GBM sensitivity to treatment after the GecKO screening.

TABLE 2 | TRAPP Subunit Essentially.

Subunit Group	Yeast Trs/Bet	Essential In Yeast	Human TrappC	Essential Hart et al[a]	Essential Blomen et al[b]	Essential Wang et al[c]	Essential in Human[d]
Core TRAPP	Bet5	Yes	TrappC1	Yes (5/5)	Yes (2/2)	Yes (4/4)	Yes (11/11)
	Bet3	Yes	TrappC3	Yes (5/5)	Yes (2/2)	No (1/4)	Yes (8/11)
	Trs23	Yes	TrappC4	Yes (4/5)	Yes (2/2)	? (2/4)	Yes (8/11)
	Trs31	Yes	TrappC5	Yes (5/5)	? (1/2)	Yes (4/4)	Yes (10/11)
Others	Trs33	No	TrappC6A	No (0/5)	No (0/2)	No (0/4)	No (0/11)
			TrappC6B	No (0/5)	No (0/2)	No (0/4)	No (0/11)
	Trs20	Yes	TrappC2	(Not tested)	No (0/2)	No (0/4)	No (0/6)
	Tca17	No	TrappC2L	No (1/5)	No (0/2)	No (1/4)	No (2/11)
	Trs85	No	TrappC8	Yes (4/5)	Yes (2/2)	Yes (3/4)	Yes (9/11)
	Trs120	Yes	TrappC9	No (0/5)	No (0/2)	No (1/4)	No (0/11)
	Trs130	Yes	TrappC10	No (0/5)	No (0/2)	No (0/4)	No (0/11)
	Trs65	No	TrappC13	Yes (3/5)	No (0/2)	No (0/4)	No (3/11)
Metazoan	NA	NA	TrappC11	Yes (5/5)	Yes (2/2)	Yes (4/4)	Yes (11/11)
	NA	NA	TrappC12	No (0/5)	No (0/2)	No (0/4)	No (0/11)

[a] *Tested in 5 cell lines (number of cell lines in which the gene is essential/number of cell lines tested; Hart et al., 2015).*
[b] *Tested in 2 cell lines (number of cell lines in which the gene is essential/number of cell lines tested; Blomen et al., 2015).*
[c] *Tested in 4 cell lines (number of cell lines in which the gene is essential/number of cell lines tested; Wang T. et al., 2015).*
[d] *Consensus: Yes, if gene is essential in at least 6/11 cell lines tested in the three studies.*
Red: *Genes essential in yeast but not in human cells.*
Green: *Gene essential in human cells, not in yeast.*

Figure 41. Essentiality of TRAPP subunits based on published data from genome-wide CRISPR screening of different cancer cell lines[54].

For the knockdown experiments, we chose 2 shRNAs targeting the mRNA of TRAPPC1.

The knockdown of TRAPPC1 was validated at the mRNA level for both of shRNAs, being shTRAPPC1-2 the most successful. After lentiviral transduction, we did not observe cell death in the TRAPPC1-knockdown U87 cell population.

Similarly to the TRAPPC1 knockout experiments, the proliferation results of TRAPPC1-knockdown cells indicated a decrease in cell proliferation rate compared to the transduced control cells. Moreover, it was observed that the shRNAs that induced a more effective knockdown of TRAPPC1 also had lower cell proliferation rates.

Taking in account the interaction of TRAPPC1 with Rab1A, we could argue that the reason why there was a decrease in cell proliferation is due to the knockout and knockdown of the TRAPPC1 gene, which impairs Rab1A activity in U87 cells, and thus, negatively affecting the cell growth through the mTORC1 signalling pathway.

Another possible explanation for the lower cell proliferation in TRAPPC1-transduced cells could be further away from the TRAPPC1 and Rab1A interaction and more focused on the fact that TRAPPC1 belongs to a complex and thus, the knockout/knockdown of TRAPPC1 may disrupt the TRAPP complex, leading to a lower cell fitness and, therefore, reduced cell proliferation.

Ramírez-Peinado et al. investigated whether the knockdown of TRAPPC13 interfered with TRAPP II formation. Results indicated that TRAPPC2 could still bind to TRAPPC4 and TRAPPC12 in the absence of TRAPPC13, which would mean that in our scenario, TRAPPC1 knockout/knockdown is not disrupting the TRAPP complex. However, we still think that this argument should be considered because, unlike TRAPPC12 and TRAPPC13, the TRAPPC1 subunit is core to all TRAPP complexes.

Furthermore, we studied the effect of TMZ treatment and X-ray irradiation to U87 cells before analysing the role of TRAPPC1 in the GBM´s sensitivity to treatment.

Radiotherapy is widely used in cancer treatment because it induces cancer cell death and cancer cell senescence. When treating GBM cells with X-ray, many things occur, some of them being the changes in cell morphology, injuries affecting cell function and molecular changes that end in metabolic alterations facilitating cell tumourigenesis. Additionally, X-ray irradiation leads to ROS generation, which can induce senescence[86]. In our study, we observed that U87 cells treated with X-rays, presented a severely decreased clonogenicity, a significant Bcl-2 gene expression and increased p21 expression together with a high significant increase in SA-ßgal activity. All these observed results point to an increased cell senescence, together with an increased apoptotic activity in cells treated with ionisation radiation.

TMZ-chemotherapy is known to cause cell damage, apoptosis, senescence and autophagy as we have previously mentioned. In our study, we observed that U87 cells treated with TMZ only presented a severely decreased clonogenicity, an increased p21 gene expression and also a high significant SA-ßgal activity. If we compare the senescence results between the two types of treatment, U87 cells seem to be more resistant to TMZ treatment. We could argue that TMZ-treated U87 cells escape apoptosis by inducing senescence whilst X-ray irradiation induces a higher level of apoptotic activity than TMZ.

Generally speaking, the tumour cell metabolism differs from the healthy cell metabolism; besides, it is also dependent on the tumour microenvironmental conditions (e.g., hypoxic vs normoxic conditions). It is well known, but not yet well understood, that cancer cells can arrange their metabolic needs based on external selection pressure. For example, in a hypoxic niche cancer cells will switch metabolic preferences and benefit from the anaerobic glycolysis pathway instead of metabolizing glucose through aerobic glycolysis.
Because TRAPP complexes mediate the contact between vesicles and target membranes, and thus, are involved in vesicle-mediated transport of proteins and lipids, we could have expected to find up- or down-regulated TRAPPC gene expression in U87 cells treated with radiotherapy and or chemotherapy. However, this was not observed in our study. The gene expression of all TRAPPC genes seem to be similar in all cell populations, and thus, unchanged. Meanwhile,

what we could observe was that in U87 cells in hypoxic conditions, TRAPPC gene expression seemed to be decreased. This is interesting as it could indicate that hypoxia downregulates TRAPPC genes and thus, intracellular trafficking. However, further experiments should be performed.

Generally, the clonogenic assay is widely used to study the differences in cell reproductive death between two conditions (treated vs untreated), aiming to test for the consequences of cell exposure to ionizing radiation and cytotoxic agents[87].

The results obtained in the clonogenic assay, regarding the TRAPPC1 role into the sensitivity to GBM treatment were difficult to interpret, due to the aforementioned decrease in cell proliferation in TRAPPC1-knockdown cells. However, when we compare the treated U87 cells to the untreated cells, they all show a decreased clonogenicity that can be explained by the effect of radiotherapy and chemotherapy in cell proliferation.
In addition to these results, we can observe an increase in the survival fraction ratio for TRAPPC1-knockdown cells compared to the shCTL-transduced cells, which would be indicating a higher clonogenicity capacity.

Based on the previous results regarding the decreased cell proliferation rate in TRAPPC1 knockout and knockdown U87 cells, we could have expected to obtain a decreased clonogenicity of knockdown cells when treated with radiotherapy and chemotherapy.

On the other hand, the observed colonies in shCTL were bigger and rounder than the TRAPPC1-knockdown U87 cell in the different treated and untreated groups. This could be due to the slower proliferation rate for TRAPPC1-knockdown cells.

The results obtained in the previous genome wide CRISPR/Cas-knockout screening performed on a GBM cell line after treatment with chemotherapy and radiotherapy, indicated that TRAPP genes seem to confer a selective sensitivity to GBM treatment. This means that we should have expected to observe a significant decrease in terms of clonogenic capacity in the TRAPPC1-knockdown cells compared to the transduced controls after treating them concomitantly with X-ray irradiation and TMZ-treatment. However, in our study, we observe no significant sensitivity to treatment in the TRAPPC1-knockdown U87 cells compared to the transduced control. Furthermore, it appears that the transduced TRAPPC1-knockdown cells may have a slight higher clonogenic capacity than control cells, which is the opposite of what we should have expected. This slight increase in clonogenicity may be due to a higher autophagic activity caused by TMZ-treatment and the alteration in mTORC1 signalling pathway as a result of the TRAPPC1 knockdown, as previously hypothesized.

Altogether, given the results obtained in this study, we cannot confirm that TRAPPC1 has a direct role in the sensitivity to GBM treatment. However, we can conclude that TRAPPC1 acts as an essential gene for cell proliferation and thus cannot be used as a therapeutical target for improving the outcome of individuals suffering from glioblastoma.

Furthermore, and as already mentioned, it would be worthy of investigation to shift the focus to a non-essential TRAPP gene. Additionally, as Rab GTPases coordinate every step of intracellular trafficking and TRAPP regulate Rab GTPases, it would be interesting to further study the relationship between non-essential TRAPP genes (e.g., TRAPPC2L) and other proteins to understand their role in intracellular trafficking, and their potential implication in chemotherapy and radiotherapy resistance in the context of GBM.

5. References

1. Sung H, Ferlay J, Siegel RL, et al. Global Cancer Statistics 2020: GLOBOCAN Estimates of Incidence and Mortality Worldwide for 36 Cancers in 185 Countries. CA: A Cancer Journal for Clinicians. 2021;71(3):209-249. doi:10.3322/caac.21660

2. Hanahan D, Weinberg RA. Hallmarks of cancer: the next generation. Cell. 2011;144(5):646-674. doi:10.1016/j.cell.2011.02.013

3. Wen PY, Weller M, Lee EQ, et al. Glioblastoma in adults: a Society for Neuro-Oncology (SNO) and European Society of Neuro-Oncology (EANO) consensus review on current management and future directions. Neuro Oncol. 2020;22(8):1073-1113. doi:10.1093/neuonc/noaa106

4. Crocetti E, Trama A, Stiller C, et al. Epidemiology of glial and non-glial brain tumours in Europe. European journal of cancer (Oxford, England : 1990). 2012;48:1532-1542. doi:10.1016/j.ejca.2011.12.013

5. Hanif F, Muzaffar K, Perveen K, Malhi SM, Simjee SU. Glioblastoma Multiforme: A Review of its Epidemiology and Pathogenesis through Clinical Presentation and Treatment. Asian Pac J Cancer Prev. 2017;18(1):3-9. doi:10.22034/APJCP.2017.18.1.3

6. Kanderi T, Gupta V. Glioblastoma Multiforme. In: StatPearls. StatPearls Publishing; 2021. Accessed September 18, 2021. http://www.ncbi.nlm.nih.gov/books/NBK558954/

7. Grech N, Dalli T, Mizzi S, Meilak L, Calleja N, Zrinzo A. Rising Incidence of Glioblastoma Multiforme in a Well-Defined Population. Cureus. 2020;12(5). doi:10.7759/cureus.8195

8. Aldape K, Zadeh G, Mansouri S, Reifenberger G, von Deimling A. Glioblastoma: pathology, molecular mechanisms and markers. Acta Neuropathol. 2015;129(6):829-848. doi:10.1007/s00401-015-1432-1

9. Wesseling P, Capper D. WHO 2016 Classification of gliomas. Neuropathol Appl Neurobiol. 2018;44(2):139-150. doi:10.1111/nan.12432

10. D'Alessio A, Proietti G, Sica G, Scicchitano BM. Pathological and Molecular Features of Glioblastoma and Its Peritumoral Tissue. Cancers (Basel). 2019;11(4):469. doi:10.3390/cancers11040469

11. Ježek P. 2-Hydroxyglutarate in Cancer Cells. Antioxidants & Redox Signaling. 2020;33(13):903-926. doi:10.1089/ars.2019.7902

12. Tommasini-Ghelfi S, Murnan K, Kouri FM, Mahajan AS, May JL, Stegh AH. Cancer-associated mutation and beyond: The emerging biology of isocitrate dehydrogenases in human disease. Science Advances. 5(5):eaaw4543. doi:10.1126/sciadv.aaw4543

13. Ou A, Yung WKA, Majd N. Molecular Mechanisms of Treatment Resistance in Glioblastoma. IJMS. 2020;22(1):351. doi:10.3390/ijms22010351

14. Molinaro AM, Taylor JW, Wiencke JK, Wrensch MR. Genetic and molecular epidemiology of adult diffuse glioma. Nat Rev Neurol. 2019;15(7):405-417. doi:10.1038/s41582-019-0220-2

15. Nørøxe DS, Poulsen HS, Lassen U. Hallmarks of glioblastoma: a systematic review. ESMO Open. 2017;1(6):e000144. doi:10.1136/esmoopen-2016-000144

16. Targeting RTK Signaling Pathways in Cancer. Accessed September 17, 2021. https://www.ncbi.nlm.nih.gov/pmc/articles/PMC4586793/

17. Comprehensive genomic characterization defines human glioblastoma genes and core pathways. Nature. 2008;455(7216):1061-1068. doi:10.1038/nature07385

18. Ehrlich PF, Shamberger RC. Chapter 30 - Wilms' Tumor. In: Coran AG, ed. Pediatric Surgery (Seventh Edition). Mosby; 2012:423-440. doi:10.1016/B978-0-323-07255-7.00030-1

19. Aubrey BJ, Kelly GL, Janic A, Herold MJ, Strasser A. How does p53 induce apoptosis and how does this relate to p53-mediated tumour suppression? Cell Death Differ. 2018;25(1):104-113. doi:10.1038/cdd.2017.169

20. Aubrey BJ, Strasser A, Kelly GL. Tumor-Suppressor Functions of the TP53 Pathway. Cold Spring Harb Perspect Med. 2016;6(5):a026062. doi:10.1101/cshperspect.a026062

21. Knudsen ES, Wang JYJ. Targeting the RB-Pathway in Cancer Therapy. Clin Cancer Res. 2010;16(4):1094. doi:10.1158/1078-0432.CCR-09-0787

22. Du W, Searle JS. The Rb Pathway and Cancer Therapeutics. Curr Drug Targets. 2009;10(7):581-589.

23. Iurlaro R, León-Annicchiarico CL, Muñoz-Pinedo C. Regulation of Cancer Metabolism by Oncogenes and Tumor Suppressors. In: Methods in Enzymology. Vol 542. Elsevier; 2014:59-80. doi:10.1016/B978-0-12-416618-9.00003-0

24. Glioblastoma_-_high_mag.jpg (4272×2848). Accessed September 17, 2021. https://upload.wikimedia.org/wikipedia/commons/7/74/Glioblastoma_-_high_mag.jpg

25. Gaillard F. Glioblastoma NOS | Radiology Case | Radiopaedia.org. Radiopaedia. Accessed September 18, 2021. https://radiopaedia.org/cases/glioblastoma-nos-16?lang=us

26. Gaillard F. Glioblastoma | Radiology Reference Article | Radiopaedia.org. Radiopaedia. Accessed September 18, 2021. https://radiopaedia.org/articles/glioblastoma

27. Visvader JE. Cells of origin in cancer. Nature. 2011;469(7330):314-322. doi:10.1038/nature09781

28. Zong H, Parada LF, Baker SJ. Cell of Origin for Malignant Gliomas and Its Implication in Therapeutic Development. Cold Spring Harb Perspect Biol. 2015;7(5):a020610. doi:10.1101/cshperspect.a020610

29. Human glioblastoma arises from subventricular zone cells with low-level driver mutations | Nature. Accessed September 18, 2021. https://www.nature.com/articles/s41586-018-0389-3

30. Lu QR, Qian L, Zhou X. Convergence of Developmental Origins and Oncogenic Pathways in Malignant Brain Tumors. Wiley Interdiscip Rev Dev Biol. 2019;8(4):e342. doi:10.1002/wdev.342

31. Ramirez YP, Weatherbee JL, Wheelhouse RT, Ross AH. Glioblastoma Multiforme Therapy and Mechanisms of Resistance. Pharmaceuticals (Basel). 2013;6(12):1475-1506. doi:10.3390/ph6121475

32. Sottoriva A, Spiteri I, Piccirillo SGM, et al. Intratumor heterogeneity in human glioblastoma reflects cancer evolutionary dynamics. Proc Natl Acad Sci U S A. 2013;110(10):4009-4014. doi:10.1073/pnas.1219747110

33. Qazi MA, Vora P, Venugopal C, et al. Intratumoral heterogeneity: pathways to treatment resistance and relapse in human glioblastoma. Ann Oncol. 2017;28(7):1448-1456. doi:10.1093/annonc/mdx169

34. PubChem. Temozolomide. Accessed September 18, 2021. https://pubchem.ncbi.nlm.nih.gov/compound/5394

35. Butler M, Pongor L, Su YT, et al. MGMT status as a clinical biomarker in glioblastoma. Trends Cancer. 2020;6(5):380-391. doi:10.1016/j.trecan.2020.02.010

36. Yan Y, Xu Z, Dai S, Qian L, Sun L, Gong Z. Targeting autophagy to sensitive glioma to temozolomide treatment. J Exp Clin Cancer Res. 2016;35:23. doi:10.1186/s13046-016-0303-5

37. Stupp R, Mason WP, van den Bent MJ, et al. Radiotherapy plus concomitant and adjuvant temozolomide for glioblastoma. N Engl J Med. 2005;352(10):987-996. doi:10.1056/NEJMoa043330

38. Photons and Protons. Accessed November 21, 2021. https://www.hopkinsmedicine.org/news/articles/photons-and-protons

39. Raviraj R, Nagaraja SS, Selvakumar I, Mohan S, Nagarajan D. The epigenetics of brain tumors and its modulation during radiation: A review. Life Sciences. 2020;256:117974. doi:10.1016/j.lfs.2020.117974

40. Gopal Krishnan PD, Golden E, Woodward EA, Pavlos NJ, Blancafort P. Rab GTPases: Emerging Oncogenes and Tumor Suppressive Regulators for the Editing of Survival Pathways in Cancer. Cancers. 2020;12(2):259. doi:10.3390/cancers12020259

41. Ramírez-Peinado S, Ignashkova TI, van Raam BJ, et al. TRAPPC13 modulates autophagy and the response to Golgi stress. J Cell Sci. 2017;130(14):2251-2265. doi:10.1242/jcs.199521

42. Endocytosis and Exocytosis: Differences and Similarities. from Technology Networks. Accessed November 21, 2021. https://www.technologynetworks.com/immunology/articles/endocytosis-and-exocytosis-differences-and-similarities-334059

43. Su M, Mei Y, Sinha S. Role of the Crosstalk between Autophagy and Apoptosis in Cancer. Journal of Oncology. 2013;2013:e102735. doi:10.1155/2013/102735

44. Nishimura T, Tooze SA. Emerging roles of ATG proteins and membrane lipids in autophagosome formation. Cell Discov. 2020;6(1):32. doi:10.1038/s41421-020-0161-3

45. Mechanisms governing autophagosome biogenesis | Nature Reviews Molecular Cell Biology. Accessed September 20, 2021. https://www.nature.com/articles/s41580-020-0241-0

46. Frontiers | A Key Pathway to Cancer Resilience: The Role of Autophagy in Glioblastomas | Oncology. Accessed November 21, 2021. https://www.frontiersin.org/articles/10.3389/fonc.2021.652133/full#h7

47. Lee SW, Kim HK, Lee NH, et al. The synergistic effect of combination temozolomide and chloroquine treatment is dependent on autophagy formation and p53 status in glioma cells. Cancer Lett. 2015;360(2):195-204. doi:10.1016/j.canlet.2015.02.012

48. Extrinsic versus intrinsic apoptosis pathways in anticancer chemotherapy | Oncogene. Accessed December 8, 2021. https://www.nature.com/articles/1209608

49. Basu A. The interplay between apoptosis and cellular senescence: Bcl-2 family proteins as targets for cancer therapy. Pharmacology & Therapeutics. Published online June 25, 2021:107943. doi:10.1016/j.pharmthera.2021.107943

50. Frenzel A, Grespi F, Chmelewskij W, Villunger A. Bcl2 family proteins in carcinogenesis and the treatment of cancer. Apoptosis. 2009;14(4):584-596. doi:10.1007/s10495-008-0300-z

51. Pawlowska E, Szczepanska J, Szatkowska M, Blasiak J. An Interplay between Senescence, Apoptosis and Autophagy in Glioblastoma Multiforme—Role in Pathogenesis and Therapeutic Perspective. International Journal of Molecular Sciences. 2018;19(3):889. doi:10.3390/ijms19030889

52. Lipatova Z, Segev N. Ypt/Rab GTPases and their TRAPP GEFs at the Golgi. FEBS Lett. 2019;593(17):2488-2500. doi:10.1002/1873-3468.13574

53. Lipatova Z, Hain AU, Nazarko VY, Segev N. Ypt/Rab GTPases: principles learned from yeast. Crit Rev Biochem Mol Biol. 2015;50(3):203-211. doi:10.3109/10409238.2015.1014023

54. Kim JJ, Lipatova Z, Segev N. TRAPP Complexes in Secretion and Autophagy. Front Cell Dev Biol. 2016;4:20. doi:10.3389/fcell.2016.00020

55. The EM structure of the TRAPPIII complex leads to the identification of a requirement for COPII vesicles on the macroautophagy pathway | PNAS. Accessed September 23, 2021. https://www.pnas.org/content/110/48/19432

56. Ishida M, E Oguchi M, Fukuda M. Multiple Types of Guanine Nucleotide Exchange Factors (GEFs) for Rab Small GTPases. Cell Struct Funct. 2016;41(2):61-79. doi:10.1247/csf.16008

57. Barrowman J, Bhandari D, Reinisch K, Ferro-Novick S. TRAPP complexes in membrane traffic: convergence through a common Rab. Nat Rev Mol Cell Biol. 2010;11(11):759-763. doi:10.1038/nrm2999

58. Zhang Y, Liu S, Wang H, et al. Elevated NIBP/TRAPPC9 mediates tumorigenesis of cancer cells through NFκB signaling. Oncotarget. 2015;6(8):6160-6178. doi:10.18632/oncotarget.3349

59. Sacher M, Shahrzad N, Kamel H, Milev MP. TRAPPopathies: An emerging set of disorders linked to variations in the genes encoding transport protein particle (TRAPP)-associated proteins. Traffic. 2019;20(1):undefined-undefined. doi:10.1111/tra.12615

60. Brunet S, Sacher M. In sickness and in health: the role of TRAPP and associated proteins in disease. Traffic. 2014;15(8):803-818. doi:10.1111/tra.12183

61. Signal transduction mediated by the Ras/Raf/MEK/ERK pathway from cytokine receptors to transcription factors: potential targeting for therapeutic intervention | Leukemia. Accessed November 20, 2021. https://www.nature.com/articles/2402945

62. Zhao SL, Hong J, Xie ZQ, et al. TRAPPC4-ERK2 Interaction Activates ERK1/2, Modulates Its Nuclear Localization and Regulates Proliferation and Apoptosis of Colorectal Cancer Cells. PLoS One. 2011;6(8):e23262. doi:10.1371/journal.pone.0023262

63. ER-Golgi network--a future target for anti-cancer therapy - PubMed. Accessed September 23, 2021. https://pubmed.ncbi.nlm.nih.gov/19595459/

64. The emerging clinical relevance of genomics in cancer medicine | Nature Reviews Clinical Oncology. Accessed September 18, 2021. https://www.nature.com/articles/s41571-018-0002-6

65. Li H, Yang Y, Hong W, Huang M, Wu M, Zhao X. Applications of genome editing technology in the targeted therapy of human diseases: mechanisms, advances and prospects. Signal Transduct Target Ther. 2020;5:1. doi:10.1038/s41392-019-0089-y

66. The next generation of CRISPR–Cas technologies and applications | Nature Reviews Molecular Cell Biology. Accessed September 18, 2021. https://www.nature.com/articles/s41580-019-0131-5

67. Sanjana NE. Genome-scale CRISPR pooled screens. Anal Biochem. 2017;532:95-99. doi:10.1016/j.ab.2016.05.014

68. LI C, BRANT E, BUDAK H, ZHANG B. CRISPR/Cas: a Nobel Prize award-winning precise genome editing technology for gene therapy and crop improvement. J Zhejiang Univ Sci B. 2021;22(4):253-284. doi:10.1631/jzus.B2100009

69. Chatterjee N, Walker GC. Mechanisms of DNA damage, repair, and mutagenesis. Environ Mol Mutagen. 2017;58(5):235-263. doi:10.1002/em.22087

70. Rao DD, Vorhies JS, Senzer N, Nemunaitis J. siRNA vs. shRNA: Similarities and differences. Advanced Drug Delivery Reviews. 2009;61(9):746-759. doi:10.1016/j.addr.2009.04.004

71. Gavrilov K, Saltzman WM. Therapeutic siRNA: Principles, Challenges, and Strategies. Yale J Biol Med. 2012;85(2):187-200.

72. Elegheert J, Behiels E, Bishop B, et al. Lentiviral transduction of mammalian cells for fast, scalable and high-level production of soluble and membrane proteins. Nature protocols. 2018;13(12):2991. doi:10.1038/s41596-018-0075-9

73. siRNA and qRT-PCR. Accessed July 2, 2022. https://www.gene-quantification.de/si-rna.html

74. Joung J, Konermann S, Gootenberg JS, et al. Genome-scale CRISPR-Cas9 knockout and transcriptional activation screening. Nat Protoc. 2017;12(4):828-863. doi:10.1038/nprot.2017.016

75. Shalem et al. - 2014 - Genome-Scale CRISPR-Cas9 Knockout Screening in Hum.pdf. Accessed November 22, 2021. https://media.addgene.org/cms/files/Zhang_lab_LentiCRISPR_library_protocol.pdf

76. lv900_datasheet_v22_1.pdf. Accessed November 22, 2021. https://www.abmgood.com/pub/media/productdocument/document//l/v/lv900_datasheet_v22_1.pdf

77. Kaina B, Beltzig L, Strik H. Temozolomide – Just a Radiosensitizer? Frontiers in Oncology. 2022;12. Accessed July 2, 2022. https://www.frontiersin.org/article/10.3389/fonc.2022.912821

78. Stewart MP, Langer R, Jensen KF. Intracellular Delivery by Membrane Disruption: Mechanisms, Strategies, and Concepts. Chem Rev. 2018;118(16):7409-7531. doi:10.1021/acs.chemrev.7b00678

79. Sneeggen M, Guadagno NA, Progida C. Intracellular Transport in Cancer Metabolic Reprogramming. Front Cell Dev Biol. 2020;8:597608. doi:10.3389/fcell.2020.597608

80. Stenmark H. Rab GTPases as coordinators of vesicle traffic. Nat Rev Mol Cell Biol. 2009;10(8):513-525. doi:10.1038/nrm2728

81. Cheng KW, Lahad JP, Kuo WL, et al. The RAB25 small GTPase determines aggressiveness of ovarian and breast cancers. Nat Med. 2004;10(11):1251-1256. doi:10.1038/nm1125

82. Rab1A is an mTORC1 activator and a colorectal oncogene - PubMed. Accessed September 23, 2021. https://pubmed.ncbi.nlm.nih.gov/25446900/

83. Cayo A, Segovia R, Venturini W, Moore-Carrasco R, Valenzuela C, Brown N. mTOR Activity and Autophagy in Senescent Cells, a Complex Partnership. International Journal of Molecular Sciences. 2021;22(15):8149. doi:10.3390/ijms22158149

84. Giuliano CJ, Lin A, Girish V, Sheltzer JM. Generating Single Cell-Derived Knockout Clones in Mammalian Cells with CRISPR/Cas9. Curr Protoc Mol Biol. 2019;128(1):e100. doi:10.1002/cpmb.100

85. Zhang W, Quevedo J, Fries GR. Essential genes from genome-wide screenings as a resource for neuropsychiatric disorders gene discovery. Transl Psychiatry. 2021;11(1):1-11. doi:10.1038/s41398-021-01447-y

86. Gupta K, Vuckovic I, Zhang S, et al. Radiation Induced Metabolic Alterations Associate With Tumor Aggressiveness and Poor Outcome in Glioblastoma. Frontiers in Oncology. 2020;10:535. doi:10.3389/fonc.2020.00535

87. Clonogenic Assay: Adherent Cells. Accessed December 10, 2021. https://www.ncbi.nlm.nih.gov/pmc/articles/PMC3197314/

88. Reifenberger G, Wirsching HG, Knobbe-Thomsen CB, Weller M. Advances in the molecular genetics of gliomas — implications for classification and therapy. Nat Rev Clin Oncol. 2017;14(7):434-452. doi:10.1038/nrclinonc.2016.204

89. Wen PY, Reardon DA. Progress in glioma diagnosis, classification and treatment. Nat Rev Neurol. 2016;12(2):69-70. doi:10.1038/nrneurol.2015.242

6. Supplementary data

	Lower-grade gliomas (WHO grade II and III)			Higher-grade gliomas (WHO grade IV)	
	IDH1/2 mutation		IDH1/2 wildtype	IDH1/2 mutation	IDH1/2 wildtype
	1p/19q codeletion	Intact 1p/19q			
Histological classification	Oligodendroglioma	Astrocytoma	Astrocytoma	Glioblastoma	Glioblastoma
Additional gene aberrations	TERT, CIC, FUBP1, NOTCH1	TP53, ATRX	TERT, EGFR, CDKN2A, MDM4, PTEN, NF1	TP53, ATRX, CDKN2A/B	EGFR, CDKN2A/B, PTEN, TERT, TP53, PIK3R1, PDGFRA, MET, CDK4, CDK6, MDM4
MGMT-promoter methylation (%)				~ 90%	~ 40%
Clinical prognosis	Good	Intermediate	Poor	Poor	Poor

Figure 1. Classification of gliomas based on the IDH1/2 enzyme mutation. This figure is a simplification of the standard classification of the WHO, together with additional information regarding the histological classification, gene aberrations, MGMT-promoter methylation and the clinical prognosis of each type of glioma[9,88,89].

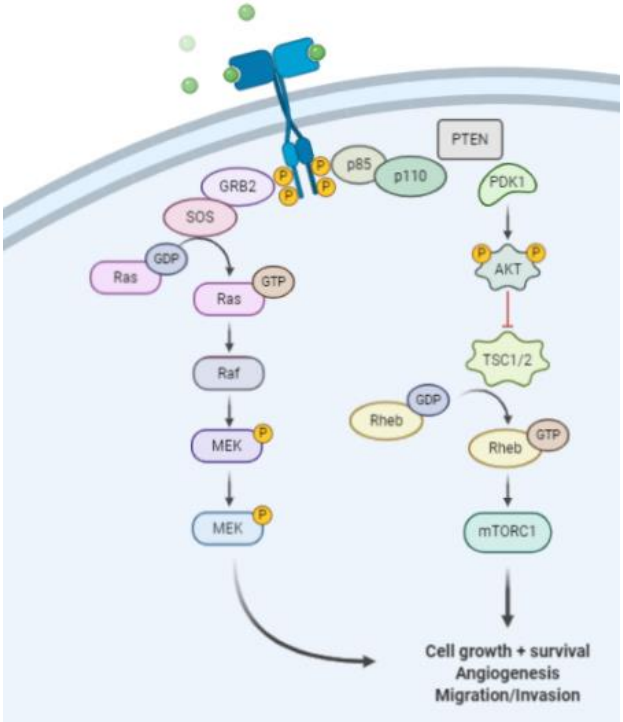

Figure 2. Schematic view of the RTK/RAS/PI3K pathways which regulate cell growth, angiogenesis and migration. Image from Biorender[17]

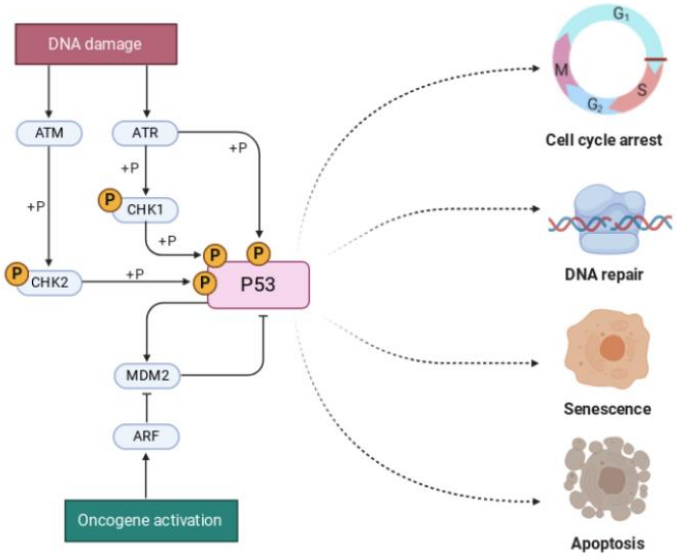

Figure 3. Diagram representing the activation of p53 upon oncogene expression and DNA damage and the variety of induced responses by p53 (e.g. growth arrest, DNA repair mechanisms and apoptosis). Image extracted from Biorender.

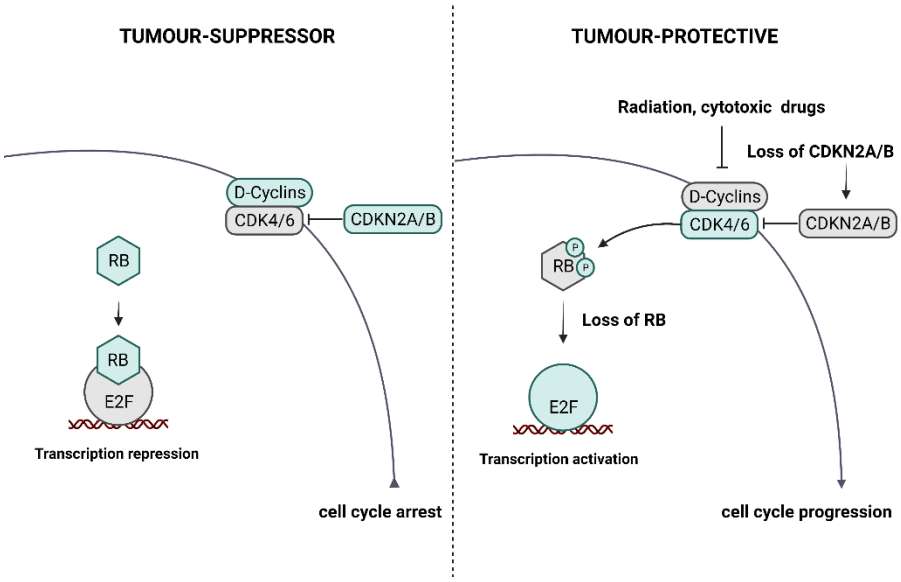

Figure 4. Diagram representing the functional interactions of the protein families participating in the Rb-pathway. The status of the RB-pathway affects cancer cell responses to radiation and other therapeutic strategies. Image created with Biorender.

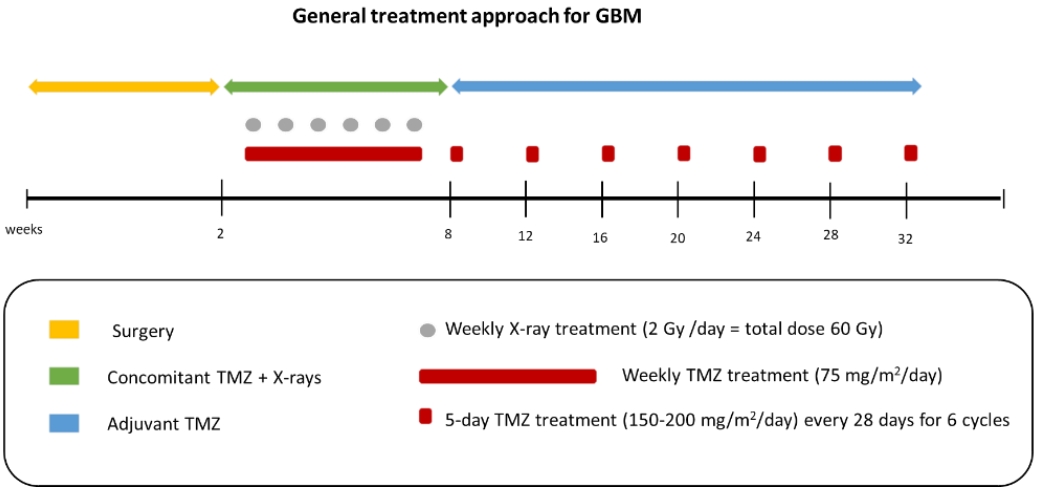

Figure 5. Schematic representation of the multimodal treatment approach for GBM. After surgery, the concomitant phase lasts six weeks, and the adjuvant phase with TMZ lasts 24 weeks. Treatment is tailored to the patient. This image was made with Microsoft PowerPoint.

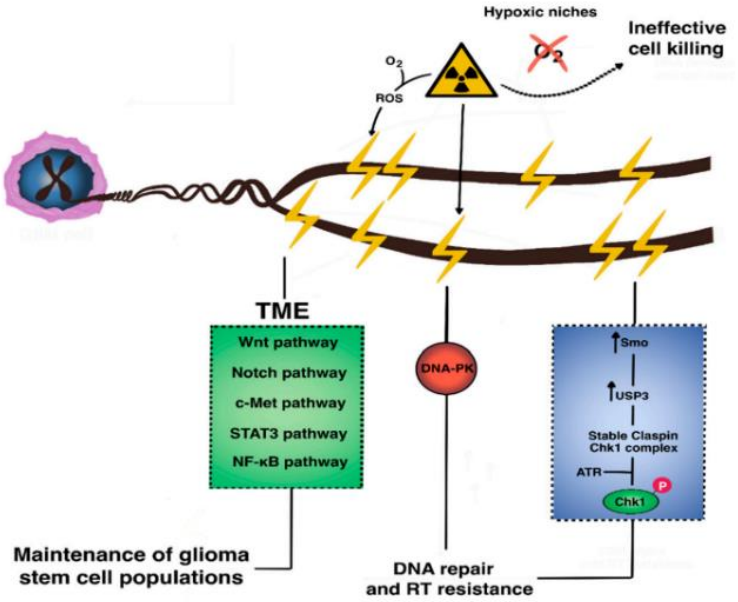

Figure 6. Resistance to radiotherapy in GBM is summarized in 3 key facts and mechanisms. The presence of hypoxic niches decreases the killing efficiency of RT, together with the TME crosstalk of Wnt, Notch, C-met, STAT3 and NF-kB pathways supporting the maintenance of GSCs and the DNA repair machinery[13].

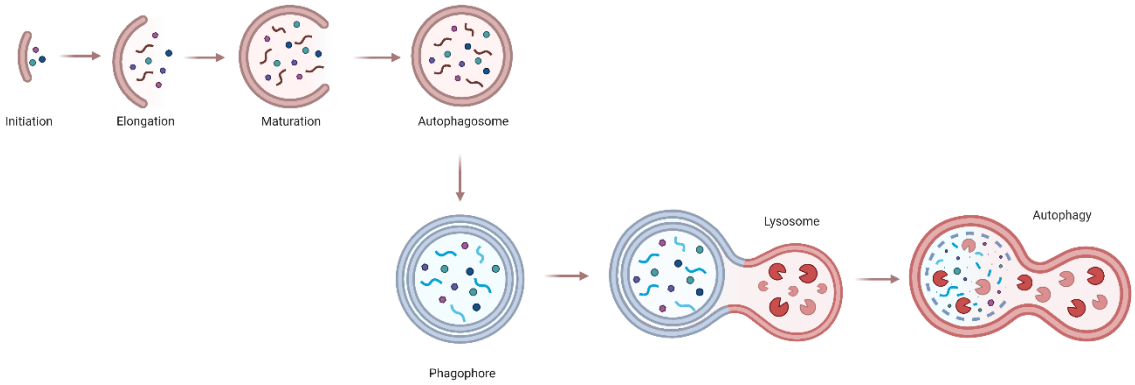

Figure 7. Overview of the autophagy process. Diagram of how autophagy works: the first step is the membrane nucleation, followed by the autophagosome generation, which transforms into a "phagophore" or an "isolation membrane". The phagophore fuses with one lysosome to degrade the sequestered cellular components. Created with Biorender

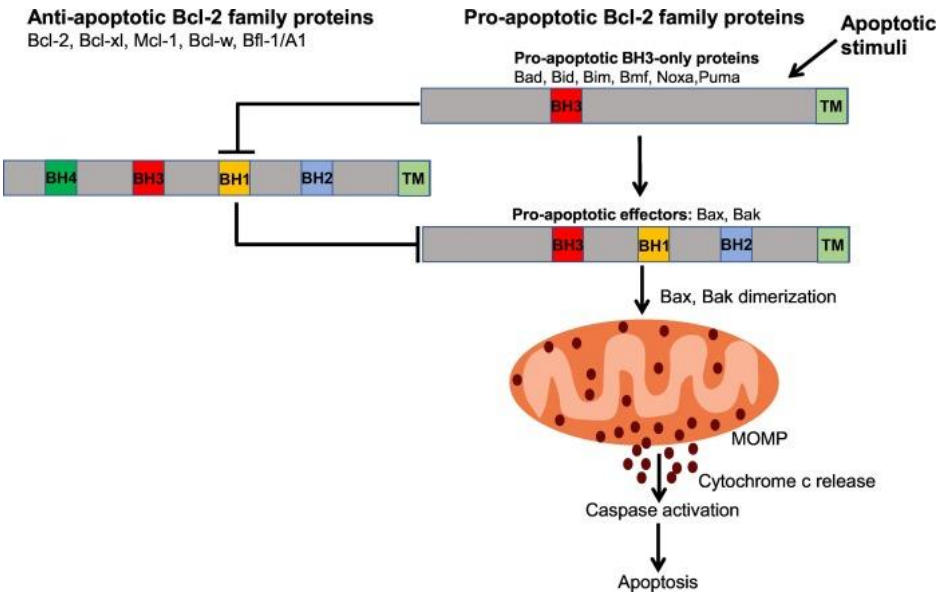

Figure 8. Intrinsic apoptotic pathway and key Bcl-2 family pro-apoptotic and anti-apoptotic regulators[49].